FORMALDEHYDE INSTRUMENT DEVELOPMENT AND BOUNDARY LAYER SULFURIC ACID: IMPLICATIONS FOR PHOTOCHEMISTRY

A Dissertation
Presented to
The Academic Faculty

by

Anne Theresa Case Hanks

In Partial Fulfillment
of the Requirements for the Degree
Doctor of Philosophy in the
School of Earth and Atmospheric Sciences

Georgia Institute of Technology
April 2008

FORMALDEHYDE INSTRUMENT DEVELOPMENT AND BOUNDARY LAYER SULFURIC ACID: IMPLICATIONS FOR PHOTOCHEMISTRY

Approved by:

Dr. Greg Huey, Advisor
School of Earth and Atmospheric Sciences
Georgia Institute of Technology

Dr. Rodney Weber
School of Earth and Atmospheric Sciences
Georgia Institute of Technology

Dr. Paul Wine
School of Chemistry and Biochemistry and
School of Earth and Atmospheric Sciences
Georgia Institute of Technology

Dr. Jennifer R. Olson
NASA Langley

Dr. David Tan
School of Earth and Atmospheric Sciences
Georgia Institute of Technology

Date Approved: March 25, 2008

To my boys: Karari, Julian, and Milo

ACKNOWLEDGEMENTS

First, I owe a debt of gratitude to my advisors David Tan and Greg Huey who have been very supportive throughout this long journey. They have spent a considerable amount of time and energy helping me and for that I am truly thankful. I have learned so much about field work, experimental design, and atmospheric chemistry.

I also owe many thanks to other group members who have helped me along the way. Joe Mastromarino taught me that lasers are not scary; through his patience and guidance I gained the experience and knowledge to design experiments and laser components. I have to thank Bob Stickel (and Speyside Scotch!) who made me smile through many tough field missions and lab experiments! I also owe many thanks to my office mates both past and present; their thoughtfulness and friendships I hold dear.

I have to thank Gao Chen and Jennifer Olson of NASA Langley for helping me with the modeling and answering any and all of my questions no matter how trivial. Never would I have thought that I would learn Fortran. Their insights and guidance have been an enormous help in completing this thesis.

Thank you to my committee, Paul Wine, Rodney Weber, and again, Jennifer Olson for comments and support.

I would also like to thank Lynn Wellage and John Murray for inspiration! Finally, I have to thank my wonderful husband, Karari, for putting up with me and my beautiful baby boy, Julian, for being perfect.

TABLE OF CONTENTS

LIST OF TABLES

LIST OF FIGURES

SUMMARY

This work presents the development of a laser-induced fluorescence technique to measure atmospheric formaldehyde. In conjunction with the technique, the design of a compact, narrow linewidth, etalon-tuned titanium:sapphire laser cavity which is pumped by the second harmonic of a kilohertz Nd:YAG laser is also presented. The fundamental tunable range is from 690-1100 nm depending on mirror reflectivities and optics kit used. The conversion efficiency is at least 25% for the fundamental, and 2-3% for intracavity frequency doubling from 3.5-4W 532 nm pump power. The linewidth is < 0.1 cm^{-1}, and the pulsewidth is 18 nsec. Applications of this cavity include the measurement of trace gas species by laser-induced fluorescence, cavity ringdown spectroscopy, and micropulse lidar in the UV-visible region.

Also presented are observations of gas-phase sulfuric acid from the NEAQS-ITCT 2K4 (New England Air Quality Study – Intercontinental Transport and Chemical Transformation) field campaign in July and August 2004. Sulfuric acid values are reported for a polluted environment and possible nucleation events as well as particle growth within the boundary layer are explored. Sulfate production rates via gas phase oxidation of sulfur dioxide are also reported. This analysis allows an important test of our ability to predict sulfuric acid concentration and probe its use as a fast time response photochemical tracer for the hydroxyl radical, OH. In comparison, the NASA time-dependent photochemical box model is used to calculate OH concentration. Nighttime H_2SO_4 values are examined to test our understanding of nocturnal OH levels and oxidation processes.

In comparison, sulfuric acid from a large ground based mission in Tecámac, México (near the northern boundary of Mexico City) during MIRAGE-Mex field campaign (March 2006) is presented. This and other measurements are used to characterize atmospheric oxidation and predict sulfuric acid and OH concentrations at the site. The observations in conjunction with the NASA LARc Photochemical box model are used to explore ozone production, nitrate and sulfate formation, and radical levels and radical production rates during the day. The one minute observations of sulfuric acid, sulfur dioxide, and aerosol surface area were again used to calculate OH levels assuming steady state, and are in good agreement with observations of OH ($R^2 = 0.7$). Photochemical activity is found to be a maximum during the morning hours, as seen in ozone and nitrate formation. Although the model predictions capture the observed diurnal profile, the model underpredicts RO_2 concentrations in the morning hours and overpredicts in the afternoon ($HO_2 + RO_2$ radical Model/observed (M/O) ~1.15 and OH M/O ~ 1.2).

CHAPTER 1

INTRODUCTION

1.1 Overview

While the composition of the atmosphere is broadly understood, the complexity of the atmosphere provides new and greater challenges for atmospheric chemists. Tropospheric *in situ* measurement techniques whether spectroscopic or chemical transformation techniques, allow for specialized measurements of trace gases, both reactive and unreactive, at the low parts-per-trillion, pptv, level. These measurements, in conjunction with chemical models and remote sensing techniques, provide the comprehensive ability to study and characterize the chemistry of trace gases. Since the Industrial Revolution, there is strong evidence to suggest concentrations of trace gases have been increasing. Figure 1.1 illustrates the increase in concentration of important greenhouse gases, CH_4, CO_2, and N_2O, for the past 1000 years as well as demonstrating the marked increase in sulfur emissions [*IPCC*, 2001]. On a global scale understanding the chemical processes, including transformation and feedbacks, in the troposphere is critical, in order to assess the anthropogenic changes to the global environment and their impact. Large scale efforts to study trace gases have included aircraft missions like NASA's Global Tropospheric Experiment (http://www-gte.larc.nasa.gov/) and various field campaigns led by NOAA (http://www.esrl.noaa.gov/csd/tropchem/), DOE, and NSF. This work presents the development of a technique and instrument to measure *in situ* formaldehyde in the troposphere and it also presents measurements of HO_x and sulfuric acid in the urban boundary layer from both an aircraft and ground-based field campaign. The next sections

offer a brief review of tropospheric ozone chemistry, in view of the fact that it is relevant and connects the species that are presented in this work.

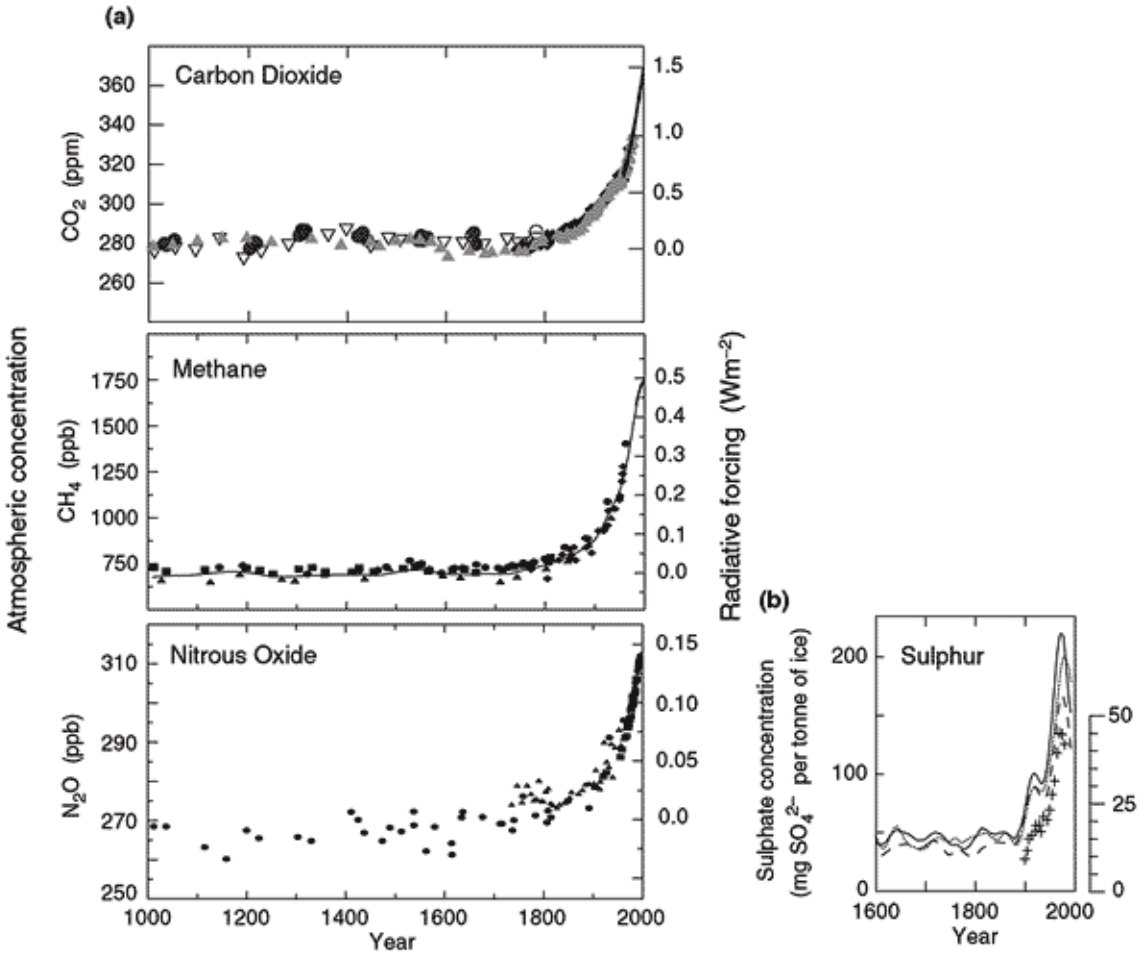

Figure 1.1: Records of changes in atmospheric composition. **(a)** Atmospheric concentrations of CO_2, CH_4 and N_2O over the past 1,000 years. The estimated radiative forcing from these gases is indicated on the right-hand scale. **(b)** Sulfate concentration in several Greenland ice cores with the episodic effects of volcanic eruptions removed (lines) and total SO_2 emissions from sources in the US and Europe (crosses), from [*IPCC*, 2001].

1.2 Ozone Chemistry

Tropospheric ozone, O_3, is defined by the Intergovernmental Panel on Climate Change, IPCC, as the third most important anthropogenic greenhouse gas behind carbon dioxide and methane[*IPCC*, 2001]. The key importance of tropospheric ozone is that it is a product of photochemistry, controlled by reactive gases including nitrogen oxides, NO_x, and volatile organic compounds, VOC, both of whose concentration vary spatially and temporally. On top of that, concentrations of ozone precursors, including methane, NO_x, CO and VOCs, have increased since the Industrial Revolution. Typical ozone concentration in remote regions is around 30-40ppbv as compared to urban centers where ozone can reach in excess of 150 ppbv [*Finlayson-Pitts and Pitts*, 2000]. Figure 1.2 is taken from the IPCC 2001 Scientific Report and shows ozone concentration for Northern Hemisphere mid-latitudes from 1970-1996, indicating that an average concentration is about 52 ppb.

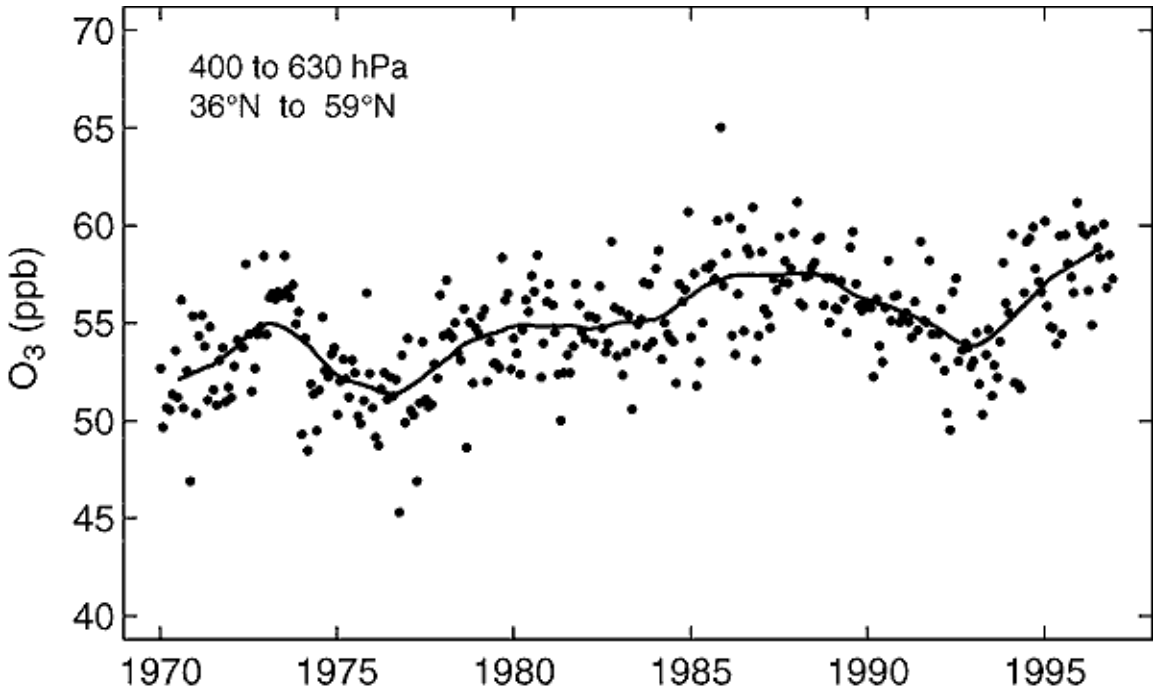

Figure 1.2: Mid-tropospheric O_3 abundance (ppb) in northern mid-latitudes (36°N-59°N) for the years 1970 to 1996. Observations between 630 and 400 hPa are averaged from nine ozone sonde stations (four in North America, three in Europe, two in Japan), following the data analysis of Logan et al. (1999) from [*IPCC*, 2001].

Ozone production is initiated by the hydroxyl radical, OH, as indicated in R1.1, but NO_x is the catalyst. It is useful to note that ozone is intimately tied to HO_x ($OH + HO_2$) through radical cycling (R1.1-7) in urban regions.

$$OH + RH \rightarrow R + H_2O \qquad \text{R1.1}$$

$$R + O_2 + M \rightarrow RO_2 + M \qquad \text{R1.2}$$

$$RO_2 + NO \rightarrow RO + NO_2 \qquad \text{R1.3}$$

$$RO + O_2 \rightarrow HO_2 + R'CHO \qquad \text{R1.4}$$

$$HO_2 + NO \rightarrow OH + NO_2 \qquad \text{R1.5}$$

$$2(NO_2 + h\nu \rightarrow NO + O) \qquad \text{R1.6}$$

$$\underline{2(O + O_2 + M \rightarrow O_3 + M)} \qquad \text{R1.7}$$

Overall: $$RH + 4O_2 + h\nu \rightarrow R'CHO + H_2O + 2O_3 \qquad \text{R1.8}$$

The overall net reaction of R1.1-7 yields 2 ozone molecules (R1.8) and some of the carbonyl compounds in this scheme can further undergo oxidation via photolysis producing additional VOCs. In remote regions (i.e. free troposphere or marine boundary layer), ozone production is dominated by methane (R1.9-16) or carbon monoxide oxidation. Methane has a long lifetime and therefore is readily available in remote regions where VOC concentrations are low.

$$OH + CH_4 \rightarrow CH_3 + H_2O \qquad \text{R1.9}$$

$$CH_3 + O_2 + M \rightarrow CH_3O_2 + M \qquad \text{R1.10}$$

$$CH_3O_2 + NO \rightarrow CH_3O + NO_2 \qquad \text{R1.11}$$

$$CH_3O + O_2 \rightarrow CH_2O + HO_2 \qquad \text{R1.12}$$

$$HO_2 + NO \rightarrow OH + NO_2 \qquad \text{R1.13}$$

$$2(NO_2 + h\nu \rightarrow NO + O) \qquad \text{R1.14}$$

$$\underline{2(O + O_2 + M \rightarrow O_3 + M)} \qquad \text{R1.15}$$

Overall: $$CH_4 + 4O_2 + h\nu \rightarrow CH_2O + H_2O + 2O_3 \qquad \text{R1.16}$$

Within the VOC or methane oxidation cycles, there are feedbacks which ultimately control ozone production and HO_x concentrations. This is a cyclical pathway which

basically involves OH oxidizing VOCs thus forming peroxy radicals that convert NO to NO_2 which is ultimately photolyzed to form ozone. This process is terminated either by radical + radical reactions (R1.17-20):

$$HO_2 + HO_2 \rightarrow H_2O_2 + O_2 \qquad \text{R1.17}$$

$$RO_2 + HO_2 \rightarrow ROOH + O_2 \qquad \text{R1.18}$$

$$OH + HO_2 \rightarrow H_2O + O_2 \qquad \text{R1.19}$$

$$RO_2 + R'O_2 \rightarrow products \qquad \text{R1.20}$$

or radical + NO_x reactions (R1.21-22):

$$OH + NO_2 \rightarrow HNO_3 \qquad \text{R1.21}$$

$$NO + RO_2 \rightarrow RONO_2 \qquad \text{R1.22}$$

Under conditions of low NO_x, the terminating processes are radical + radical reactions. In this chemical regime, ozone production is NO_x limited. Ozone production approximately increases linearly with NO_x concentration available. However, at a certain point NO_x loss rates are greater than peroxy radical loss rates because the termination steps involving NO_x and radicals are faster due to reaction rates than R1.17-20. In this chemical regime, the ozone formation rate slows, decreasing with increasing NO_x concentration and is said to be VOC-limited. Therefore, NO_x is an important control of peroxy radical concentrations. This is illustrated in a model simulation for a regional ozone event in the eastern United States as in figure 1.3 [*Sillman et al.*, 1990].

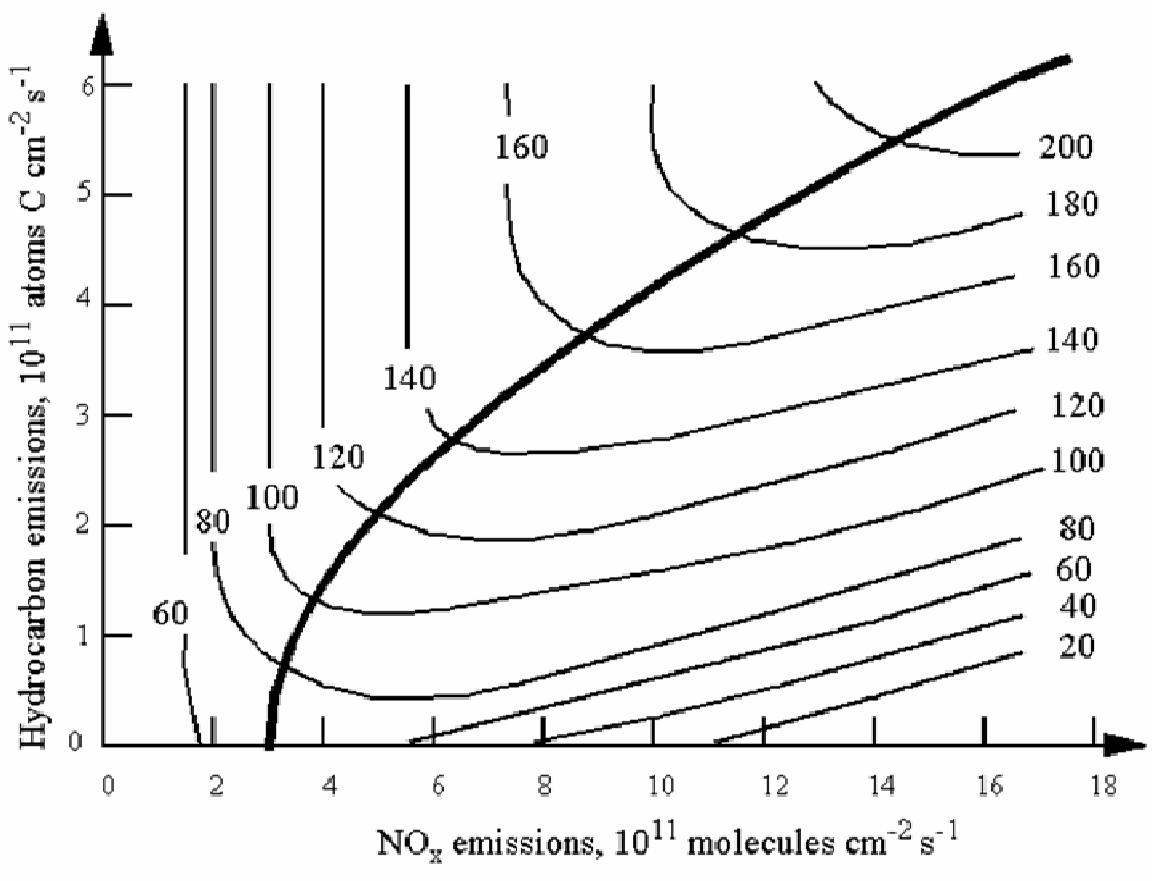

Figure 1.3 Simulated ozone concentrations (ppbv) as a function of NOx and hydrocarbon emissions. The thick line divides the NOx-limited and VOC-limited chemical regimes. Figure from [*Sillman et al.*, 1990].

The ozone isopleths to the left of the thick line are in the NO_x limited regime in which ozone concentration increases with increasing NO_x with no sensitivity to VOC concentrations. To the right of the thick line is the VOC-limited regime, here the ozone concentration decreases with increasing NO_x and increases with increasing VOCs. Ozone production in the United States is primarily in the NO_x limited regime [*Jacob*, 1999].

Ozone production in certain regions can begin in the NO_x-limited regime and then switch to VOC-limited. This balance between the NO_x-limited and VOC-limited chemical regimes and the point at which crossover can have implications in policy and

regulations for urban areas [*Cardelino and Chameides*, 1990; *Cohan et al.*, 2007; *Roth et al.*, 2005; *Stone*, 2005]. There is also an intense focus to properly identify the ozone concentrations expected from the NO_x-limited or VOC-limited regimes within models [*Kleinman et al.*, 1997; *Kleinman*, 2005; *Sillman et al.*, 1995; *Sillman et al.*, 1997; *Stein et al.*, 2005].

Trends of surface ozone both in remote region and urban areas continue to present challenges as most ozone monitoring stations are in the northern mid-latitudes [*WMO* -- http://www.wmo.ch/pages/prog/arep/gaw/reactive_gases.html#surfaceozone]. Another challenge is the complexity of ozone production chemistry from VOC and NO_x; this can yield different ozone concentrations depending on the chemical model used [*Olson et al.*, 1997].

The urban environment is susceptible to increased pollution due to the increase in population and an increase of vehicles and industries emitting primary pollutants. *Lawrence et al.*, [2007] used the 3-D global model MATCH (Model of Atmospheric Transport and Chemistry) to understand the global impact of pollution from megacities on all continents and found that long-range export of low level pollutants were strongest in the mid to high latitudes especially Eurasia. NO_x emissions rates from Asia exceed the amount from North America and Europe, a trend currently continuing [*Akimoto*, 2003]. Therefore, tropospheric ozone levels are projected to increase in many Asian megacities as result of the increasing NO_x and VOC emissions [*Guttikunda et al.*, 2005]. Within the United States, Houston has been identified as having some of the highest ozone mixing ratios and is notable for its many industries, producing large amounts of VOCs [*Brock et al.*, 2003]. Ozone production rates there can range from 50-150 ppb hr^{-1} due to the high

concentration of reactive hydrocarbons and available NO_x [*Kleinman et al.*, 2002]. In spite of this, the Environmental Protection Agency reported that there has been a 12% decreases in the maximum daily 8-hour averaged ozone concentration within the United States[*EPA*, 2002; *Jacob*, 1999].

Mexico City, on the other hand, is one of the most polluted cities and the most populated in North America. [*Fast and Zhong*, 1998] noted that the Mexican standard ozone of 110 ppb was exceeded at 19 monitoring stations almost every day and the variation of ozone concentration varied greatly among the stations. Results from the 2003 Mexico City Metropolitan Area (MCMA-2003) confirmed that the large loadings of reactive VOCs in the greater area contributed to high OH reactivities during the day, combined with high NO_x levels, ozone production rates surpass 50 ppb/hr soon after sunrise [*Ren et al.*, 2006b]. Median ozone concentration observed by *Shirley et al* [2006] during MCMA-2003 was 115 ppbv.

1.3 HO_x Importance and Measurement Techniques

While NO_x and VOCs are fundamental in ozone formation, HO_x participation is significant and describes the oxidative capacity of the atmosphere (See Figure 1.4). Many ground-based and aircraft studies to measure HO_x mixing ratios have been conducted around the world [*Cantrell et al.*, 2003a; *Kanaya and Akimoto*, 2002; *Kanaya et al.*, 2007; *Ren et al.*, 2003a; *Ren et al.*, 2006b]. Few of these studies have focused on an intensely polluted environment such as Mexico City.

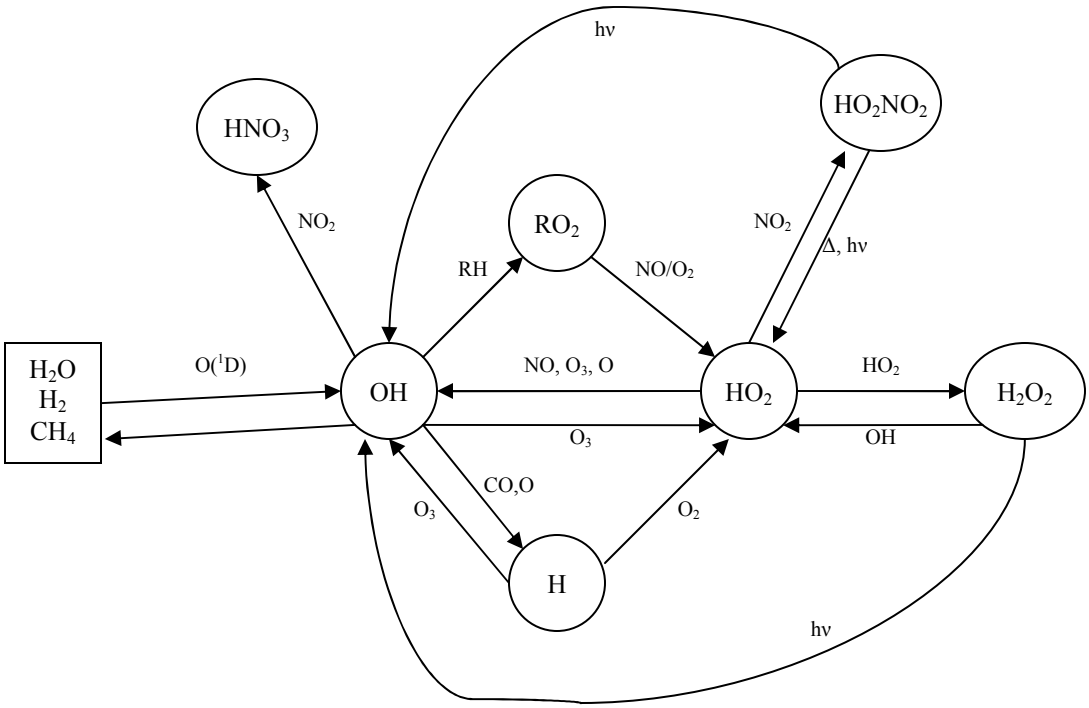

Figure 1.4: Schematic representation of important HO_x reactions and controls in troposphere

Current measurement techniques to measure the hydroxyl radical include long-path optical absorption spectroscopy (DOAS), laser-induced fluorescence (LIF) and chemical ionization mass spectrometry (CIMS). A brief description of each follows: DOAS employs a 3 km path length folded into a 20 m multi-reflection optical cell; a picosecond laser centered on 308 nm is used to detect 6 different OH absorption lines [*Dorn et al.*, 1995]. The detection limit for a 5 minute integration time is 2×10^5 molecules cm^{-3}. This technique only quantifies OH and has mainly been employed in ground-based studies [*Brauers et al.*, 2001; *Hofzumahaus et al.*, 1991; *McKeen et al.*, 1997]. The second spectroscopic technique is laser-induced fluorescence. Again using 308 nm, the $X^2\Pi$ ground state of OH can be excited to the first electronic state, $A^2\Sigma$. At

low pressure, the fluorescence lifetime can be extended allowing for observation of the fluorescence signal and discrimination of scattered light [*Hard et al.*, 1984]. Current level of detection of OH is around 2.5×10^5 molec cm^{-3} in 10 minutes [*Cantrell et al.*, 2003a]. OH can also be measured by the CIMS technique; OH is reacted with isotopically labeled $^{34}SO_2$ and undergoes a chemical conversion sequence to form $H_2{}^{34}SO_4$ which is detected using quadrupole mass spectrometry as $H^{34}SO_4^-$ (99 amu) [*Tanner et al.*, 1997]. This technique has been involved in both ground based studies and on various airborne platforms. Current limit of detection is around 1.3×10^5 molecules cm^{-3} in 10 minutes [*Sjostedt et al.*, 2007].

Recently, in Germany, an intercomparison between LIF and DOAS in an atmosphere simulation chamber in which there were controlled air masses sampled found excellent agreement between the instruments ($r^2 = 0.89$) [*Schlosser et al.*, 2007]. During PEM-TROPICS B, an intercomparsion of OH measurements which included LIF and CIMS, aboard the DC-8 and WP3-B respectively, was carried out in the marine boundary layer. The results indicated no obvious discrepancies in the OH measurement techniques [*Davis et al.*, 2001]. In rural Germany, a ground-based intercomparison of LIF and DOAS revealed excellent agreement ($r^2 = 0.81$) in OH concentration measured within the same air mass [*Brauers et al.*, 1996]. The first successful intercomparisons between the OH measurement techniques, CIMS, LIF and DOAS, were ground-based, occurring in rural areas; results at Fitz Peak, Colorado yielded a correlation coefficient of $R^2 = 0.62$ due to the fact that different air was sampled [*Eisele et al.*, 1994; *McKeen et al.*, 1997].

Within the urban environment, Ren et al., [2006] observed median OH concentration to be 1.4×10^6 molecules cm^{-3} in New York City. During the MCMA-2003

field campaign, OH concentration ranged from 5-8×10^6 molecules cm^{-3} while HO_2 spanned a much greater range, 15 -60 pptv [*Ren et al.*, 2006b]. Other observed OH concentrations ranged from 1×10^6 molecules cm^{-3} to 7 ×10^6 molecules cm^{-3} for urban environments in North America [*Brune et al.*, 2002; *George et al.*, 1999; *Ren et al.*, 2006b]. In remote regions, typical OH concentrations vary from 1-6 × 10^6 molecules cm^{-3} [*Mauldin et al.*, 1999a; *Sjostedt et al.*, 2007].

Recently, there have been reported measurements of nighttime OH (> 10^6 molecules cm^{-3}) using the LIF technique [*Faloona et al.*, 2001a; *Geyer et al.*, 2003; *Ren et al.*, 2003a]. As OH is produced photochemically, a nonphotochemical explanation for the presence of nighttime OH has been postulated; ozonolysis of VOCs and the oxidation of VOCs via NO_3 then subsequent chemistry has been suggested as a possible mechanisms for nighttime production of OH radicals [*Platt et al.*, 1990], although the mechanism by which OH is produced at night is poorly understood. Another source for nighttime OH which has been postulated is ozonlysis of alkenes, although such work have been model focused [*Ariya et al.*, 2000].

Hydroperoxy (HO_2) and peroxy (RO_2) radical measurement are complimentary to OH measurements. In fact, quantitative detection of these radicals relies on the interconversion between OH and HO_2/RO_2 (Figure 1.6). Ambient measurement techniques consist of Ion Molecule Reaction-Mass Spectrometry (IMR-MS), CIMS, and LIF (HO_2 radicals only). The IMR-MS [*Reiner et al.*, 1997; 1998; *Reiner et al.*, 1999] and CIMS [*Cantrell et al.*, 2003b; *Edwards et al.*, 2003; *Sjostedt et al.*, 2007] techniques are analogous in nature. Peroxy radicals (HO_2 + RO_2) are converted to OH by addition of high concentration of NO in the presence of O_2. The converted OH is then detected by

conversion to sulfuric acid. This chemical conversion sequence depends heavily on the concentration of NO. For the sum of HO_2+RO_2 ,the IRM-MS has a detection limit in 1 minute of 0.5 pptv [*Hanke et al.*, 2002] and the CIMS estimates 37% uncertainty for peroxy measurements [*Sjostedt et al.*, 2007]. Finally, the LIF technique only measures HO_2 radicals and, again, uses the conversion of HO_2 to OH via NO [*Brune et al.*, 1995; *Hard et al.*, 1984; *Kanaya et al.*, 2001]. Fluorescence of the converted OH is detected after excitation by 308 nm as described previously. The LIF technique only measures HO_2 radicals because the reaction of RO_2 with NO at low pressure is limited due to decreased concentration of species. The current limit of detection is about 0.15 pptv [*Cantrell et al.*, 2003a].

1.4 Formaldehyde Importance in the Atmosphere and Measurement Techniques

Formaldehyde (HCHO), as stated above, is a key reactive intermediate in the methane oxidation cycle and the photooxidation of hydrocarbons. It is the most abundant carbonyl species in the atmosphere and exerts a substantial influence on the oxidizing power of the atmosphere [*Crutzen et al.*, 1999]. In the continental boundary layer, formaldehyde is primarily produced from the photooxidation of isoprene and terpenes emitted from plants and other vegetation. It is also emitted directly into the atmosphere by vegetation and by anthropogenic sources including combustion and biomass burning [*Smith et al.*, 2002]. In the free troposphere, the primary source of HCHO is photooxidation of methane in the presence of NO; other sources include the photooxidation of larger hydrocarbons [*Carlier et al.*, 1986].

Formaldehyde concentrations range from several 10s of pptv in the free troposphere to several ppbv in urban areas. HCHO decomposes by two photolytic pathways. Reaction 1.17 occurs at wavelengths less than 360 nm. Reaction 1.18 serves as a source of HO_x within the free troposphere (R1.18-21), [*Jaegle et al.*, 2000] and dominates in urban conditions when ozone is suppressed by reaction with NO [*Jenkin et al.*, 2000]. As such, it is an integral part of the dynamic relationship between tropospheric O_3, NO_x, and HO_x

$$HCHO + h\nu(\lambda < 360nm) \rightarrow H_2 + CO \qquad \text{R1.17}$$

$$HCHO + h\nu(\lambda < 340nm) \rightarrow 2HO_2 + CO \qquad \text{R1.18}$$

$$HO_2 + NO \rightarrow NO_2 + OH \qquad \text{R1.19}$$

$$NO_2 + h\nu \rightarrow NO + O \qquad \text{R1.20}$$

$$O + O_2 \rightarrow O_3 \qquad \text{R1.21}$$

Another possible fate of HCHO in the atmosphere is chemical oxidation by OH, which also generates HCO radicals, leading to a minor amount of ozone and free radicals. The contribution of formaldehyde decomposition to the total HO_x production in the free troposphere is significant as seen in two recent NASA field programs, the Subsonic Assessment Ozone and Nitrogen Oxide Experiment (SONEX) and the Pacific Exploratory Mission - Tropics –B (PEM-Tropics B). It was demonstrated in PEM-Tropics B that at higher altitudes, photolysis of formaldehyde and peroxides governed half of the total HO_x and about 35% of HO_x production was attributed to formaldehyde photolysis alone as shown in Figure 1.5 [*Tan et al*., 2001]. The SONEX mission established that the principal source of HO_x throughout the middle and upper troposphere in this region and time of year is formaldehyde [*Jaegle et al.*, 2000].

Elevated formaldehyde levels have been observed in the arctic boundary layer, more specifically directly above the snowpack and in firn air. In fact, the levels are sufficiently high that known gas phase chemistry does not fully account for measured HCHO concentrations. These elevated levels of HCHO indicate significant levels of snow-phase photochemistry, which has potential implications for atmospheric chemistry at high latitudes as well as the glacial ice core record and paleoclimate reconstructions. Several explanations have been proposed to explain the high concentration of formaldehyde within the arctic. [*Deserves*, 1994] measured gas-phase formaldehyde in the polar night and attributed the elevated levels to long-range transport from Eurasia. In the spring of 1996 in Summit, Greenland, it was found that within firn air, HCHO concentrations increased with depth and had a mean value of 190 pptv, significantly lower than 230 pptv mean atmospheric value measured 1-meter above the snow pack; it was proposed that the high concentration was due to desorption from ice crystals as temperature increases [*Hutterli et al.*, 1999]. After the polar sunrise in 1998 in Alert, Canada elevated gas-phase formaldehyde concentrations were observed (52 pptv to 690 pptv) and a simple gas-phase steady-state calculation could not explain the high-observed levels; [*Sumner and Shepson*, 1999] speculated that the elevated levels were due to photochemistry within the quasi-liquid layer of the snowpack. During ISCAT (Investigation of Sulfur Chemistry of Antarctic Troposphere) 2000, a detailed budget analysis of HO_x was performed and it was found that formaldehyde and hydrogen peroxide snow emissions accounted for 46% of gas-phase HO_x at the South Pole [*Chen et al.*, 2004].

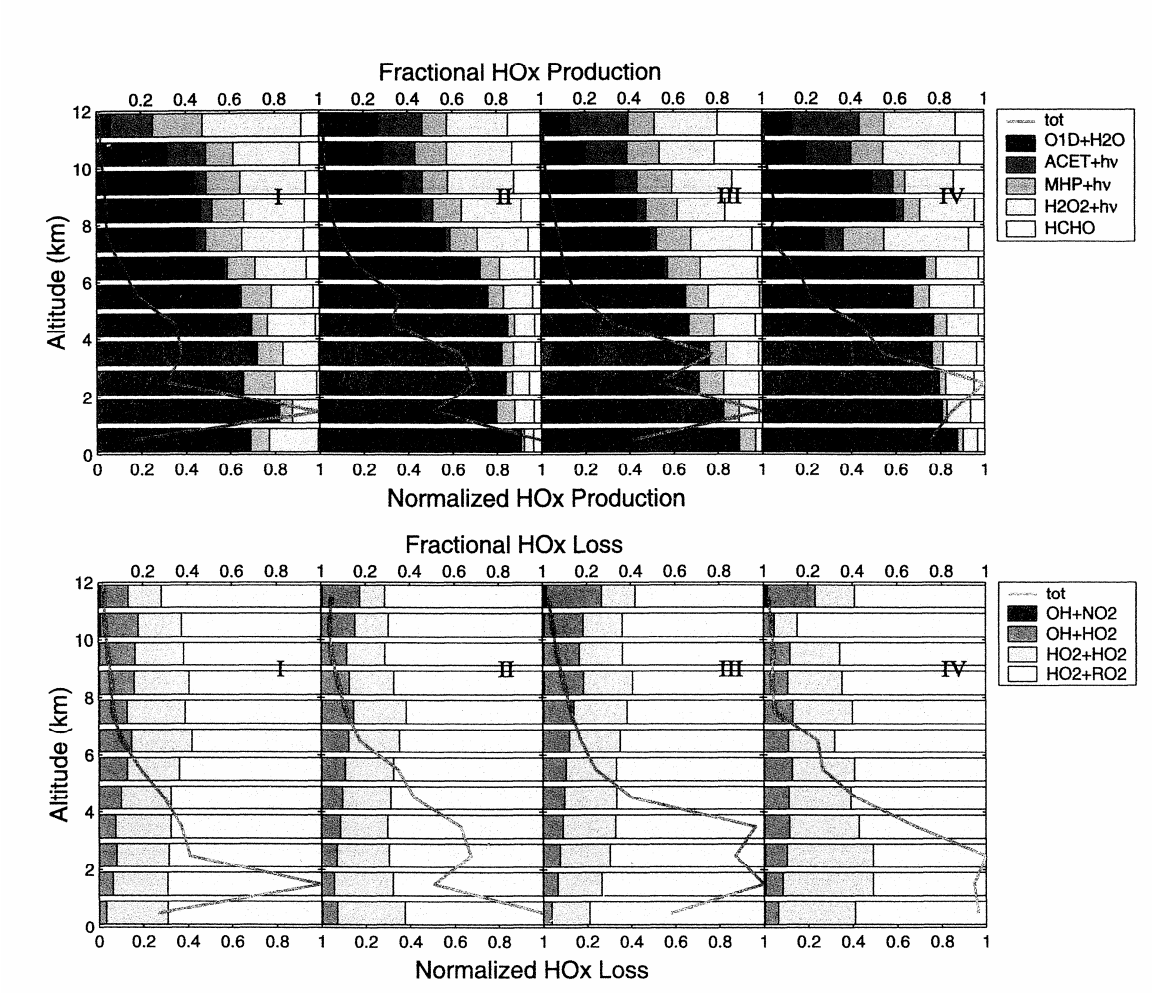

Figure 1.5: Altitude profiles of total (solid line) and fractional HOx production in the Pacific Ocean on PEM-Tropics B within the following regions: (I) north of the equator and west of 130W longitude; (II) south of the equator and west of 170W longitude; (III) south of the equator and east of 170W longitude; and (IV) North of the equator and east of 130W longitude. [*Tan et al*., 2001]

Attempts to quantify atmospheric HCHO have developed steadily over the years. Methods for detecting formaldehyde have included spectroscopic and nonspectrocopic

techniques. The spectroscopic techniques used include tunable diode laser absorption spectroscopy [*Mackay et al.*, 1996; *McKeen et al.*, 1997] and long path absorption [*McKeen et al.*, 1997]. Nonspectroscopic methods include a coil enzyme method [*Heikes et al.*, 1996], an impregnated-cartridge 2,4-dinitrophenylhydrazine (DNPH) method [*Zhou and Mopper*, 1990], and aqueous-scrubber DNPH derivization followed by high performance liquid chromatography [*Lee and Zhou*, 1993]. It should be noted that current instruments continue to have difficulties measuring the particularly low concentrations of HCHO in the free troposphere and/or arctic boundary layer with good time resolution. The continuing inability to reconcile the difference between observed and calculated formaldehyde concentrations [*Heikes et al.*, 1996; *Jacob et al.*, 1996] demands a thorough reexamination of the current capability of experimental measurements and the models. [*Wagner et al.*, 2002] concluded that over the past 10 years, model-measurement comparisons point to a lack in understanding of the current HCHO behavior in the free troposphere and no consistent explanation can reconcile the discrepancies of model-measurement HCHO studies.

1.5 Sulfuric Acid in the Atmosphere: Photochemistry and Aerosols

Sulfur dioxide is a common intermediate in the oxidation of reduced sulfur compounds in the troposphere [*Brasseur et al.*, 1999]. Natural sources of sulfur dioxide include dimethyl sulfide oxidation, volcanoes and biomass burning. Most sulfur dioxide which is directly emitted is due to anthropogenic activities including combustion and refining processes. Hence, this is the chief factor for the increase in sulfur in the atmosphere since the Industrial Revolution (see Figure 1.1). The total anthropogenic emissions of SO_2 have remained globally constant over the past 20 years, however, concentrations have been changing on the region scale [*Brasseur et al*., 1999]. In contrast, remote regions find little sulfur dioxide, typical concentrations are less than 100 pptv [*Stecher et al.*, 1997]. This is illustrated in Figure 1.6 as it shows the result of a global simulation for the monthly average SO_2 distribution in the lowest layer [*Berglen et al.*, 2004]. Oxidation of SO_2 by the hydroxyl radical, OH, and subsequent conversion of the SO_2-adduct leads to the formation of gas-phase sulfuric acid, H_2SO_4.

$$OH + SO_2 \rightarrow HOSO_2 \qquad \text{R1.22}$$

$$HOSO_2 + O_2 \rightarrow SO_3 + HO_2 \qquad \text{R1.23}$$

$$SO_3 + 2H_2O \rightarrow H_2SO_4 + H_2O \qquad \text{R1.24}$$

It has also been recognized that sulfuric acid has been responsible for acid precipitation and long range transport of acidic pollutants. Clean air initiatives were enacted (National Acid Precipitation Assessment Program and the Clean Air Act in 1990) to reduce SO_2

and NO_x emissions. [*Frost et al.*, 2006] found that over a period of 10 years

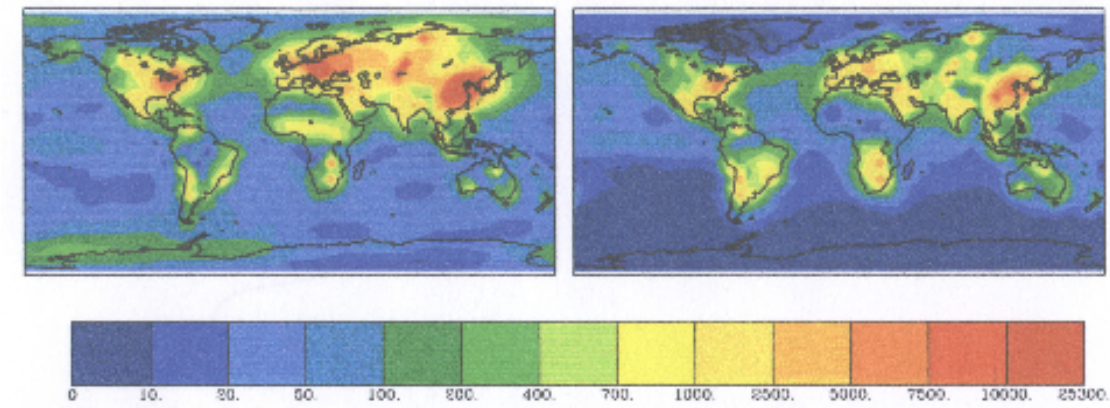

Figure 1.6: Monthly average SO_2 in ppt at the ground from a model run using the 1996 anthropogenic emission inventory from [*Berglen et al.*, 2004].

the decrease in NO_x emissions from power plants in the northeast United States was around 50% while the decrease in SO_2 emissions was marginal.

Sulfuric acid is also an important precursor to particles in the atmosphere. Extensive research has been conducted to determine the relationship of gaseous sulfuric acid and the formation and growth of new particles [*Eisele and McMurry*, 1997; *Kulmala et al.*, 2004a; *McMurry et al.*, 2005]; however, there are only a modest number of publications reporting gas-phase H_2SO_4 measurements and its trends within the troposphere. Measurement techniques for sulfuric acid in the atmosphere include CIMS and IMR-MS as described in section 1.3.

Published values for gas-phase sulfuric acid within the troposphere are concentrated in remote regions where there is relatively unpolluted air. [*Weber et al.*, 1997] reported daytime concentrations ranging between 10^6 and 10^7 molecules cm^{-3} in Idaho Hills. Higher concentrations of sulfuric acid from 10^7 to 10^8 molecules cm^{-3} were observed in the equatorial regions between Hawaii and Tahiti [*Weber et al.*, 2001]. In

the marine boundary layer, [*Berresheim et al.*, 2002] measured a mean daytime gas-phase sulfuric acid concentration of 1.0 x 10^7 molecules cm^{-3} which was correlated to concurrent measurements of SO_2 and OH. In comparison, sulfuric acid concentrations at a forested site in Finland were determined to have a mean of 2.9 x 10^6 molecules cm^{-3} [*Boy et al.*, 2005]. A mean sulfuric acid concentration was observed at a polluted site in Heidelberg, Germany to be 3.46 x 10^6 molecules cm^{-3} [*Fiedler et al.*, 2005] which is comparable to the clean sites previously stated.

The primary loss mechanism of gas-phase sulfuric acid is scavenging by aerosol particles. Vertical profiles of stratospheric aerosols established sulfuric acid as a primary aerosol component [*Arnold et al.*, 1998]. Sulfuric acid has also been confirmed to be present in particles in the troposphere [*Eisele and McMurry*, 1997; *Kulmala et al.*, 2004b; *McMurry et al.*, 2005]. Within the upper troposphere it has been suggested that homogeneous bimolecular nucleation of H_2SO_4 and H_2O is responsible for observations of new particle formation [*Arnold et al.*, 1997]. Although the mechanism is not completely understood, it is generally acknowledged that sulfuric acid is a crucial species participating in nucleation.

These nucleation events can lead to new particle formation and an increase in the number concentration of aerosol by factors of two to ten [*Stolzenburg et al.*, 2005]. Recently, new particle formation was demonstrated to occur in flow-tube experiments for H_2SO_4 concentrations of 7 x 10^6 molecule cm^{-3} or greater [*Berndt et al.*, 2005]. This concentration is consistent with field observations of new particle formation by nucleation of gas phase species [*McMurry et al.*, 2005; *Weber et al.*, 1999]. Additional mechanisms besides H_2SO_4 and water have been suggested to account for nucleation

events. Most notably ternary nucleation with ammonia, NH_3, has been discussed [*Weber et al.*, 1998]. Laboratory studies have revealed enhanced nucleation rates when NH_3 is present [*Ball et al.*, 1999; *Fiedler et al.*, 2005; *Fleming et al.*, 2006]. This is consistent with model studies of nucleation rates for atmospheric conditions in the H_2SO_4-NH_3 – H_2O system [*Korhonen et al.*, 1999; *Kulmala et al.*, 2002].

1.6 References

Akimoto, H. (2003), Global air quality and pollution, *Science*, *302*(5651), 1716-1719.

Arnold, F., J. Schneider, K. Gollinger, H. Schlager, P. Schulte, D. E. Hagen, P. D. Whitefield, and P. vanVelthoven (1997), Observation of upper tropospheric sulfur dioxide- and acetone-pollution: Potential implications for hydroxyl radical and aerosol formation, *Geophysical Research Letters*, *24*(1), 57-60.

Arnold, F., J. Curtius, S. Spreng, and T. Deshler (1998), Stratospheric aerosol sulfuric acid: First direct in situ measurements using a novel balloon-based mass spectrometer apparatus, *Journal of Atmospheric Chemistry*, *30*(1), 3-10.

Ball, S. M., D. R. Hanson, F. L. Eisele, and P. H. McMurry (1999), Laboratory studies of particle nucleation: Initial results for H2SO4, H2O, and NH3 vapors, *Journal of Geophysical Research-Atmospheres*, *104*(D19), 23709-23718

Berglen, T. F., T. K. Berntsen, I. S. A. Isaksen, and J. K. Sundet (2004), A global model of the coupled sulfur/oxidant chemistry in the troposphere: The sulfur cycle, *Journal of Geophysical Research-Atmospheres*, *109*(D19), 27.

Berndt, T., O. Boge, F. Stratmann, J. Heintzenberg, and M. Kulmala (2005), Rapid formation of sulfuric acid particles at near-atmospheric conditions, *Science*, *307*(5710), 698-700.

Berresheim, H., T. Elste, H. G. Tremmel, A. G. Allen, H. C. Hansson, K. Rosman, M. Dal Maso, J. M. Makela, M. Kulmala, and C. D. O'Dowd (2002), Gas-aerosol relationships of H2SO4, MSA, and OH: Observations in the coastal marine boundary layer at Mace Head, Ireland, *Journal of Geophysical Research-Atmospheres*, *107*(D19), 12.

Boy, M., M. Kulmala, T. M. Ruuskanen, M. Pihlatie, A. Reissell, P. P. Aalto, P. Keronen, M. Dal Maso, H. Hellen, H. Hakola, R. Jansson, M. Hanke, and F. Arnold (2005), Sulphuric acid closure and contribution to nucleation mode particle growth, *Atmospheric Chemistry and Physics*, *5*, 863-878.

Brasseur, G. P., J. J. Orlando, and G. S. Tyndall (1999), *Atmospheric Chemistry and Global Change*, Oxford University Press, New York.

Brauers, T., U. Aschmutat, U. Brandenburger, H. P. Dorn, M. Hausmann, M. Hessling, A. Hofzumahaus, F. Holland, C. PlassDulmer, and D. H. Ehhalt (1996), Intercomparison of tropospheric OH radical measurements by multiple folded long-path laser absorption and laser induced fluorescence, *Geophysical Research Letters*, *23*(18), 2545-2548.

Brauers, T., M. Hausmann, A. Bister, A. Kraus, H. P. Dorn, and Qz (2001), OH radicals in the boundary layer of the Atlantic Ocean 1. Measurements by long-path laser absorption spectroscopy, *Journal of Geophysical Research-Atmospheres*, *106*(D7), 7399-7414.

Brock, C. A., M. Trainer, T. B. Ryerson, J. A. Neuman, D. D. Parrish, J. S. Holloway, D. K. Nicks, G. J. Frost, G. Hubler, F. C. Fehsenfeld, J. C. Wilson, J. M. Reeves, B. G. Lafleur, H. Hilbert, E. L. Atlas, S. G. Donnelly, S. M. Schauffler, V. R. Stroud, and C. Wiedinmyer (2003), Particle growth in urban and industrial plumes in Texas, *Journal of Geophysical Research-Atmospheres*, *108*(D3).

Brune, W., H. Harder, M. Martinez, I. Faloona, D. Tan, J. B. Simpas, R. Lesher, L. Jeagle, D. Jacob, and J. Crawford (2002), Global atmospheric oxidation chemistry: What are measurements telling us?, *Abstracts of Papers of the American Chemical Society*, *224*, U300-U300.

Brune, W. H., P. S. Stevens, and J. H. Mather (1995), MEASURING OH AND HO2 IN THE TROPOSPHERE BY LASER-INDUCED FLUORESCENCE AT LOW-PRESSURE, *Journal of the Atmospheric Sciences*, *52*(19), 3328-3336.

Cantrell, C. A., G. D. Edwards, S. Stephens, R. L. Mauldin, M. A. Zondlo, E. Kosciuch, F. L. Eisele, R. E. Shetter, B. L. Lefer, S. Hall, F. Flocke, A. Weinheimer, A. Fried, E. Apel, Y. Kondo, D. R. Blake, N. J. Blake, I. J. Simpson, A. R. Bandy, D. C. Thornton, B. G. Heikes, H. B. Singh, W. H. Brune, H. Harder, M. Martinez, D. J. Jacob, M. A. Avery, J. D. Barrick, G. W. Sachse, J. R. Olson, J. H. Crawford, and A. D. Clarke (2003a), Peroxy radical behavior during the Transport and Chemical Evolution over the Pacific (TRACE-P) campaign as measured aboard the NASA P-3B aircraft, *Journal of Geophysical Research-Atmospheres*, *108*(D20), 21.

Cantrell, C. A., G. D. Edwards, S. Stephens, R. L. Mauldin, M. A. Zondlo, E. Kosciuch, F. L. Eisele, R. E. Shetter, B. L. Lefer, S. Hall, F. Flocke, A. Weinheimer, A. Fried, E. Apel, Y. Kondo, D. R. Blake, N. J. Blake, I. J. Simpson, A. R. Bandy, D. C. Thornton, B. G. Heikes, H. B. Singh, W. H. Brune, H. Harder, M. Martinez, D. J. Jacob, M. A. Avery, J. D. Barrick, G. W. Sachse, J. R. Olson, J. H. Crawford, and A. D. Clarke (2003b), Peroxy radical behavior during the Transport and Chemical Evolution over the Pacific (TRACE-P) campaign as measured aboard the NASA P-3B aircraft, *Journal of Geophysical Research-Atmospheres*, *108*(D20).

Cardelino, C. A., and W. L. Chameides (1990), NATURAL HYDROCARBONS, URBANIZATION, AND URBAN OZONE, *Journal of Geophysical Research-Atmospheres*, *95*(D9), 13971-13979.

Carlier, P., H. Hannachi, and G. Mouvier (1986), THE CHEMISTRY OF CARBONYL-COMPOUNDS IN THE ATMOSPHERE - A REVIEW, *Atmospheric Environment*, *20*(11), 2079-2099.

Chen, G., D. Davis, J. Crawford, L. M. Hutterli, L. G. Huey, D. Slusher, L. Mauldin, F. Eisele, D. Tanner, J. Dibb, M. Buhr, J. McConnell, B. Lefer, R. Shetter, D. Blake, C. H. Song, K. Lombardi, and J. Arnoldy (2004), A reassessment of HOx South Pole chemistry based on observations recorded during ISCAT 2000., *Atmospheric Environment*, *38*, 5451-5461.

Cohan, D. S., J. W. Boylan, A. Marmur, and M. N. Khan (2007), An integrated framework for multipollutant air quality management and its application in georgia, *Environmental Management*, *40*(4), 545-554.

Crutzen, P. J., M. G. Lawrence, and U. Poschl (1999), On the background photochemistry of tropospheric ozone, *Tellus Series a-Dynamic Meteorology and Oceanography*, *51*(1), 123-146.

Davis, D., G. Grodzinsky, G. Chen, J. Crawford, F. Eisele, L. Mauldin, D. Tanner, C. Cantrell, W. Brune, D. Tan, I. Faloona, B. Ridley, D. Montzka, J. Walega, F. Grahek, S. Sandholm, G. Sachse, S. Vay, B. Anderson, M. Avery, B. Heikes, J. Snow, D. O'Sullivan, R. Shetter, B. Lefer, D. Blake, N. Blake, M. Carroll, and Y. Wang (2001), Marine latitude/altitude OH distributions: Comparison of Pacific Ocean observations with models, *Journal of Geophysical Research-Atmospheres*, *106*(D23), 32691-32707.

Deserves, C. (1994), GAS-PHASE FORMALDEHYDE AND PEROXIDE MEASUREMENTS IN THE ARCTIC ATMOSPHERE, *Journal of Geophysical Research-Atmospheres*, *99*(D12), 25391-25398.

Dorn, H. P., U. Brandenburger, T. Brauers, and H. Hausmann (1995), A NEW IN-SITU LASER LONG-PATH ABSORPTION INSTRUMENT FOR THE MEASUREMENT OF TROPOSPHERIC OH RADICALS, *Journal of the Atmospheric Sciences*, *52*(19), 3373-3380.

Edwards, G. D., C. A. Cantrell, S. Stephens, B. Hill, O. Goyea, R. E. Shetter, R. L. Mauldin, E. Kosciuch, D. J. Tanner, and F. L. Eisele (2003), Chemical ionization mass spectrometer instrument for the measurement of tropospheric HO2 and RO2, *Analytical Chemistry*, *75*(20), 5317-5327.

Eisele, F. L., G. H. Mount, F. C. Fehsenfeld, J. Harder, E. Marovich, D. D. Parrish, J. Roberts, and M. Trainer (1994), INTERCOMPARISON OF TROPOSPHERIC OH AND ANCILLARY TRACE GAS MEASUREMENTS AT FRITZ-PEAK-OBSERVATORY, COLORADO, *Journal of Geophysical Research-Atmospheres*, *99*(D9), 18605-18626.

Eisele, F. L., and P. H. McMurry (1997), Recent progress in understanding particle nucleation and growth, *Philosophical Transactions of the Royal Society of London Series B-Biological Sciences*, *352*(1350), 191-200.

EPA (2002), Air Quality Trends Summary Report, edited by E. P. Agency, Washington DC.

Faloona, I., D. Tan, W. Brune, J. Hurst, D. Barket, T. L. Couch, P. Shepson, E. Apel, D. Riemer, T. Thornberry, M. A. Carroll, S. Sillman, G. J. Keeler, J. Sagady, D. Hooper, and K. Paterson (2001), Nighttime observations of anomalously high levels of hydroxyl radicals above a deciduous forest canopy, *Journal of Geophysical Research-Atmospheres*, *106*(D20), 24315-24333.

Fast, J. D., and S. Y. Zhong (1998), Meteorological factors associated with inhomogeneous ozone concentrations within the Mexico City basin, *Journal of Geophysical Research-Atmospheres*, *103*(D15), 18927-18946.

Fiedler, V., M. Dal Maso, M. Boy, H. Aufmhoff, J. Hoffmann, T. Schuck, W. Birmili, M. Hanke, J. Uecker, F. Arnold, and M. Kulmala (2005), The contribution of sulphuric acid to atmospheric particle formation and growth: a comparison between boundary layers in Northern and Central Europe, *Atmospheric Chemistry and Physics*, *5*, 1773-1785.

Finlayson-Pitts, B., and J. Pitts (2000), *Chemistry of Upper and Lower Atmosphere*, 1st ed., Academic Press, San Diego.

Fleming, Z. L., P. S. Monks, A. R. Rickard, D. E. Heard, W. J. Bloss, P. W. Seakins, T. J. Still, R. Sommariva, M. J. Pilling, R. Morgan, T. J. Green, N. Brough, G. P. Mills, S. A. Penkett, A. C. Lewis, J. D. Lee, A. Saiz-Lopez, and J. M. C. Plane (2006), Peroxy radical chemistry and the control of ozone photochemistry at Mace Head, Ireland during the summer of 2002, *Atmospheric Chemistry and Physics*, *6*, 2193-2214.

Frost, G. J., S. A. McKeen, M. Trainer, T. B. Ryerson, J. A. Neuman, J. M. Roberts, A. Swanson, J. S. Holloway, D. T. Sueper, T. Fortin, D. D. Parrish, F. C. Fehsenfeld, F. Flocke, S. E. Peckham, G. A. Grell, D. Kowal, J. Cartwright, N. Auerbach, and T. Habermann (2006), Effects of changing power plant NOx emissions on ozone in the eastern United States: Proof of concept, *Journal of Geophysical Research-Atmospheres*, *111*(D12), 19.

George, L. A., T. M. Hard, R. J. O'Brien, and Pz (1999), Measurement of free radicals OH and HO2 in Los Angeles smog, *Journal of Geophysical Research-Atmospheres*, *104*(D9), 11643-11655.

Geyer, A., K. Bachmann, A. Hofzumahaus, F. Holland, S. Konrad, T. Klupfel, H. W. Patz, D. Perner, D. Mihelcic, H. J. Schafer, A. Volz-Thomas, and U. Platt (2003), Nighttime formation of peroxy and hydroxyl radicals during the BERLIOZ campaign: Observations and modeling studies, *Journal of Geophysical Research-Atmospheres*, *108*(D4), 16.

Guttikunda, S. K., Y. H. Tang, G. R. Carmichael, G. Kurata, L. Pan, D. G. Streets, J. H. Woo, N. Thongboonchoo, and A. Fried (2005), Impacts of Asian megacity emissions on regional air quality during spring 2001, *Journal of Geophysical Research-Atmospheres*, *110*(D20), 27.

Hanke, M., J. Uecker, T. Reiner, and F. Arnold (2002), Atmospheric peroxy radicals: ROXMAS, a new mass-spectrometric methodology for speciated measurements of HO2 and Sigma RO2 and first results, *International Journal of Mass Spectrometry*, *213*(2-3), 91-99.

Hard, T. M., R. J. Obrien, C. Y. Chan, and A. A. Mehrabzadeh (1984), TROPOSPHERIC FREE-RADICAL DETERMINATION BY FAGE, *Environmental Science & Technology*, *18*(10), 768-777

Heikes, B., B. McCully, X. Zhou, Y. N. Lee, K. Mopper, X. Chen, G. Mackay, D. Karecki, H. Schiff, T. Campos, and E. Atlas (1996), Formaldehyde methods comparison in the remote lower troposphere during the Mauna Loa photochemistry experiment 2, *Journal of Geophysical Research-Atmospheres*, *101*(D9), 14741-14755.

Hofzumahaus, A., H. P. Dorn, J. Callies, U. Platt, D. H. Ehhalt, and Fv (1991), TROPOSPHERIC OH CONCENTRATION MEASUREMENTS BY LASER LONG-PATH ABSORPTION-SPECTROSCOPY, *Atmospheric Environment Part a-General Topics*, *25*(9), 2017-2022.

Hutterli, M., R. Rothlisberger, and R. C. Bales (1999), Atmopshere-to-snow-to-firn transfer studies of HCHO at Summit, Greenland, *Geophys. Res. Lett.*(26), 1691-1694.

IPCC (2001), *Climate Change 2001: The Scientific Basis. Contribution of Working Group I to the Thrid Assessment Report of the Intergovermental Panel on Climate Change*, Cambridge University Press, Cambridge, United Kingdom.

Jacob, D. (1999), *Introduction to Atmospheric Chemistry*, Princeton University Press, Princeton.

Jacob, D. J., B. G. Heikes, S. M. Fan, J. A. Logan, D. L. Mauzerall, J. D. Bradshaw, H. B. Singh, G. L. Gregory, R. W. Talbot, D. R. Blake, and G. W. Sachse (1996), Origin of ozone and NOx in the tropical troposphere: A photochemical analysis of aircraft observations over the South Atlantic basin, *Journal of Geophysical Research-Atmospheres*, *101*(D19), 24235-24250.

Jaegle, L., D. J. Jacob, W. H. Brune, I. Faloona, D. Tan, B. G. Heikes, Y. Kondo, G. W. Sachse, B. Anderson, G. L. Gregory, H. B. Singh, R. Pueschel, G. Ferry, D. R. Blake, and R. E. Shetter (2000), Photochemistry of HOx in the upper troposphere at northern midlatitudes, *Journal of Geophysical Research-Atmospheres*, *105*(D3), 3877-3892.

Jenkin, M. E., K. C. Clemitshaw, and El (2000), Ozone and other secondary photochemical pollutants: chemical processes governing their formation in the planetary boundary layer, *Atmospheric Environment*, *34*(16), 2499-2527.

Kanaya, Y., Y. Sadanaga, J. Hirokawa, Y. Kajii, and H. Akimoto (2001), Development of a ground-based LIF instrument for measuring HOx radicals: Instrumentation and calibrations, *Journal of Atmospheric Chemistry*, *38*(1), 73-110.

Kanaya, Y., and H. Akimoto (2002), Direct measurements of HOx radicals in the marine boundary layer: Testing the current tropospheric chemistry mechanism, *Chemical Record*, *2*(3), 199-211.

Kanaya, Y. G., R. Q. Cao, S. G. Kato, Y. K. Miyakawa, Y. Kajii, H. Tanimoto, Y. Yokouchi, M. Mochida, K. Kawamura, and H. Akimoto (2007), Chemistry of OH and HO2 radicals observed at Rishiri Island, Japan, in September 2003: Missing daytime sink of HO2 and positive nighttime correlations with monoterpenes, *Journal of Geophysical Research-Atmospheres*, *112*(D11), 17.

Kleinman, L. I., P. H. Daum, J. H. Lee, Y. N. Lee, L. J. Nunnermacker, S. R. Springston, L. Newman, J. WeinsteinLloyd, and S. Sillman (1997), Dependence of ozone production on NO and hydrocarbons in the troposphere, *Geophysical Research Letters*, *24*(18), 2299-2302.

Kleinman, L. I., P. H. Daum, Y. N. Lee, L. J. Nunnermacker, S. R. Springston, J. Weinstein-Lloyd, and J. Rudolph (2002), Ozone production efficiency in an urban area, *Journal of Geophysical Research-Atmospheres*, *107*(D23), 12.

Kleinman, L. I. (2005), The dependence of tropospheric ozone production rate on ozone precursors, *Atmospheric Environment*, *39*(3), 575-586.

Korhonen, P., M. Kulmala, A. Laaksonen, Y. Viisanen, R. McGraw, and J. H. Seinfeld (1999), Ternary nucleation of H2SO4, NH3, and H2O in the atmosphere, *Journal of Geophysical Research-Atmospheres*, *104*(D21), 26349-26353.

Kulmala, M., P. Korhonen, I. Napari, A. Karlsson, H. Berresheim, and C. D. O'Dowd (2002), Aerosol formation during PARFORCE: Ternary nucleation of H2SO4, NH3, and H2O, *Journal of Geophysical Research-Atmospheres*, *107*(D19), 11.

Kulmala, M., V. M. Kerminen, T. Anttila, A. Laaksonen, and C. D. O'Dowd (2004a), Organic aerosol formation via sulphate cluster activation, *Journal of Geophysical Research-Atmospheres*, *109*(D4), 7.

Kulmala, M., H. Vehkamaki, T. Petajda, M. Dal Maso, A. Lauri, V. M. Kerminen, W. Birmili, and P. H. McMurry (2004b), Formation and growth rates of ultrafine atmospheric particles: a review of observations, *Journal of Aerosol Science*, *35*(2), 143-176.

Lee, Y. N., and X. L. Zhou (1993), METHOD FOR THE DETERMINATION OF SOME SOLUBLE ATMOSPHERIC CARBONYL-COMPOUNDS, *Environmental Science & Technology*, *27*(4), 749-756.

Mackay, G. I., D. R. Karecki, and H. I. Schiff (1996), Tunable diode laser absorption measurements of H2O2 and HCHO during the Mauna Loa observatory photochemistry experiment, *Journal of Geophysical Research-Atmospheres*, *101*(D9), 14721-14728.

Mauldin, R. L., D. J. Tanner, and F. L. Eisele (1999), Measurements of OH during PEM-Tropics A, *Journal of Geophysical Research-Atmospheres*, *104*(D5), 5817-5827.

McKeen, S. A., G. Mount, F. Eisele, E. Williams, J. Harder, P. Goldan, W. Kuster, S. C. Liu, K. Baumann, D. Tanner, A. Fried, S. Sewell, C. Cantrell, and R. Shetter (1997), Photochemical modeling of hydroxyl and its relationship to other species during the Tropospheric OH Photochemistry Experiment, *Journal of Geophysical Research-Atmospheres*, *102*(D5), 6467-6493

McMurry, P. H., M. Fink, H. Sakurai, M. R. Stolzenburg, R. L. Mauldin, J. Smith, F. Eisele, K. Moore, S. Sjostedt, D. Tanner, L. G. Huey, J. B. Nowak, E. Edgerton, and D. Voisin (2005), A criterion for new particle formation in the sulfur-rich Atlanta atmosphere, *Journal of Geophysical Research-Atmospheres*, *110*(D22), 10.

Olson, J., M. Prather, T. Berntsen, G. Carmichael, R. Chatfield, P. Connell, R. Derwent, L. Horowitz, S. X. Jin, M. Kanakidou, P. Kasibhatla, R. Kotamarthi, M. Kuhn, K. Law, J. Penner, L. Perliski, S. Sillman, F. Stordal, A. Thompson, and O. Wild (1997), Results from the Intergovernmental Panel on Climatic Change Photochemical Model Intercomparison (PhotoComp), *Journal of Geophysical Research-Atmospheres*, *102*(D5), 5979-5991.

Platt, U., G. Lebras, G. Poulet, J. P. Burrows, and G. Moortgat (1990), PEROXY-RADICALS FROM NIGHTTIME REACTION OF NO3 WITH ORGANIC-COMPOUNDS, *Nature*, *348*(6297), 147-149

Reiner, T., M. Hanke, and F. Arnold (1997), Atmospheric peroxy radical measurements by ion molecule reaction mass spectrometry: A novel analytical method using amplifying chemical conversion to sulfuric acid, *Journal of Geophysical Research-Atmospheres*, *102*(D1), 1311-1326.

Reiner, T., M. Hanke, and F. Arnold (1998), Aircraft-borne measurements of peroxy radicals in the middle troposphere, *Geophysical Research Letters*, *25*(1), 47-50.

Reiner, T., M. Hanke, F. Arnold, H. Ziereis, H. Schlager, and W. Junkerman (1999), Aircraft-borne measurements of peroxy radicals by chemical conversion/ion molecule reaction mass spectrometry: Calibration, diagnostics, and results, *Journal of Geophysical Research-Atmospheres*, *104*(D15), 18647-18659.

Ren, X. R., G. D. Edwards, C. A. Cantrell, R. L. Lesher, A. R. Metcalf, T. Shirley, and W. H. Brune (2003), Intercomparison of peroxy radical measurements at a rural site using laser-induced fluorescence and Peroxy Radical Chemical Ionization

Mass Spectrometer (PerCIMS) techniques, *Journal of Geophysical Research-Atmospheres*, *108*(D19), 9.

Ren, X. R., W. H. Brune, A. Oliger, A. R. Metcalf, J. B. Simpas, T. Shirley, J. J. Schwab, C. H. Bai, U. Roychowdhury, Y. Q. Li, C. X. Cai, K. L. Demerjian, Y. He, X. L. Zhou, H. L. Gao, and J. Hou (2006), OH, HO2, and OH reactivity during the PMTACS-NY Whiteface Mountain 2002 campaign: Observations and model comparison, *Journal of Geophysical Research-Atmospheres*, *111*(D10), 12.

Roth, P. M., S. D. Reynolds, and T. W. Tesche (2005), Air quality modeling and decisions for ozone reduction strategies, *Journal of the Air & Waste Management Association*, *55*(10), 1558-1573.

Schlosser, E., B. Bohn, T. Brauers, H. P. Dorn, H. Fuchs, R. Haseler, A. Hofzumahaus, F. Holland, F. Rohrer, L. O. Rupp, M. Siese, R. Tillmann, and A. Wahner (2007), Intercomparison of two hydroxyl radical measurement techniques at the atmosphere simulation chamber SAPHIR, *Journal of Atmospheric Chemistry*, *56*(2), 187-205.

Sillman, S., J. A. Logan, and S. C. Wofsy (1990), THE SENSITIVITY OF OZONE TO NITROGEN-OXIDES AND HYDROCARBONS IN REGIONAL OZONE EPISODES, *Journal of Geophysical Research-Atmospheres*, *95*(D2), 1837-1851.

Sillman, S., K. I. Alwali, F. J. Marsik, P. Nowacki, P. J. Samson, M. O. Rodgers, L. J. Garland, J. E. Martinez, C. Stoneking, R. Imhoff, J. H. Lee, L. Newman, J. Weinsteinlloyd, and V. P. Aneja (1995), PHOTOCHEMISTRY OF OZONE FORMATION IN ATLANTA, GA - MODELS AND MEASUREMENTS, *Atmospheric Environment*, *29*(21), 3055-3066.

Sillman, S., D. Y. He, C. Cardelino, and R. E. Imhoff (1997), The use of photochemical indicators to evaluate ozone-NOx-hydrocarbon sensitivity: Case studies from Atlanta, New York, and Los Angeles, *Journal of the Air & Waste Management Association*, *47*(10), 1030-1040.

Sjostedt, S., L. G. Huey, D. J. Tanner, J. Peischl, G. Chen, J. E. Dibb, B. Lefer, M. A. Hutterli, A. J. Beyersdorf, N. J. Blake, D. R. Blake, D. Sueper, T. Ryerson, J. Burkhart, and A. Stohl (2007), Observations of hydroxyl and the sum of peroxy radical at Summit, Greenland during summer 2003, *Atmospheric Environment*, *41*, 5122-5137.

Smith, G. D., L. T. Molina, and M. J. Molina (2002), Measurement of radical quantum yields from formaldehyde photolysis between 269 and 339 nm, *J Phys Chem A*, *106*(7), 1233-1240.

Stecher, H. A., G. W. Luther, D. L. MacTaggart, S. O. Farwell, D. R. Crosley, W. D. Dorko, P. D. Goldan, N. Beltz, U. Krischke, W. T. Luke, D. C. Thornton, R. W. Talbot, B. L. Lefer, E. M. Scheuer, R. L. Benner, J. G. Wu, E. S. Saltzman, M. S. Gallagher, and R. J. Ferek (1997), Results of the gas-phase sulfur intercomparison

experiment (GASIE): Overview of experimental setup, results and general conclusions, *Journal of Geophysical Research-Atmospheres*, *102*(D13), 16219-16236.

Stein, A. F., E. Mantilla, and M. M. Millan (2005), Using measured and modeled indicators to assess ozone-NOx-VOC sensitivity in a western Mediterranean coastal environment, *Atmospheric Environment*, *39*(37), 7167-7180.

Stolzenburg, M. R., P. H. McMurry, H. Sakurai, J. N. Smith, R. L. Mauldin, F. L. Eisele, and C. F. Clement (2005), Growth rates of freshly nucleated atmospheric particles in Atlanta, *Journal of Geophysical Research-Atmospheres*, *110*(D22), 10.

Stone, B. (2005), Urban heat and air pollution - An emerging role for planners in the climate change debate, *Journal of the American Planning Association*, *71*(1), 13-25.

Sumner, A. L., and P. B. Shepson (1999), Snowpack production of formaldehyde and its effect on the Arctic troposphere, *Nature*, *398*(6724), 230-233.

Tanner, D. J., A. Jefferson, and F. L. Eisele (1997), Selected ion chemical ionization mass spectrometric measurement of OH, *Journal of Geophysical Research-Atmospheres*, *102*(D5), 6415-6425.

Wagner, V., R. von Glasow, H. Fischer, and P. J. Crutzen (2002), Are CH2O measurements in the marine boundary layer suitable for testing the current understanding of CH4 photooxidation?: A model study, *Journal of Geophysical Research-Atmospheres*, *107*(D3), 14.

Weber, R. J., J. J. Marti, P. H. McMurry, F. L. Eisele, D. J. Tanner, and A. Jefferson (1997), Measurements of new particle formation and ultrafine particle growth rates at a clean continental site, *Journal of Geophysical Research-Atmospheres*, *102*(D4), 4375-4385.

Weber, R. J., M. R. Stolzenburg, S. N. Pandis, and P. H. McMurry (1998), Inversion of ultrafine condensation nucleus counter pulse height distributions to obtain nanoparticle (similar to 3-10 nm) size distributions, *Journal of Aerosol Science*, *29*(5-6), 601-615

Weber, R. J., P. H. McMurry, R. L. Mauldin, D. J. Tanner, F. L. Eisele, A. D. Clarke, and V. N. Kapustin (1999), New particle formation in the remote troposphere: A comparison of observations at various sites, *Geophysical Research Letters*, *26*(3), 307-310.

Weber, R. J., G. Chen, D. D. Davis, R. L. Mauldin, D. J. Tanner, F. L. Eisele, A. D. Clarke, D. C. Thornton, and A. R. Bandy (2001a), Measurements of enhanced H2SO4 and 3-4 nm particles near a frontal cloud during the First Aerosol Characterization Experiment (ACE 1), *Journal of Geophysical Research-Atmospheres*, *106*(D20), 24107-24117.

Weber, R. J., K. Moore, V. Kapustin, A. Clarke, R. L. Mauldin, E. Kosciuch, C. Cantrell, F. Eisele, B. Anderson, and L. Thornhill (2001b), Nucleation in the equatorial Pacific during PEM-Tropics B: Enhanced boundary layer H2SO4 with no particle production, *Journal of Geophysical Research-Atmospheres*, *106*(D23), 32767-32776.

Zhou, X. L., and K. Mopper (1990), APPARENT PARTITION-COEFFICIENTS OF 15 CARBONYL-COMPOUNDS BETWEEN AIR AND SEAWATER AND BETWEEN AIR AND FRESH-WATER - IMPLICATIONS FOR AIR SEA EXCHANGE, *Environmental Science & Technology*, *24*(12), 1864-1869.

CHAPTER 2

MEASUREMENT OF FORMALDEHYDE BY LASER-INDUCED FLUORESCENCE

2.1 Summary

The development of a laser-induced fluorescence (LIF) formaldehyde (HCHO) detection instrument capable of measuring parts-per-trillion-by-volume (pptv) levels of formaldehyde in ambient air is presented. This approach employs excitation of the lowest-lying electronic state of formaldehyde along the $A^1A_2 \leftarrow X^1A_1$ transition at 353.16 nm and measurement of fluorescence in the 400-450 nm range. The instrument is capable of sampling air with a signal integration time of 1-minute. The 2-sigma limit of detection is 40 pptv/minute. We have identified no significant chemical interferences for this measurement scheme.

2.2 Laser-Induced Fluorescence Scheme and Instrument Description

The LIF spectroscopic scheme employs excitation of the lowest-lying electronic state of formaldehyde along the $A^1A_2 \leftarrow X^1A_1$ transition at 353.16 nm, as shown in Figure 2.1, with a linewidth of 0.8 cm^{-1}. There are transitions with larger cross-sections at shorter wavelengths (*e.g.*, near 314, 327, and 338 nm); however, the photolytic yield for HCHO at these wavelengths is unity. Since the photolysis quantum yield, Φ, increases with decreasing wavelength and approaches unity below 340nm, the lowest lying electronic absorption band needs to be excited.

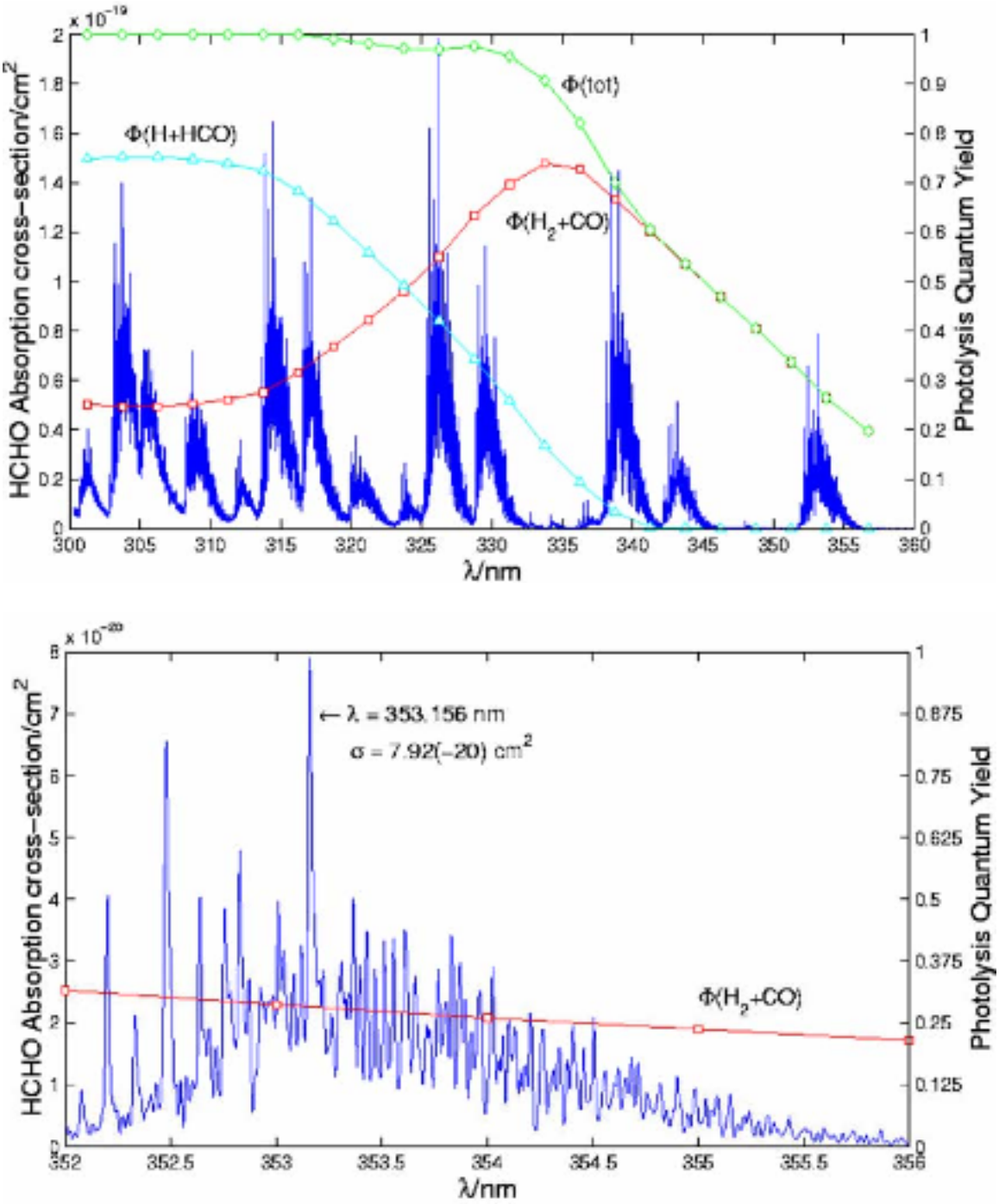

Figure 2.1: (a.) Formaldehyde Absorption Spectrum with photolytic quantum yields for two photolysis pathways and for the total photolytic yield. (b.) The expanded region of interest, 352-356 nm, shows the minimal quantum yield and the excitation line that is used in the LIF-technique and its cross-section.

Even excitation of the A state leads to photodissociation of a fraction of the excited state population:

$$HCHO(S_0) + h\nu \rightarrow HCHO(S_1) \rightarrow HCHO^*(S_0) \rightarrow H_2 + CO \qquad \text{R2.1}$$

Electronically excited formaldehyde relaxes to an in-plane vibrationally hot molecule in the S_0 manifold, a portion of which subsequently dissociates to form molecular hydrogen and carbon monoxide. The excitation wavelength, 353.156 nm, was chosen in order to correspond to the strongest HCHO absorption peak in the region where photolytic decomposition is at a minimum. The estimated photolytic quantum yields for HCHO at this wavelength is 0.28 [*Sander et al.*, 2003].

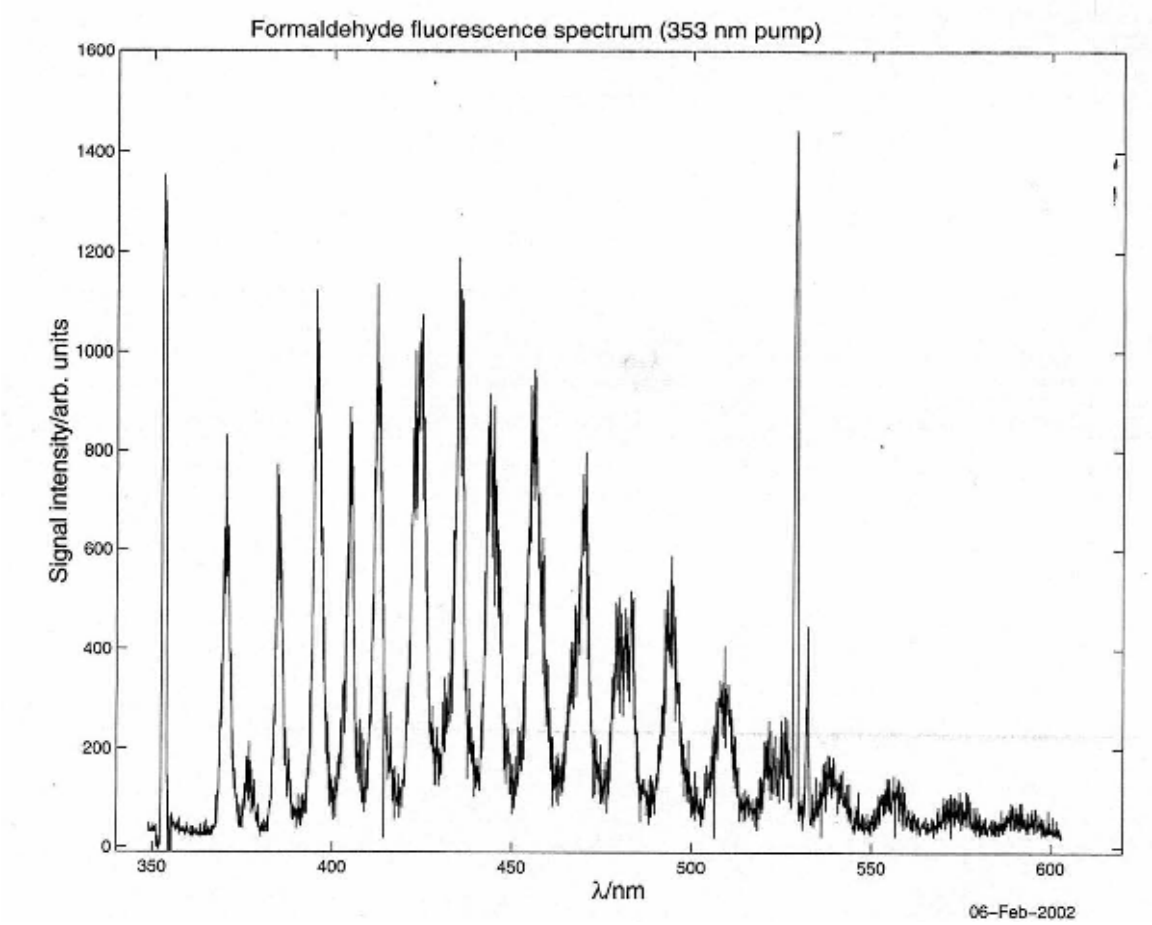

Figure 2.2: Fluorescence spectrum of HCHO in dry nitrogen at atmospheric pressure following excitation from 353.156 nm laser pulse. The peak around 353 nm is leakage probe beam (353.156 nm) and the peak centered about 532 nm is green leakage from the OPOs.

The HCHO fluorescence spectrum following excitation at 353 nm is shown in Figure 2.2. There are a number of strong features in the fluorescence band between 390 and 525 nm. In practice, it was found that monitoring several fluorescence features between 400 and 450 nm gave better signal to noise ratio than monitoring a single strong line (the peak near 435 nm) with a narrow bandpass interference filter.

The formaldehyde instrument is shown in Figure 2.3. The LIF sensor is composed of (1) laser system, (2) ambient sample cell, (3) collection optics, (4) reference cell, (5) data acquisition system and (6) calibration system.

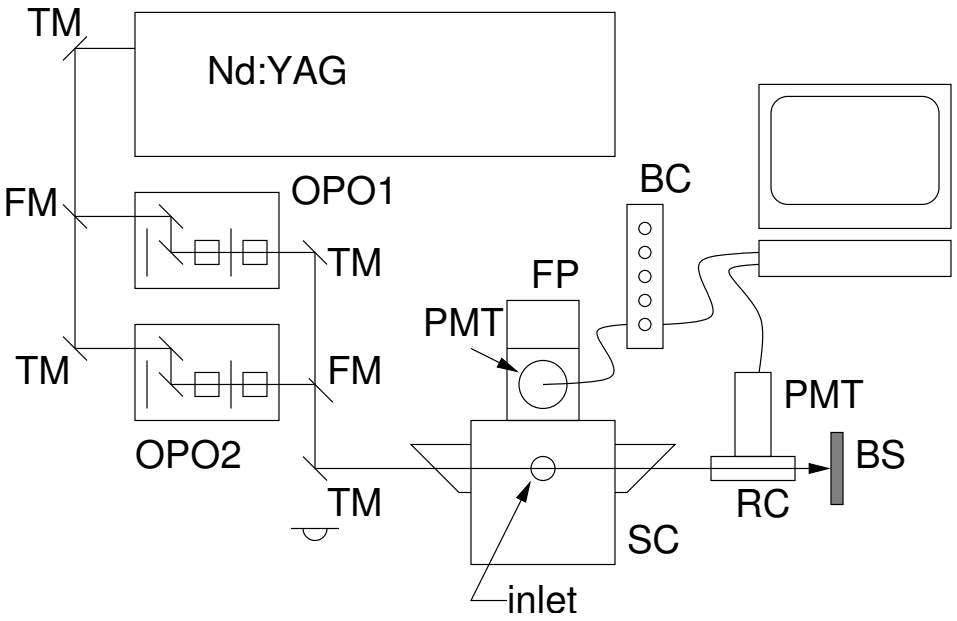

Figure 2.3: General block diagram of experimental set-up for HCHO LIF instrument: TM: turning mirror; FM: New Focus Motorized Flipper (Model 8892-K), toggles in sync for on/offline entrance into sample cell; OPO1 Online OPO generates 353.156 nm; OPO 2: Offline OPO generates 355.57 nm; SC: Sample Cell with Brewster Angle Windows; FP: Filter pack; PMT: R331 PMT (Hamamatsu); BC: Boxcar Averager; RC: Reference Cell; BS: Beam Stop.

Currently, a Spectra Physics 290 Nd:YAG laser operating at 10Hz pulse repetition frequency and homebuilt optical-parametric-oscillators (OPOs) are used to generate the target wavelengths, one for the on-line wavelength and one for the offline. The OPOs are independent optical cavities that convert a high-energy photon at 532 nm into two lower energy photons, a signal photon and an idler photon. Energy is conserved in this process, such that $\omega_{532} = \omega_{signal} + \omega_{idler}$, where $\omega_{signal} > \omega_{idler}$. The OPO cavity, as shown in Figure 2.4, is comprised of a high reflector, an output coupler, a pump mirror that

reflects the 532 nm beam and transmits the ~700 nm signal beam, and a β-barium borate (BBO) nonlinear crystal (U-Oplaz Corporation, Chatsworth, CA) in which the parametric oscillation takes place. The output coupler doubles as a retroreflector for the 532 nm pump beam: this "double-pass" arrangement enables low beam divergence, excellent mode structure, and a relatively narrow linewidth of ~0.5 cm^{-1} without the use of intracavity line narrowing elements in a compact (~15 cm) and very simple cavity. This in turn provides good conversion efficiencies from the pump to the signal and for frequency doubling of the signal. Narrower linewidths down to 0.11 cm^{-1} have been achieved using an intracavity etalon operating on the idler beam; however, the etalon also introduced a frequency jitter, probably from increased sensitivity to thermal fluctuations which were not sufficiently controlled in this version of the instrument. The data presented here were taken with etalon-free cavities. The OPO has a conversion efficiency of 24% to the signal beam: 250 mJ of the 2nd harmonic of the Nd:YAG laser at 532 nm are used to pump each OPO, generating about 60 mJ of signal output (706 nm for online and 711 nm for offline). The signal beam is then frequency doubled via a second BBO crystal external to the cavity to generate 10 mJ of the target online/offline wavelengths, 353.156 nm/355.76 nm, respectively. A Burleigh 4500 wavemeter (Burleigh Instruments, Victor, NY) is used to determine the wavelengths of the OPO outputs. By toggling between these two wavelengths, and comparing the fluorescence intensity of the on/offline conditions, the concentration of HCHO can be determined.

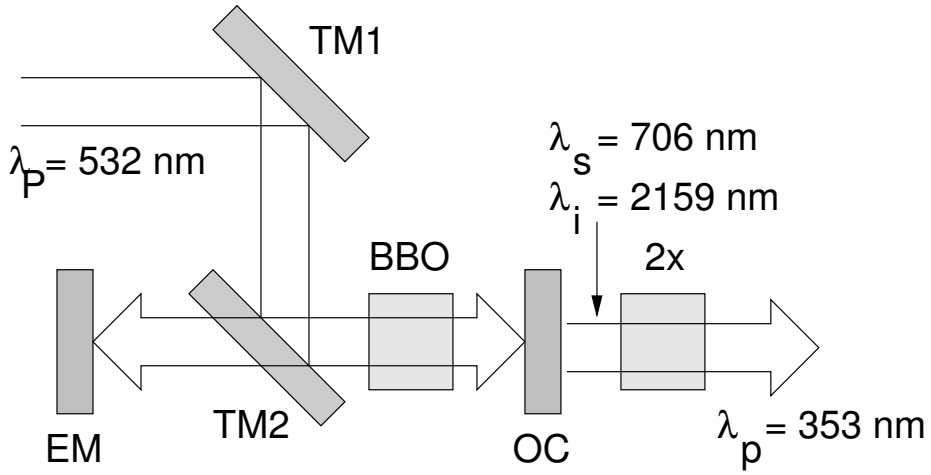

Figure 2.4: Diagram of Optical Parametric Oscillators includes turning mirrors (TM), end mirror (EM), output coupler (OC), BBO crystal (BBO), doubling crystal (2x). The signal (λ_s) and idler (λ_i) produced by the OPO is 706 nm and 2159 nm, respectively. The signal is frequency doubled to produce the 353 nm probe beam (λ_p).

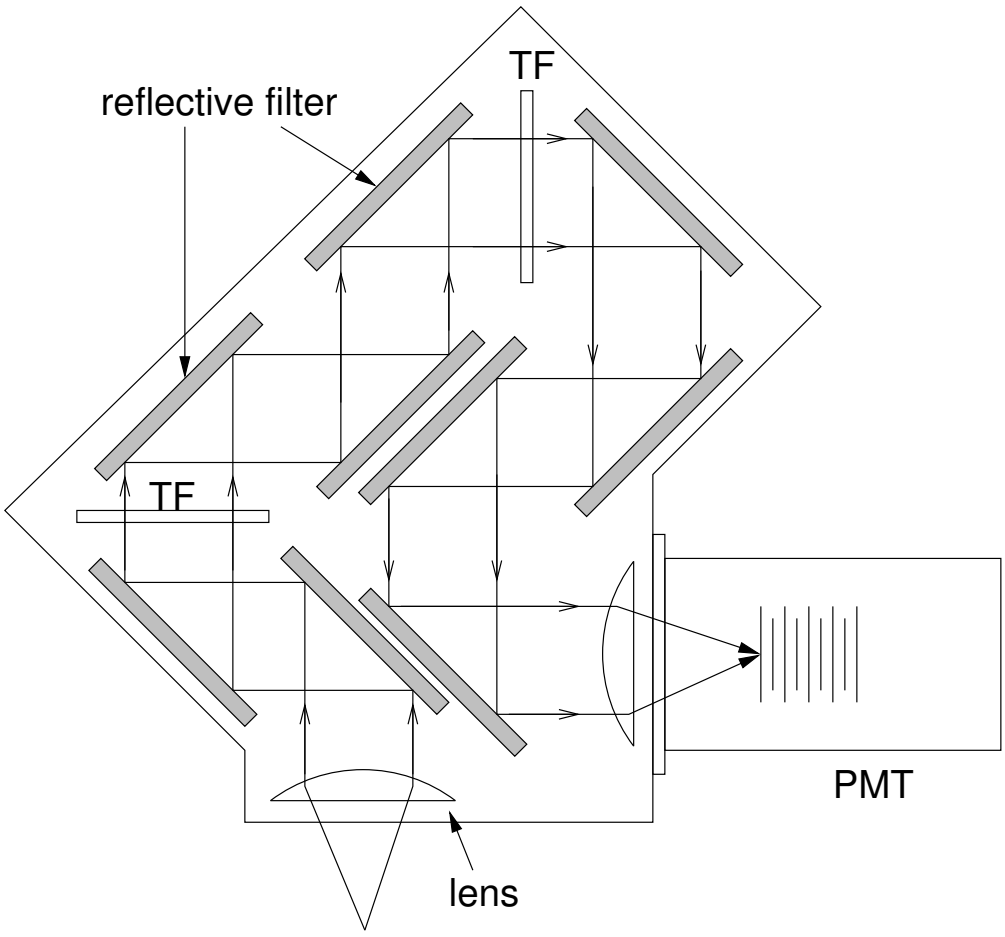

Figure 2.5: Schematic of Filter pack, contains 9 reflective dichroics with a bandwidth of 400-450 nm, 2 transmission filters, and 2 2-inch focal length collimating lens. PMT: Photomultiplier Tube; TF: The lines with arrows indicate the direction of light travel.

Air is drawn into the sample cell at ambient pressure at ~20 standard liters per minute (slpm). The sample is probed by the UV radiation at right angles to the flow. The UV probe beam enters the sample cell through Brewster's angle windows held at 7 inches from the sample volume to minimize the laser scatter contribution to the background signal. The fluorescence is detected at right angles to both the main flow and the probe beam. The internal volume of the cell is ~20 L, resulting in a residence time of 1 minute. The large internal volume arises from the need to minimize wall fluorescence (see below), but puts a lower limit on the time resolution of the instrument.

Sampling at reduced pressure in a multipass fluorescence cell was found to be impractical with low repetition rate giant pulse lasers because of pulse diameter and linewidth. Low pressure sampling reduces the background from Rayleigh scatter and extends the gas-phase fluorescence lifetime of the analyte; however, the loss in number density is significant and is usually made up for by extending the sample volume by means of a multipass cell, such as a White cell or a Herriott cell. In a White cell, the beam waist is at one of the mirrors; in a Herriott cell, the beam waist is equidistant from the mirrors, in the sampling region. The high peak irradiances of a giant pulse laser (on the order of 400 MW/cm^2 for a 10 mJ pulse and a 0.5 mm spot size) will destroy a White cell mirror and saturate the sample volume in a Herriott cell.

A folded filter pack was constructed to minimize the background signal by filtering out any scattering from the pump wavelength and thereby increase the signal to noise ratio [*Sandholm et al.*, 1997] as illustrated in Figure 2.5. A lens with a focal length of 3 inches collects the fluorescence into the filter pack perpendicular to the axis of the laser beam. The collected light is sent to a series of nine dichroic mirrors (ZC&R Coatings) coated to maximize reflectivity of the HCHO fluorescence wavelengths and to maximize the transmission of the probe wavelengths, which passes through the mirrors and are absorbed by the filter pack housing. A broad bandpass filter further attenuates the probe wavelengths and passes the desired fluorescence. Finally, 2 long-pass filters (Schott Glass Technologies: KV389, KV399) are employed to further reject the laser probe wavelength. The filtered-fluorescence output of the folded filter pack is focused onto a photomultiplier tube (PMT --Hamamatsu R331) with a 3-inch focal length lens.

A number of different spectral filtration schemes have been explored, including filter packs based purely on transmission filters. It was thought that a narrowband filter centered at the strong 435 nm fluorescence feature (Andover Corporation, 436FS05) with a bandwidth of ± 5 nm would help to reject the laser scatter and transmit the strong HCHO fluorescence peaks centered around 435 nm. These features typically have a ~10 nm bandwidth, providing a good match for the interference filter. However, it was found that a broadband transmission filter (70 nm bandwidth centered at 425 nm) in conjunction with a reflective filter pack delivered a better signal to background ratio than a narrowband filter in conjunction with either a reflective filter pack or as part of a transmission filter pack.

The measurement is currently background limited. Extensive testing of the background signal indicates that the background is dominated by what appears to be fluorescence of the cell walls. It was found that by purging the cell with nitrogen, probing with the 355 nm third harmonic from the YAG, and passing the signal through a monochromator, detectable signal occurred from 390 nm to over 500 nm. The red-shifted nature of the signal precludes scattering as the primary contributor to the background; its presence in a cell containing pure N_2 indicates that the signal is fluorescence, which we attribute to the cell walls. The scatter itself is effectively rejected by the filter pack. The sample cell was designed with a large internal volume to minimize the fluorescence background by reducing the background intensity in the detector field of view, although in practice background levels remained high.

The signal from the R331 PMT is taken into a boxcar amplifier (Stanford Research Systems, SR250), here used in single-shot mode as a gated pre-amplifier. It

was found that the cell fluorescence signal damps 15-20 nanoseconds more quickly than does the HCHO fluorescence. Use of the boxcar enabled the temporal rejection of most of the cell fluorescence and amplifies the fluorescence tail. This amplification is not strictly necessary but simplifies data acquisition by minimizing digitization artifacts (it could also be done in the data acquisition program itself). The data acquisition system tracks the signal and holds the signal level after a user-selectable gate. The track and hold system is VXI based and acquires data on up to 12 channels on a single-shot basis (*i.e.* each data point is recorded on a shot-to-shot basis.) There are also 24 analog inputs with 1 Hz acquisition for parameters that do not vary quickly (temperature, *e.g.*)

A reference cell is used to track any wavelength drifts due to temperature variations or other fluctuations in the laser. The reference cell is a small fluorescence cell using a small flow of nitrogen with a high concentration of formaldehyde to generate a strong fluorescence signal. Two narrow band interference filters centered at 435 nm are stacked in front of a Hamamatsu R928 PMT to reject laser scatter. The reference cell fluorescence is sufficiently strong in order not to require time-gating or sophisticated optical filtration. Photodiodes (Thorlabs, DET110) are used to monitor the power of the probe beam wavelengths of the on/offline cavities.

Calibrations for the LIF technique were done in the laboratory by standard addition. The gas-phase HCHO was generated via a bubbler in which dry nitrogen of a constant flow was passed over an aqueous HCHO solution of known concentration. The gas-phase concentration of HCHO was calculated from the aqueous concentration and the Henry's law coefficient ($H_{HCHO} = 2.97 \times 10^3$ M atm^{-1}, [*Betterton*, 1988]). Aqueous

solutions were made from 37% HCHO (Fisher Scientific, lot #023112) and diluted volumetrically with deionized ultra filtered water (Fisher Scientific, lot #034586).

The gas-phase HCHO concentrations derived from the aqueous HCHO solutions were verified at higher concentrations by using the absolute Beer's law absorption measurement. The absorption experiment employed a Cadmium lamp (Pen-Ray Lamp, Light Source 90-0071-03) and 1-meter path length glass cell. Absorption and lamp stability were monitored at the 325.5 nm line ($\sigma_{HCHO}=6.2 \times 10^{-20}$, [*Cantrell et al.*, 1990].

Absorption measurements were obtained for high aqueous concentrations of formaldehyde ranging from 2M to 12M. The data were compared to that of [*Ledbury and Blair*, 1925] and closely resembled their results. A non-linear relationship between the gas- and aqueous-phase concentrations is expected; however, the Beer's Law absorption measurement available to us does not have the sensitivity at low molar concentrations to determine the nonlinearity. [*Dong and Dasgupta*, 1986] explored the equilibrium behavior of HCHO at lower aqueous-phase concentrations (μM HCHO(aq) range). An exponential relationship between the aqueous-phase HCHO concentration and the gas-phase HCHO concentration exists as

$$\left[HCHO_{aq}\right] = 16650\left[HCHO_{g}\right]^{1.0789} \qquad \text{R2.2}$$

Our data are in good agreement with the data obtained by *Ledbury and Blair* [1925] and *Dong and Dasgupta* [1986], verifying the calculations of our gas-phase formaldehyde concentration used for our calibration.

2.3 Results and Discussion

The HCHO LIF sensor will be used to measure trace amounts of atmospheric formaldehyde, in the free troposphere and within the boundary layer. Typical concentrations of HCHO above the snowpack as reported by [*Sumner et al.*, 2002] ranged from 52 pptv to 690 pptv and within the free troposphere are typically 10 to several hundreds of pptv. It is therefore necessary to calibrate the instrument at low concentrations, particularly below 500 pptv. The calibration plot of HCHO in zero air at ambient air pressure is shown in Figure 2.6. This plot shows 1-minute averages and 2-sigma error bars. This gives a limit of detection of 40 pptv/minute. Longer integration times reduce the detection limit by the square root of the detection time.

The quenching effect of oxygen was tested and it was found that a 20% mixing ratio of oxygen and 80% of nitrogen by volume created a 23-25% reduction in signal compared to the signal using pure nitrogen as the carrier gas. Water vapor quenching was not quantified. [*Mohlmann*, 1985] found no noticeable quenching effect due to water vapor with large concentrations of HCHO present within the system.

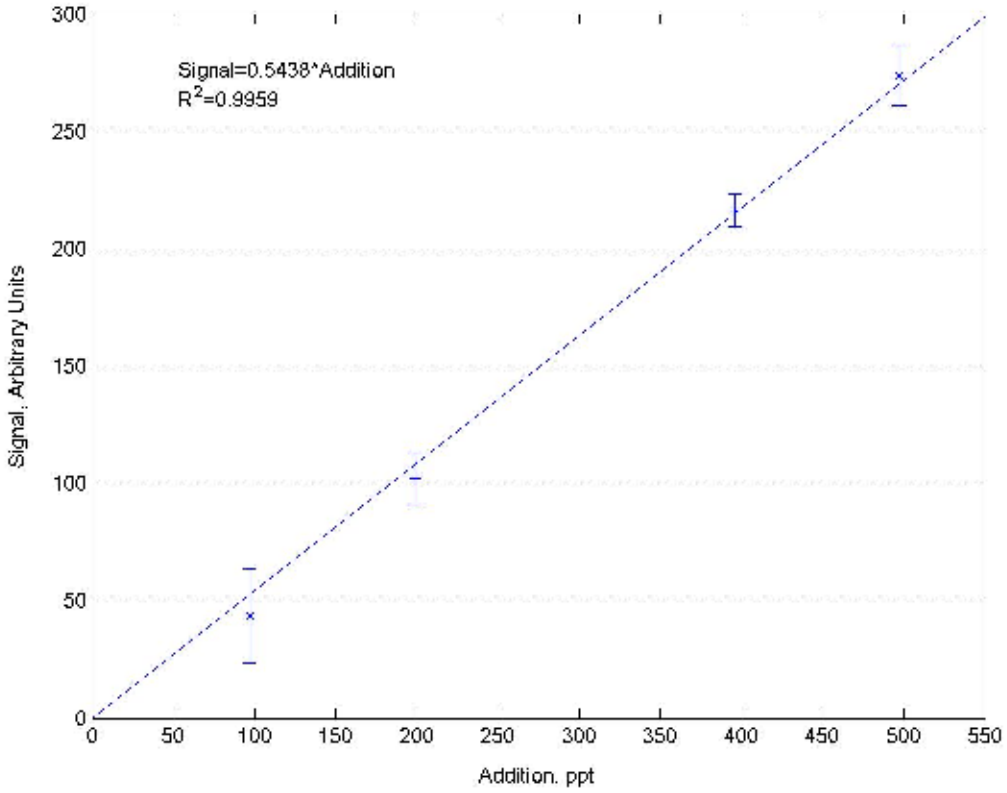

Figure 2.6: HCHO Calibration of LIF sensor. Data points are 1-mintue averages, or 600 shots, with 2-sigma error bars and a best-fit line.

An evaluation of potential chemical interferences was carried out in order to quantify any artifact signal. Table 2.1 presents the species tested and the results in equivalent signal of HCHO. Several species such as NO_2, HONO, BrO, OClO, and other halogen oxides have large absorption cross-sections at 353 nm; however, these species have near-unity photolysis quantum yields [*Sander et al.*, 2003]. With the exception of NO_2 and HONO (in urban areas), the species also have very low mixing ratios in the troposphere. $BrONO_2$ and $ClONO_2$, species present in the marine polar boundary layer, have large cross sections near 353 nm, but these have photolytic quantum yields of unity; these species were not tested and are not expected to interfere.

Table 2.1: Evaluation of Potential Chemical Interferences: Most species with absorption near 353 nm have near unity photolysis yields and do not interfere. 9,10-Diphenylanthracene was used to represent large bulky molecules which may be present in atmosphere

Species	Equivalent signal of HCHO
N_2	--
SO_2	10^{-3}
NO	--
NO_2	10^{-3}
NH_3	--
CH_3I	--
H_2O_2	--
Acetone	--
9,10 -Diphenylanthracene	--

In the planetary boundary layer, there are many hydrocarbon species with concentrations comparable to that of formaldehyde, including isoprene, aldehydes such as acetaldehyde and propanal, lightweight ketones and peroxides. Many of these do not fluoresce and those that do have no absorption features near 353 nm. 9,10-diphenylanthracene (Aldrich, Lot # 06408AB) has a large absorption cross section (~8600 cm^{-1}/M) at 353 nm and a peak in the fluorescence spectrum from 400-450 nm and was used to represent large bulky organic compounds that might absorb and fluoresce in the same region as formaldehyde: it showed no signal interference, presumably because it, like other aromatic hydrocarbons large enough to absorb in the near UV, has negligible vapor pressure. We do not expect a significant interference from large aromatic molecules. In industrialized regions, sulfur dioxide is present in significant mixing ratios. However, sulfur dioxide has a cross-section of 10^{-22} cm^2 [*Finlayson-Pitts and Pitts*, 2000] around 353 nm, which is over two orders magnitude smaller than HCHO at this

wavelength. There is nonetheless a small interference from SO_2 (Scott Marin, JJ20282), equivalent to one part per thousand of HCHO (that is, 1 ppbv SO_2 provides a signal comparable to 1 pptv HCHO). It is conceivable that under certain unusual conditions, such as in the plume of a volcano, SO_2 may be a significant interferant. Anthropogenic outflow is also often marked by elevated levels of SO_2; however, formaldehyde is also usually elevated in such air masses. Under most conditions, SO_2 is not expected to be a significant interferant.

2.4 Futher Development:

A downsized version of this instrument is currently under construction in order to accommodate a greater range of possible field missions and to improve the detection limit. A 5 kHz repetition rate YAG laser (Lightwave Electronics, Q201-HD) will be used to produce a high-repetition rate photon counting system. The YAG will be used to pump a single Ti:sapphire laser using etalon tuning alternately to generate the online and offline wavelengths, a simplification from the 2-cavity system currently in use. A reduced pressure technique also known as FAGE (fluorescence assay with gas expansion) will be employed to reduce the collisional quenching and lengthen the fluorescence lifetime; ultimately scattering such as Rayleigh, Raman, or Mie decreases linearly with pressure, reducing the background [*Hard et al.*, 1984]. These improvements and additional sample cell redesign work (i.e. multipass sample cell) will improve the limit of detection below 40 ppt/minute.

2.5 References

Betterton, E. A., M.R. Hoffman (1988), Henry's law constants of some environmentally important aldehydes, *Environ. Sci. Technol.*, *22*(12), 415-418.

Cantrell, C. A., J. A. Davidson, A. H. McDaniel, R. E. Shetter, and J. G. Calvert (1990), TEMPERATURE-DEPENDENT FORMALDEHYDE CROSS-SECTIONS IN THE NEAR-ULTRAVIOLET SPECTRAL REGION, *Journal of Physical Chemistry*, *94*(10), 3902-3908.

Dong, S., and P. K. Dasgupta (1986), ON THE FORMALDEHYDE-BISULFITE-HYDROXYMETHANE-SULFONATE EQUILIBRIUM, *Atmospheric Environment*, *20*(8).

Finlayson-Pitts, B., and J. Pitts (2000), *Chemistry of Upper and Lower Atmosphere*, 1st ed., Academic Press, San Diego.

Hard, T. M., R. J. Obrien, C. Y. Chan, and A. A. Mehrabzadeh (1984), TROPOSPHERIC FREE-RADICAL DETERMINATION BY FAGE, *Environmental Science & Technology*, *18*(10), 768-777

Ledbury, W., and E. W. Blair (1925), The partial formaldehyde vapour pressures of aqueous solutions of formaldehyde. Part II, *Journal of the Chemical Society*, *127*, 2832-2839 Article The partial formaldehyde vapour pressures of aqueous solutions of formaldehyde. Part II

Mohlmann, G. R. (1985), Formaldehyde detection in air by laser-induced fluorescence, *Applied Spectroscopy*, *39*(1), 98-101.

Sander, S., W. B. DeMore, R. Golden, R. Hanson, M. Kurlyo, C. Howard, A. Ravishankara, C. Kolb, and M. Molina (2003), Chemical Kinetics and Photochemical Data for Use in Stratospheric Modeling, *JPL Publication*.

Sandholm, S., S. Smyth, R. Bai, and J. Bradshaw (1997), Recent and future improvements in two-photon laser-induced fluorescence NO measurement capabilities, *Journal of Geophysical Research, [Atmospheres]*, *102*(D23), 28651-28661.

Sumner, A. L., P. B. Shepson, A. M. Grannas, J. W. Bottenhiem, K. G. Anlauf, D. Worthy, W. H. Schroeder, A. Steffen, F. Domine, S. Perrier, and S. Houdier (2002), Atmopsheric chemistry of formaldehyde in the Arctic troposphere at Polar Sunrise, and the influence of the snowpack, *Atmos. Env.*, *36*, 2553-2562.

CHAPTER 3

DEVELOPMENT OF A NARROW-LINEWIDTH, TUNABLE UV, TI:SAPPHIRE LASER FOR ENVIRONMENTAL SENSING

3.1 Summary

The description of a compact, narrow linewidth, etalon-tuned titanium:sapphire laser cavity designed for field environmental sensing which is pumped by the second harmonic of a kilohertz Nd:YAG laser is presented here. The fundamental tunable range is from 690-1100 nm depending on mirror reflectivities and optics kit used. The conversion efficiency is at least 25% for the fundamental, and 2-3% for intracavity frequency doubling from 3.5-4W 532 nm pump power. The linewidth is < 0.1 cm^{-1}, and the pulsewidth is 18 nsec. Applications of this cavity include the measurement of trace gas species by laser-induced fluorescence, cavity ringdown spectroscopy, and micropulse lidar in the UV-visible region.

3.2 Laser Instruments in Atmospheric Research

Air quality and climate are largely determined by atmospheric composition and chemistry, which in turn are controlled by the concentrations of trace chemical species. For many of these species, laser-induced fluorescence (LIF) has proven to be a sensitive and selective probe of their atmospheric concentrations [*Bradshaw et al.*, 1999; *Wennberg et al.*, 1994]. Such species include OH and HO_2 [*Brune et al.*, 1998], NO and NO_2 [*Bradshaw et al.*, 1999; *Thornton et al.*, 2000], HCHO [*Mohlmann*, 1985], NO_3 [*Wood et al.*, 2003] and atomic Hg [*Rodgers et al.*, 1982]. Cavity ringdown spectroscopy (CRS) has also recently been used to measure NO_3 [*King et al.*, 2000; *Wood et al.*, 2003]

at pptv levels. For each of these, a narrow-linewidth, tunable light source in the visible or ultraviolet is required. Stability and robustness to environmental changes in temperature, pressure, and vibration are also required; a compact size and the capability for extended unattended operation are highly desirable.

Current laser-based instruments used for measuring trace gases use dye lasers and sometimes optical parametric oscillators (OPOs). In fact, a modified version of a two-decade old Chromatix dye laser serves as the basis for many LIF-based field instruments with pptv sensitivity [*Brune et al.*, 1998; *Thornton et al.*, 2000; *Wennberg et al.*, 1994]. Dye lasers are well-established, commercially available, and can access a wide range of wavelengths. Dyes, however, degrade with time (relatively quickly in certain wavelength ranges) and are toxic and require inflammable solvents. OPOs have the advantage of great tunability and have the added benefit of being all solid-state; however, parametric oscillation is a nonlinear process and generally suffers from relatively high oscillation thresholds, thereby limiting its utility.

3.3 Description of Laser Cavity

The laser uses a bent cavity 20 cm in length of the optical axis (Figure 3.1). The gain medium is a titanium sapphire rod 22 mm long and 4 mm in diameter, with end faces cut at Brewster's angle, a Ti_2O_3 dopant concentration of 4%, and an absorption coefficient at 532 nm (α) of 1.29/cm. It is mounted in a water-cooled aluminum jacket. The nominal fundamental tuning range is 690 nm to 1100 nm; the actual tuning range is determined by the reflectivity curves of the end mirror and output coupler used, and a series of appropriately coated mirrors will be needed to access the full gain curve. For LIF

purposes, the output is intracavity frequency doubled and possibly externally mixed, in which case a blue cutoff of 700 nm is more realistic.

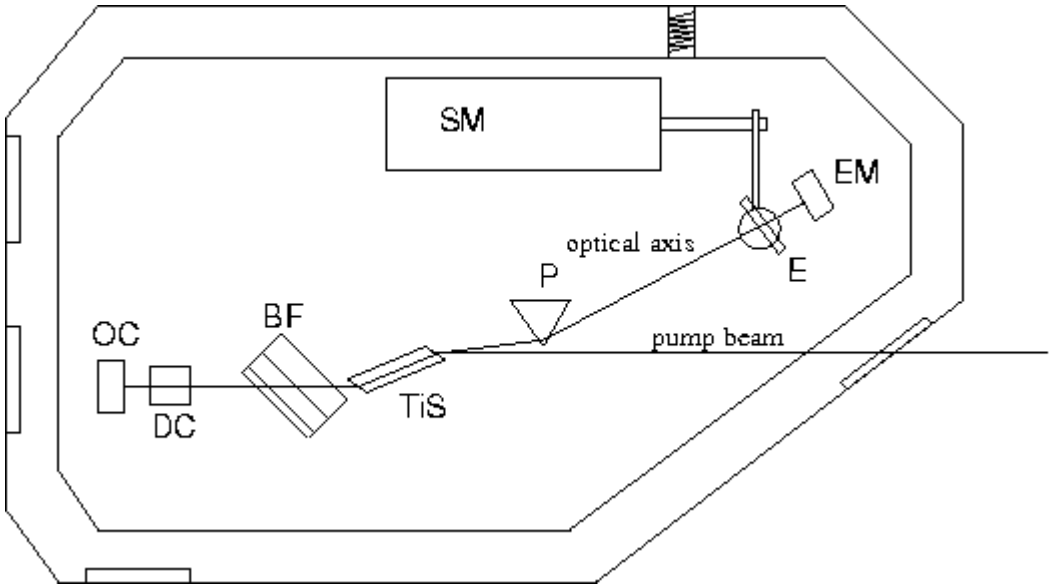

Figure 3.1: The Ti:sapphire cavity configuration includes the OC: Output coupler; EM: End Mirror; BF: Birefringent Filter; Ti:S: Ti:sapphire rod; DC: BBO doubling crystal; P: Isosceles Prism; E: Etalon; SM: Stepper Motor. The optical length of the cavity is 20 cm and enclosed in an aluminum housing to maintain constant pressure and temperature.

For our purposes, we operate the cavity at 706 nm and at 784 nm. In both cases the output is intracavity doubled to 353 nm (a formaldehyde absorption feature) and 392 nm (mixed with 1-2W of 532 nm doubled YAG light to probe the 226 nm feature of NO), respectively; hence the output couplers chosen are fully reflective at the fundamental wavelengths. In the event that the fundamental is desired, output coupling of 2-4% is recommended.

The output coupler is a 12.7 mm diameter flat, the 12.7 mm diameter end mirror is concave with a 10 cm focal length. For the 353 nm (392 nm) cavity, the mirror coating is

centered at 694 nm (800 nm) with R > 99% from 670-730 nm (766-844 nm). An isosceles Brewster's angle prism (CVI Lasers, IB-12.4-69.1-UV) between the Ti:sapphire rod and the end mirror bends the optical axis to prevent interference with the pump beam. A three-plate (4 mm, 2 mm, 1 mm thick) birefringent filter stack (Lambda Research, BIR-25.4) is set at Brewster's angle between the gain medium and the output coupler for rough tuning and line narrowing. Fine tuning and further line-narrowing are accomplished by means of an intracavity etalon between the prism and end mirror. The etalon is attached to a computer controlled stepper motor (Oriental Motors, DRL28PB1-03). The choice of etalon depends on application and species studied; for our purposes, the etalon used has a free spectral range of 10 cm^{-1} and a finesse of 6, resulting in a laser linewidth of 0.07 cm^{-1}, as measured on a Burleigh WA-4500 pulsed wavemeter (Figure 2). The etalon tuning range is set by the free spectral range: this is not a limitation because the absorption features probed are quite narrow (0.1 to 1 cm^{-1}.) To tune over a greater range, or to access a different range of wavelengths, the birefringent filter stack must be manually adjusted. Finally, a 5 mm long Type I β-barium borate (BBO) crystal ($\theta=56^{o}$) is set between the birefringent filter and the output coupler, near the nominal beam waist for optimal intracavity frequency doubling and to minimize polarization losses of the doubled light. The entire laser cavity fits in a custom-built 0.5" thick aluminum housing (5" x 9" by 4.5") with a 0.5" thick acrylic cover which can be sealed against pressure changes. Temperature-regulated heating elements (Minco Thermofoil heaters) affixed to the outside of the housing and insulation around the housing control the temperature of the laser.

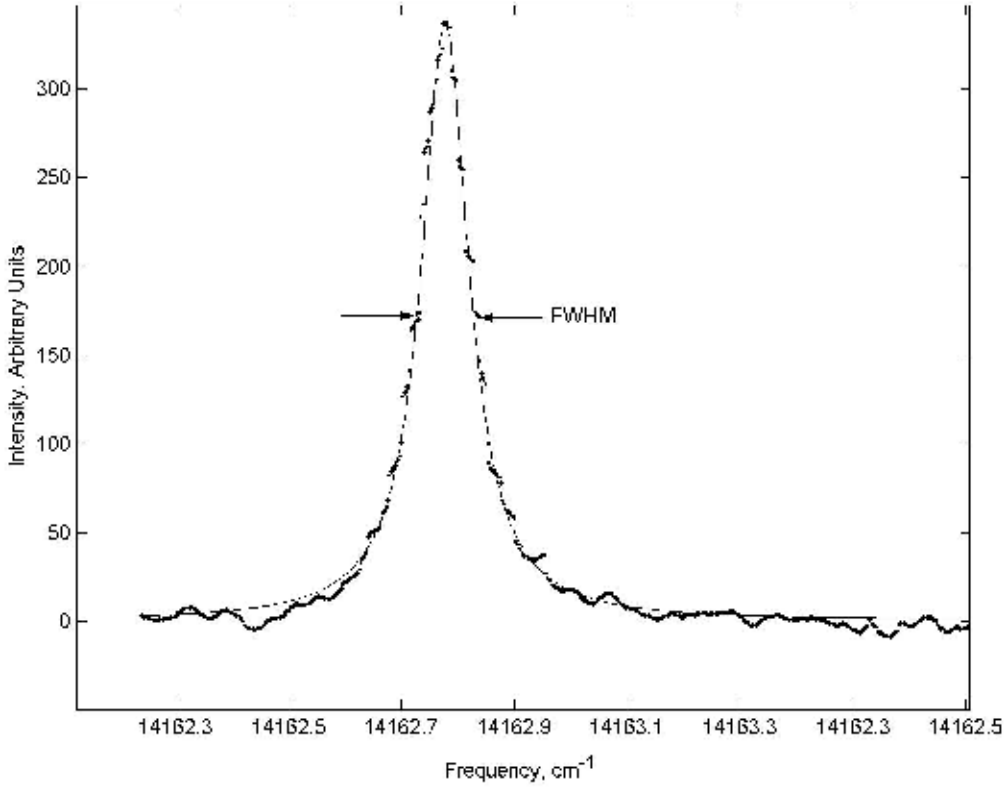

Figure 3.2: The linewidth of the fundamental output of the Ti:sapphire cavity at full-width half-max (FWHM) is 0.07 cm^{-1}. The solid line is a Lorenztian fit.

The pump beam, from a DPSS laser operating near 532 nm, enters the laser housing through a Brewster's angle window. In our case, we use a Lightwave Q201 Nd:YAG laser; however, any appropriate YAG, YLF, or glass laser may be used. The Q201 is operated at 9.5 kHz, where it provides > 12.5 W of green light with a pulse width of 22 ns. This is enough to pump at least 2-3 Ti:sapphire cavities, depending on the wavelength and output power required. Conversion efficiency to the fundamental is at least 25%, again depending on wavelength and with the appropriate output coupling: *e.g.*, with 3.6 W of pump power, we have achieved 900 mW of 706 nm light with a fully reflective ouput coupler. Conversion efficiency from the pump to the intracavity doubled

output is 2-3%. The pulsewidth for the fundamental as well as the doubled output is about 18 ns. Figure 3.3 shows the beam profile of the fundamental: it is somewhat elliptical, with a Gaussian transverse mode. The beam divergence is 0.56 (0.83) mrads in the major (minor) axis. Power and frequency stability are excellent compared to comparable dye lasers: experiments with an open cavity show 1-second power fluctuations of 5% over a 20 minute period.

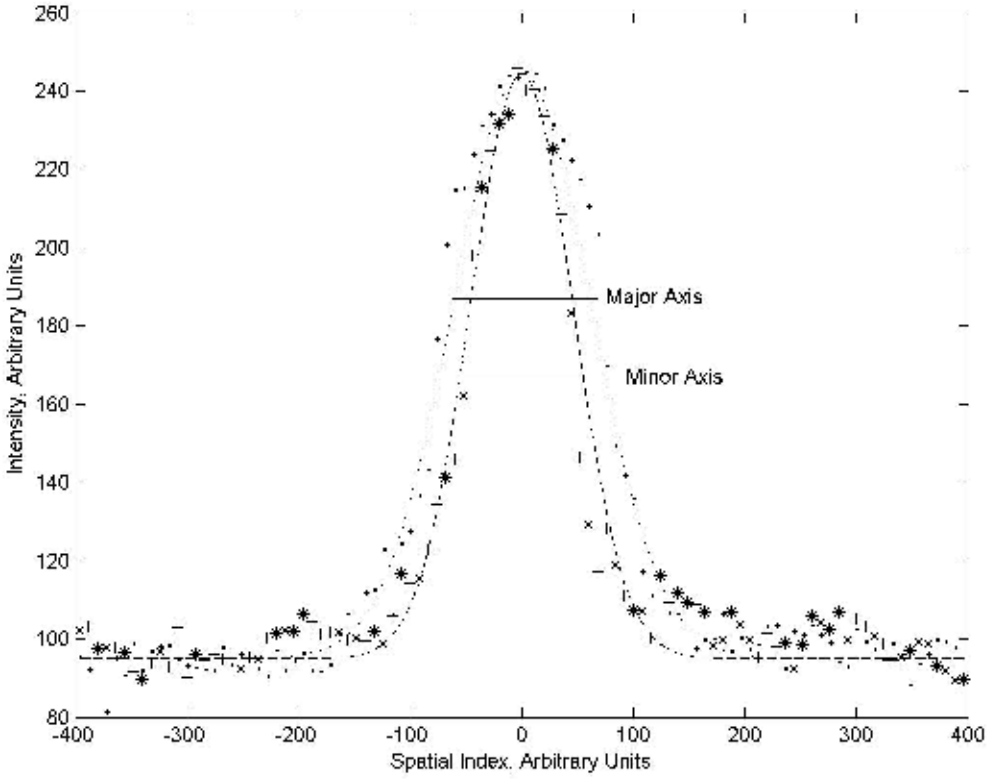

Figure 3.3: The 706 nm beam profile from a CCD camera at ~2m distance. The abscissa refers to the spatial index in arbitrary units (CCD pixels). The dots (stars) represent the profile of the major (minor) axis and the dash-dot (dash-dash) line is its corresponding Gaussian fit.

In normal operation, the cavity is etalon-tuned alternately onto a strong absorption feature and a nearby absorption minimum. The signal from the "online" condition contains fluorescence from the analyte as well as background scattering, the "offline" condition provides the background, and the difference signal is taken to be proportional to the analyte concentration. Figure 3.4 shows a time series illustrating this behavior: the top panel shows the signal from a reference cell, a cell filled with a high concentration of analyte (in this case NO) through which a part of the beam is passed, and used to ensure that the laser frequency does not drift and to indicate the online/offline status of the laser. The difference between the online and offline conditions is quite evident. The bottom panel shows the difference signal taken from the sample cell, a multipass White cell into which ambient air is drawn. This difference signal is converted to a concentration by means of a calibration factor determined by standard addition of a calibration gas.

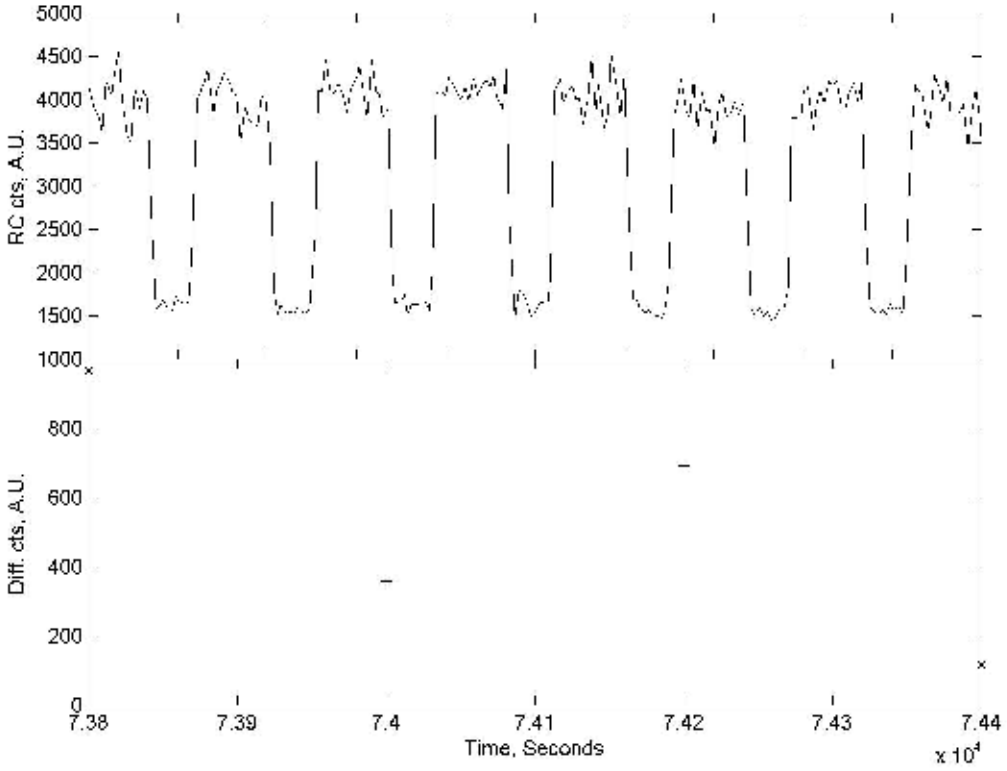

Figure 3.4: Reference cell signal (top) and difference signal from the ambient sampling cell (bottom) during normal operation of the instrument, when the etalon is alternately tuned on and off the absorption feature. The reference cell signal is a one-second average; the ambient cell signal is a two-minute average difference signal. See text for details.

The laser described here is intended for use on a variety of observational platforms, including unpressurized, high altitude aircraft as well as unattended monitoring on ground-based platforms. An early version has flown on NASA's DC-8 airborne laboratory during the INTEX-NA field campaign. It is tunable from 690 nm to at least 1 micron (350 nm to at least 500 nm in the UV), depending on mirror coatings, and with mixing or third harmonic generation can access deep UV wavelengths. The narrow linewidth enables efficient probing of the spectroscopic feature, and in conjunction with the relatively narrow pulsewidth enable efficient spectral and temporal filtration of the

signal. Finally, it can be pumped by compact, relatively low power DPSS doubled YAG lasers.

3.4 References

Bradshaw, J., et al. (1999), Photofragmentation two-photon laser-induced fluorescence detection of NO2 and NO: Comparison of measurements with model results based on airborne observations during PEM-Tropics A, *Geophysical Research Letters*, *26*(4), 471-474.

Brune, W. H., et al. (1998), Airborne in-situ OH and HO2 observations in the cloud-free troposphere and lower stratosphere during SUCCESS, *Geophysical Research Letters*, *25*(10), 1701-1704.

King, M. D., et al. (2000), A new method for the atmospheric detection of the nitrate radical (NO3), *Atmospheric Environment*, *34*(5), 685-688.

Mohlmann, G. R. (1985), FORMALDEHYDE DETECTION IN AIR BY LASER-INDUCED FLUORESCENCE, *Applied Spectroscopy*, *39*(1), 98-101.

Rodgers, M. O., et al. (1982), SEQUENTIAL 2-PHOTON LASER-INDUCED FLUORESCENCE DETECTION OF MERCURY, *Optics Letters*, *7*(8), 359-361.

Thornton, J. A., et al. (2000), Atmospheric NO2: In situ laser-induced fluorescence detection at parts per trillion mixing ratios, *Analytical Chemistry*, *72*(3), 528-539.

Wennberg, P. O., et al. (1994), AIRCRAFT-BORNE, LASER-INDUCED FLUORESCENCE INSTRUMENT FOR THE IN-SITU DETECTION OF HYDROXYL AND HYDROPEROXYL RADICALS, *Review of Scientific Instruments*, *65*(6), 1858-1876.

Wood, E. C., et al. (2003), Prototype for in situ detection of atmospheric NO3 and N2O5 via laser-induced fluorescence, *Environmental Science & Technology*, *37*(24), 5732-5738.

CHAPTER 4

BOUNDARY LAYER SULFURIC ACID MEASUREMENTS DURING NEAQS-ITCT 2K4: IMPLICATIONS FOR PHOTOCHEMISTRY AND AEROSOLS

4.1 Summary

We report values of gas-phase sulfuric acid, H_2SO_4, from the New England Air Quality Study 2004 as measured by Chemical Ionization Mass Spectrometry (CIMS). The mean sulfuric acid value for daytime boundary layer is 2.06×10^7 molecules cm^{-3} for the Northeastern U.S. Because aerosol scavenging is efficient, sulfuric acid observations provide a simple tool for calculating steady-state hydroxyl radical concentration and thus tests our ability to predict H_2SO_4 levels. The hydroxyl radical concentrations are compared with the output of the NASA photochemical box model. Model to steady-state value for the field campaign is 1.68. However, good agreement was found between model predictions and steady state calculations of OH when VOC variability could be captured in the model. Several night flights occurred, making it possible to calculate steady state OH at a fast time response of 1 second. In the New York City area, OH was calculated to have a maximum concentration of 1.5×10^6 molecules cm^{-3}, although the median value was 3.3×10^5 molecules cm^{-3}. Relatively high sulfuric acid levels were observed at night but appear to be produced by NO_3 initiated chemistry. A dimensionless parameter, *L*, was also calculated for 8 daytime flights to determine when nucleation was possible. The *L* parameter indicated nucleation was possible 10% of the time for the flights examined and mainly occurred within urban plumes.

4.2 Methods

4.2.1 Instrumentation

The NEAQS-ITCT 2K4 field campaign focused on chemical transformation and transport of polluted air as well as emission characterization from urban areas along the Eastern United States and point sources along the Ohio Valley. The NOAA WP-3D aircraft was based out of Portsmouth, New Hampshire for the duration of the study. It was equipped to measure a suite of trace gases, aerosol properties, and meteorological conditions. Pertinent measurements used in this analysis are indicated with references in Table 4.1. A description of the P3 flight plans and payload can be found in [*Fehsenfeld et al.*, 2006]. Relevant flights for this analysis include daytime boundary layer flights in the Ohio Valley and New York City regions and several night flights in the greater New York City region.

Table 4.1: Measurements and Techniques aboard the WP-3D aircraft during NEAQS-ITCT 2K4

Measurement	Technique	Reference
O_3	Chemiluminescence	[*Ryerson et al.*, 1998]
NO	Chemiluminescence	[*Ryerson et al.*, 1999]
Canister VOCs	GC/FID, GC-MS	[*Schauffler et al.*, 1999]]
SO_2	UV pulsed fluorescence	[*Ryerson et al.*, 1998]
H_2SO_4	CIMS	[*Eisele and Tanner*, 1993]
NO_3, N_2O_5	Cavity Ring-Down Spectroscopy	[*Dube et al.*, 2006]
Aerosol Size Distribution	Nucleation Mode Aerosol Size Spectrometer	[*Brock et al.*, 2000; *Brock et al.*, 2003]
CO	VUV fluorescence	[*Holloway et al.*, 2000]
NH_3	CIMS	[*Neuman et al.*, 2002]
Actinic Flux	Spectrally Resolved Radiometer, Nadir & Zenith	
Aircraft Diagnostics[a]	Commercial sensors	---
Water Vapor	Tunable Diode Laser	---

[a] Diagnostics include temperature, pressure, longitude, latitude, altitude, relative humidity and dew point. For more information on the NOAA WP-3D payload, please refer to *Fehsenfeld et al*., [2006]

4.2.1.1 CIMS Instrument

Gas-phase H_2SO_4 was measured by chemical ionization mass spectrometry (CIMs) as described in detail by [*Sjostedt et al.*, 2007]. The CIMs instrument was mounted underneath the starboard wing. Figure 4.1 is a schematic of the CIMS instrument within nose cone of the wingpod. A brief description of the instrument and technique is given here. The inlet assembly is based on the work of [*Eisele et al.*, 1997]. It consists of a shroud which straightens the air flow and connects to two reducing air ducts thus resulting in a reduction of air speed from ~100-150 m/s to ~0.5 m/s. This design produces laminar flow while preventing interaction with the wall. Ions are produced by a ^{210}Po foil in air doped with nitric acid. The alpha particles from the foil form positive ions and thermalized electrons within the carrier gas. These electrons initiate the formation of the nitrate ion (NO_3^-) and nitric acid clusters [*Eisele*, 1989; *Fehsenfeld et al.*, 1975], thus permitting selective detection of sulfuric acid via HSO_4^- (97 amu) by reaction (R4.1)

$$H_2SO_4 + NO_3^- \cdot (HNO_3) \rightarrow HSO_4^- \cdot (HNO_3) + HNO_3 \qquad \text{R4.1}$$

On some flights the sum of HO_2 +RO_2 was measured by addition of $^{34}SO_2$ and NO [*Edwards et al.*, 2003; *Sjostedt et al.*, 2007]. The peroxy chemical conversion scheme is depicted in reactions (R4.2-4.7).

$$HO_2 + NO \rightarrow OH + NO_2 \qquad \text{R4.2}$$

$$OH + {}^{34}SO_2 + M \rightarrow H{}^{34}SO_3 + M \qquad \text{R4.3}$$

$$H{}^{34}SO_3 + O_2 \rightarrow HO_2 + {}^{34}SO_3 \qquad \text{R4.4}$$

$${}^{34}SO_3 + 2H_2O \rightarrow\rightarrow H_2{}^{34}SO_4 + H_2O \qquad \text{R4.5}$$

$$OH + NO + M \rightarrow HONO + M \qquad \text{R4.6}$$

$$NO_2 + HO_2 + M \rightarrow HO_2NO_2 + M \qquad \text{R4.7}$$

The resulting reactions transform HO_2 and RO_2 radicals to $H_2{}^{34}SO_4$ which can be distinguished from ambient sulfuric acid ($H_2{}^{32}SO_4$). The sensitivity of sulfuric acid was determined by photolysis of water vapor to produce a known concentration of OH radicals which were then converted via reaction with $^{34}SO_2$ to sulfuric acid [*Sjostedt et al.*, 2007]. The H_2SO_4 detection limit for the field campaign was typically 6×10^5 molecules cm^{-3} in 1 second and for peroxy radicals the limit of detection in 1 second was 2×10^7 molecules cm^{-3}. The accuracy for H_2SO_4 was estimated to be 35% and 45% for RO_2 radicals.

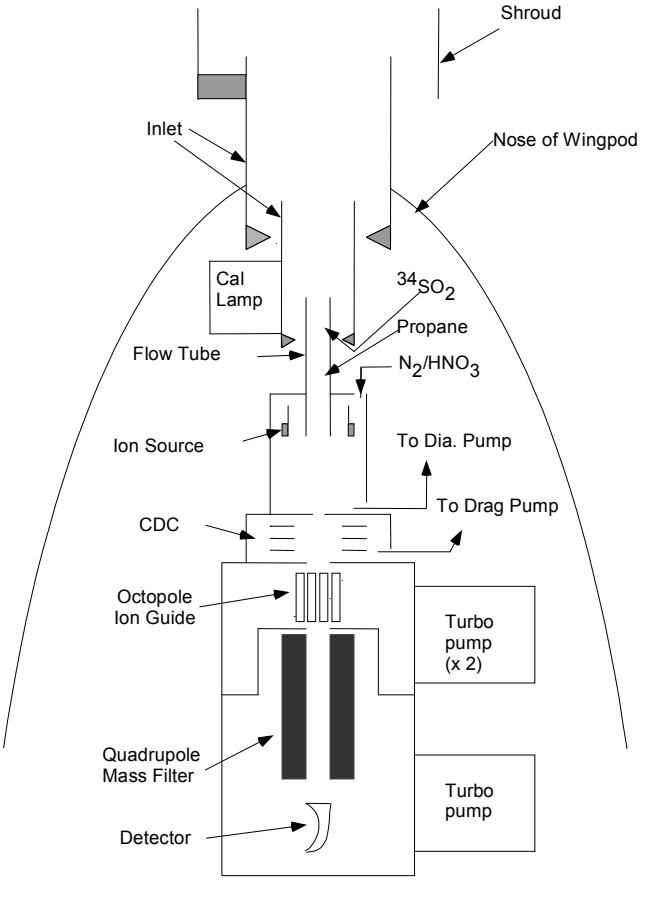

Figure 4.1: Diagram of CIMS instrument within the nose cone of the wingpod

4.2.2 Model Description

The NASA time-dependent photochemical model [*Crawford et al.*, 1999; *Olson et al.*, 2006] was used to calculate OH concentrations in order to compare them with the OH calculated from measured aerosol surface data and sulfuric acid concentrations. Details of the model and a chemical reaction scheme can be found elsewhere [*Crawford et al.*, 1999] although it is important to note that updates to the model have occurred, reflecting more current reaction rate coefficients [*Sander*, 2003]. The model calculations were constrained to measured meteorological values such as temperature, pressure, and dew point, as well as photolytic fluxes and species including O_3, CO, NO and H_2O. The species calculated by the model in which a diurnal estate was found whereby the variations in the individual species diurnal cycles attained equilibrium.

Model runs were performed on a one second data merger time resolution which required interpolation of species with longer time resolution such as volatile organic compounds (VOCs). VOC concentrations were measured by a whole air sampling technique followed by gas chromatography [*Schauffler et al.*, 1999; *Schauffler et al.*, 2003]. Whole air samples were taken approximately every 5 minutes with an intergration time on the order of 20 sec. The VOC data were interpolated either as a function of time or based on a 1^{st} order polynomial relationship of CO levels depending the conditions. The CO correlation was used when a reasonable correlation was found between CO and VOC levels ($R^2 > 0.50$).

4.2.3 Nucleation Parameterization

McMurry et al. [2005] have defined a dimensionless parameter, *L*, which expresses whether new particle formation via nucleation can occur.

$$L = \frac{\bar{c} A_{Fuchs}}{4\beta_{11} N_1} \qquad \text{E4.1}$$

where

$\bar{c}$ = mean thermal speed of cluster

A_{Fuchs} = Fuchs surface area

$$= \frac{4\pi}{3} \int_{D_{p\min}}^{\infty} D_p^2 \left(\frac{Kn + Kn^2}{1 + 1.71Kn + 1.33Kn^2} \right) n(D_p) dD_p \qquad \text{E4.2}$$

Kn = Cluster Knudsen number

D_p = diameter of preexisting particle

$D_{p\,min}$ = minimum diameter

β_{11} = Collision frequency function

N_1 = Concentration of clusters

For simplification, the concentration of clusters, N, is assumed to be the measured sulfuric acid concentration. The parameter *L* in equation (E4.1) describes the ratio of the coagulation of new clusters relative to their growth via condensation of sulfuric acid. Therefore nucleation from the gas phase would occur when $L < 1$ since condensation is dominant and when $L > 1$ nucleating clusters would be lost to preexisting particles. This calculation was used to determine possible nucleation events, how often they occur during the NEAQS-ITCT 2K4 campaign, and to validate the consistency of this parameterization when compared to observations.

4.3 Results and Discussion

4.3.1 Sulfuric Acid Observations

The H_2SO_4 measurements were performed as part of the NEAQS-ITCT 2k4 study during July of 2004. The campaign consisted of 18 flights; the CIMS instrument measured

sulfuric acid for 13 flights. Figure 4.2 depicts a standard flight in which much variability of sulfuric acid is encountered. It is a time series plot of 06 August 2004 measured gas-phase sulfuric acid. Boundary layer height for each flight was determined by observation of a temperature inversion or a sharp decrease in water vapor mixing ratio with altitude. The average boundary layer height was 2000 meters.

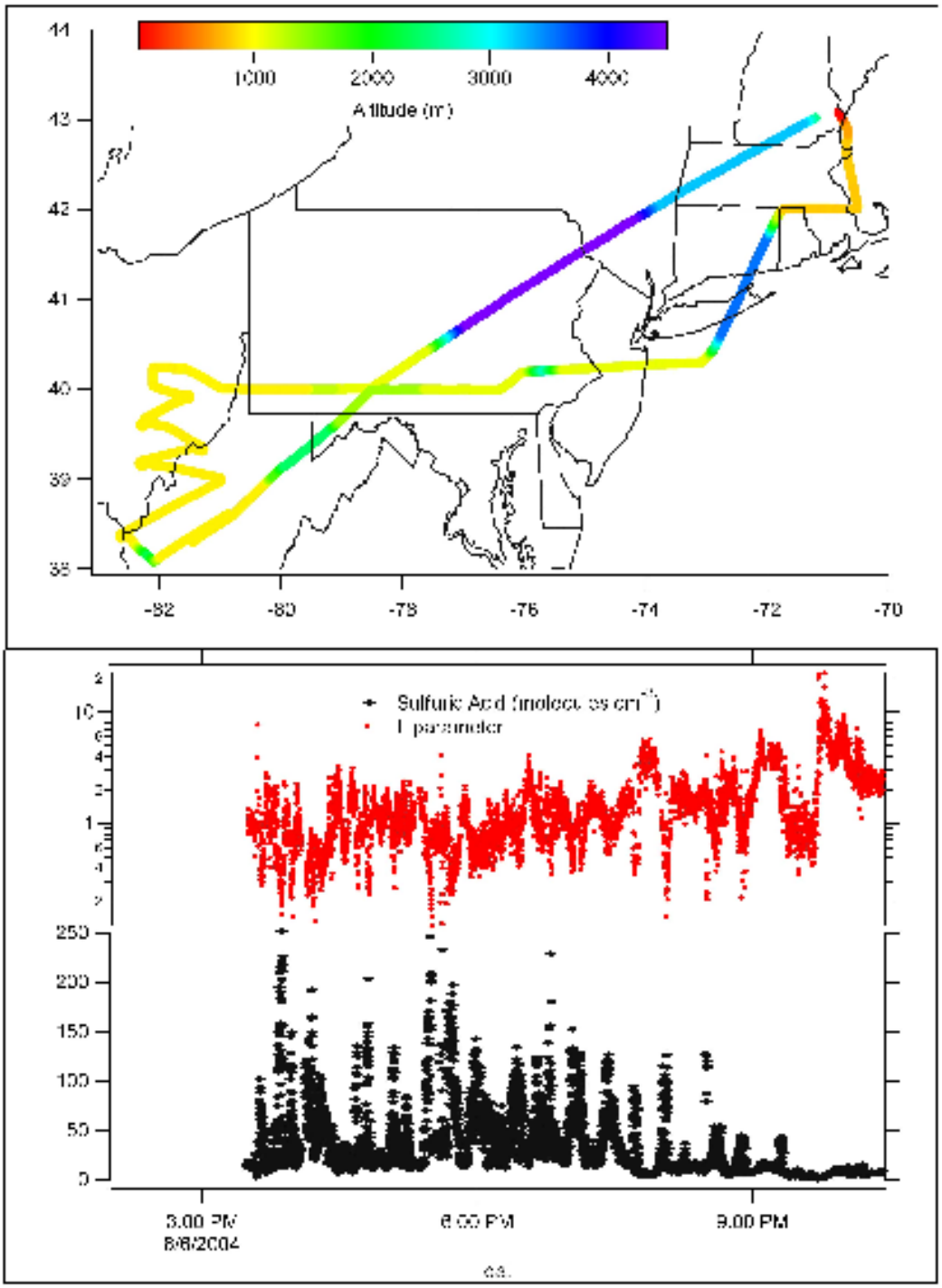

Figure 4.2: Top panel shows flight path which is color coded for altitude for the 06 August 2004 WP-3D flight. The bottom panel shows total 1 second measured gas-phase sulfuric acid within the boundary layer (black diamonds) and calculated *L* parameter (red circles). Boundary layer height was 2300 meters. Sulfuric acid is quite variable within the Midwest. The median sulfuric acid concentration observed for the NEAQS mission was 1.52×10^7 molecules cm^{-3}.

Table 4.2 presents data statistics for measured gas phase sulfuric acid at different altitude bins (every 500 m) for day and night. The WP-3 flew below 6500 meters the entire campaign and most of the CIMS measured sulfuric acid data were collected at altitudes between 200 and 4000 meters. The mean daytime sulfuric acid number density for the entire mission within the boundary layer was 2.06×10^{7} molecules cm^{-3} (median value: 1.52×10^{7} molecules cm^{-3}). Recent literature values report sulfuric acid concentration in the range of 10^{6} to 10^{8} molecules cm^{-3}. Since formation of sulfuric acid occurs through photochemistry, nighttime values are expected to be low. In fact, observed boundary layer sulfuric acid number densities for the entire mission during night hours (8:30 pm to 7 am, local) have mean and median values of 4.55×10^{6} and 1.7×10^{6} molecules cm^{-3} respectively. Nighttime sulfuric acid is addressed below (see section 4.3.3 Nighttime H_2SO_4 and OH).

Table 4.2: Data Statistics for Measured Total Gas-Phase Sulfuric Acid[a] in Altitude Bins

Altitude (m)	Day Mean	Day Median	Day Minimum	Day Maximum	Night Mean	Night Median	Night Minimum	Night Max
0-499	1.87	1.48	0.0091	54.2	0.289	0.166	0.0144	9.10
500-999	2.28	1.61	0.0089	33.5	0.506	0.176	0.0091	19.9
1000-1499	1.42	0.956	0.0101	25.1	0.497	0.158	0.0092	12.7
1500-1999	9.91	0.851	0.0106	9.22	0.268	0.166	0.0081	1.89
2000-2499	1.14	0.614	0.0169	12.2	0.220	0.111	0.0088	2.08
2500-2999	1.18	0.576	0.0131	11.7	0.137	0.0746	0.0088	1.20
3000-3499	0.488	35.8	0.0129	11.9	0.0979	0.0692	0.0119	1.81
3500-3999	0.415	0.350	0.0538	0.954	0.229	0.189	206383	1.04

[a]Sulfuric acid is reported as number density ($\times 10^7$molecules cm^{-3}). Day is defined as 7 am to 8:30 pm, local. Typical boundary layer height was around 1800 meters

4.3.2 Sulfuric Acid as a Photochemical Tracer

In the atmosphere, sulfuric acid is in effect formed from the reaction of SO_2 + OH, this being the rate limiting step in reactions 1-3, and its primary sink is loss to aerosols. For this reason, we think H_2SO_4 may be used as a photochemical tracer within the boundary layer to monitor the hydroxyl radical levels as its lifetime is of the order of minutes and it should reach steady state. Assuming that H_2SO_4 is irreversibly lost to aerosol scavenging, the average lifetime was 3 minutes for the NEAQS mission. As a result, the OH concentration can be calculated through a steady state approximation assuming diffusion limited uptake of H_2SO_4 by the aerosol, $R_{AerosolUptake}$,

$$[OH]_{ss} = \frac{R_{AerosolUptake}}{k[SO_2]} \qquad \text{E4.3}$$

$$R_{AerosolUptake} = \left(\frac{4}{v\alpha}\right)^{-1} A n_x \qquad \text{E4.4}$$

where v is the molecular speed, α is the mass accommodation coefficient, A is the Fuchs surface area, and n_x is $[H_2SO_4]_{(g)}$ [*Jacob*, 2000]. For this analysis, the value of the mass accommodation coefficient used was 0.7 as suggested by [*Chen et al.*, 2005]. Hydroxyl radical concentrations were calculated using equation 13 for sulfur dioxide concentrations > 1 ppbv. This filter was applied because sulfur dioxide was measured via pulsed UV fluorescence [*Ryerson et al.*, 1999] with a detection limit on the order of a few hundred pptv. We estimate measurement uncertainty as 30% for the sulfuric acid measurement; therefore the hydroxyl radical calculation has this inherent error associarted. Sulfate production was also calculated using equation (E4.4). The mean value was 0.1 μg m^{-3} hr^{-1}. The maximum sulfate production calculated was 3.8 μg m^{-3} hr^{-1}. Within power plant plumes, mean production was calculated to be 0.72 μg m^{-3} hr^{-1} while urban plumes had a mean production value 0.02 μg m^{-3} hr^{-1}. Observed sulfate for the NEAQS campaign had a mean of 3 μg m^{-3} in the boundary layer and sulfate represented 37% of the fine particle mass of non-biomass burning aerosols [*Peltier et al.*, 2007].

The mean steady state OH concentration calculated from the observed sulfuric acid for the total mission is 5.19×10^6 molecules cm^{-3} (median: 4.5×10^6 molecules cm^{-3}. As a way to evaluate this method, OH concentrations were also calculated by using the NASA Photochemical box model for day flights. This method provided a mean concentration of 5×10^6 molecules cm^{-3} (median: 5.2×10^6 molecules cm^{-3}). The NASA model (M) over predicts OH concentration when compared to the steady state calculation (SS) where the median value is 1.36 (overall 1 second $R^2 = 0.16$). The combination of

using the CO interpolation when there was good correlation and the linear interpolation in portions where there was not good correlation provided the best overall M/SS. The 1 second model output was also averaged for 1 minute to smooth any data variations. This did not have a great impact on overall M/SS (median M/SS = 1.32, R^2= 0.22). A good example to study the relationship of OH and H_2SO_4 occurred on the flight on 06 August 2004.

4.3.2a 06 August 2004

Figure 4.2 shows the WP-3D flight track for 06 August 2004. The boundary layer height was determined to be ~2300 meters. The focus of this flight was primarily on the coal burning Ohio valley power plants, as a result, high SO_2 and sulfuric acid concentrations were observed. Much of the flight was in the boundary layer as indicated on the color code in figure 4.2. Mean sulfuric acid observed on 06 August 2004 is 3.4×10^7 molecules cm^{-3} (median: 2.11×10^7 mol cm^{-3}).

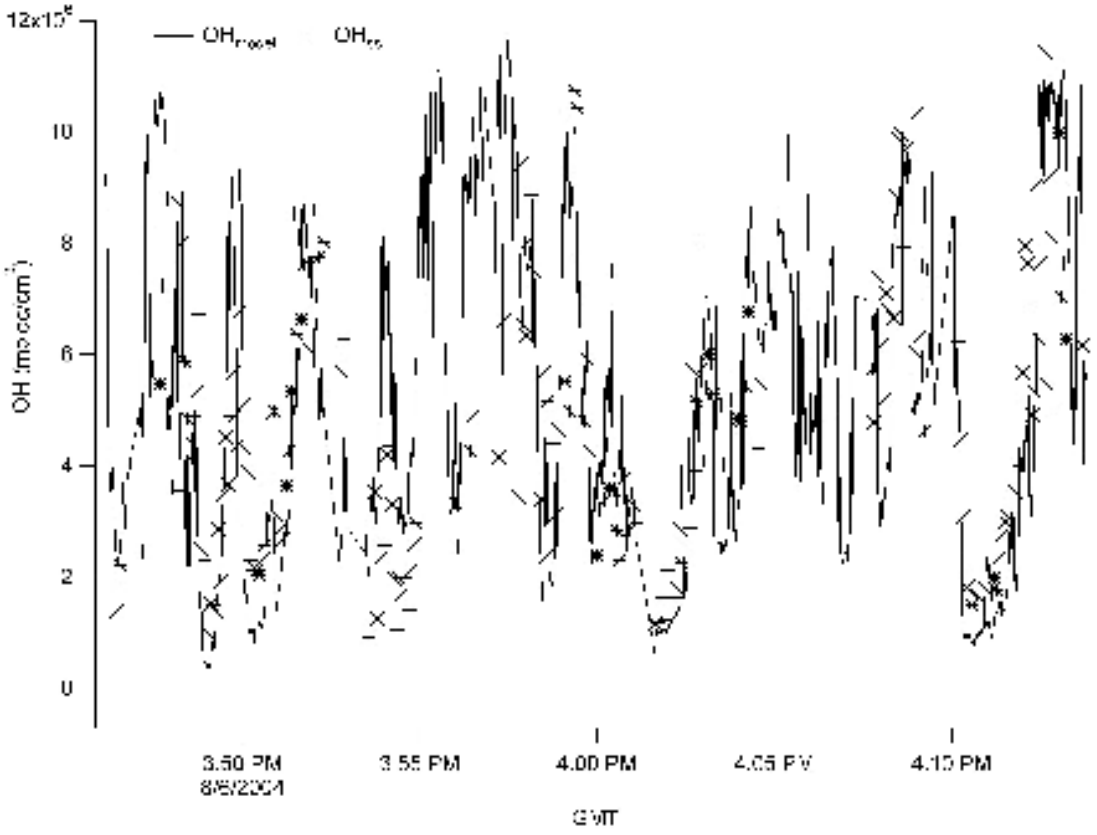

Figure 4.3: Time series plot for the Ohio valley flight on 06 August 2004. Graph illustrates the ability to used sulfuric acid as a photochemical tracer. The steady state calculation captures the variance in the OH concentration as indicated by the [OH] concentration obtained from the NASA photochemical model ([OH]model, solid line) and steady state approximation ($[OH]_{ss}$ *).

Because of the large number of power plants located in this region, this flight encountered plumes rich in SO_2. The average correlation of VOCs and CO was high with an $R^2 \geq 0.6$. The mean steady state OH concentration calculated from the observed sulfuric acid is 5.2×10^6 molecules cm^{-3}. In comparison, the mean OH concentration acquired from the NASA photochemical model was 5.8×10^6 molecules cm^{-3}. A time series plot in figure 4.3 represents the ability of the steady state calculation to capture the variance in the OH concentration. The variation in the $[OH]_{ss}$ can be attributed to the variation in the H_2SO_4 observations. Figure 4.4 presents a scatter plot of model to steady

state [OH]. A linear regression yields a slope of 0.99 and an intercept of 6.68×10^5 molecules cm^{-3}. For this flight, there is excellent agreement between model (M) and steady state calculation (SS) for OH values where average value of M/SS = 1.13 and median value = 1.09 ($R^2 = 0.6$). The model tends to slightly over predict OH when compared to the steady state but it is well within error bars of the sulfuric acid measurement alone. The air mass encountered during this flight is polluted continental with a relatively high hydrocarbon load. These results indicate that the steady state calculation captures the daytime OH variation sufficiently when the VOCs are well correlated to the CO concentration. This also suggests that sulfuric acid levels may be a good photochemical tracer for OH in high sulfur environments and may be particularly useful when VOCs can be well captured in a model. Finally, these results indicate that models will not do a good job of predicting H_2SO_4 levels in environments where the variability of VOCs and SO_2 are not well understood.

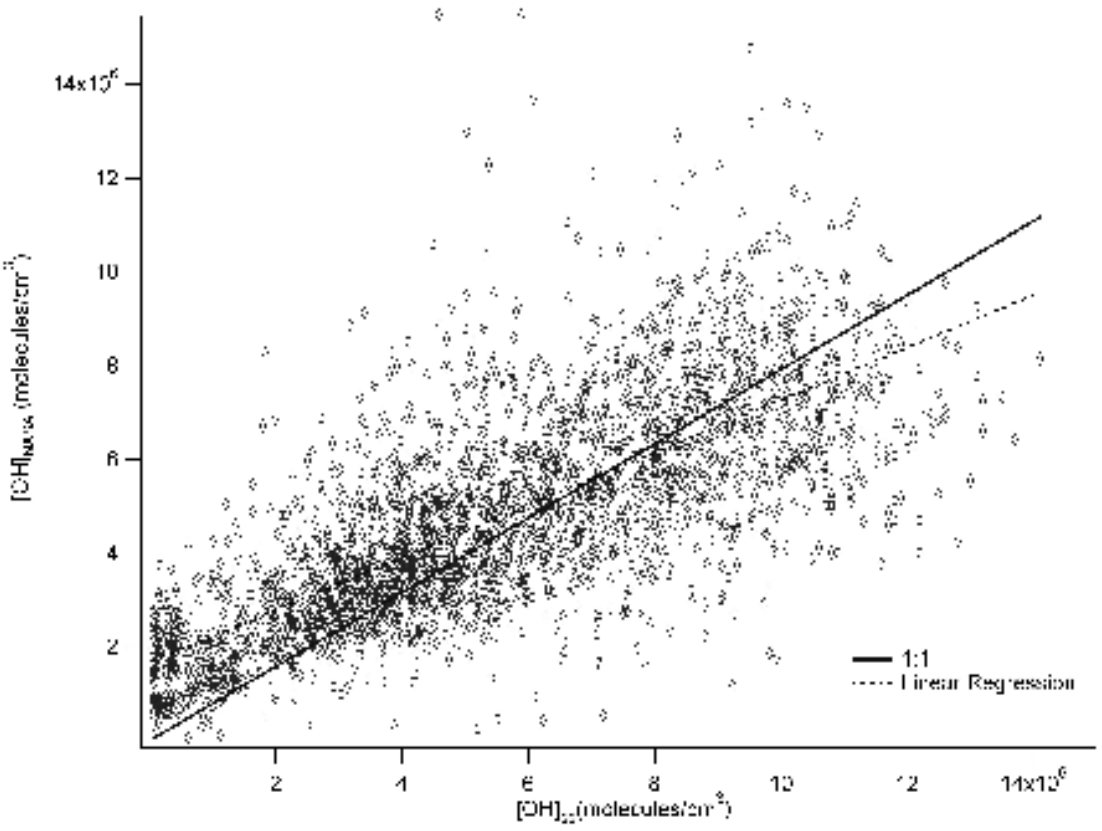

Figure 4.4: Scatter plot of predicted versus steady state calculated OH radical concentration for 06 August 2004. The linear regression equation is $[OH]_{model} = 6.68e5 + 0.99[OH]_{ss}$. $R^2 = 0.6$ and N = 2786

4.3.3 Nighttime H_2SO_4 and OH

In recent years, there have been several reports of significant OH levels at night (> 10^6 molecules cm^{-3}) [*Faloona et al.*, 2001b; *Geyer et al.*, 2003; *Ren et al.*, 2003b; *Ren et al.*, 2003d]. During the day, OH is produced photochemically; hence, a nonphotochemical explanation for the presence of nighttime OH has been postulated; ozonolysis of VOCs and the oxidation of VOCs via NO_3 then subsequent chemistry has been suggested as a possible mechanisms for nighttime production of OH radicals [*Platt et al.*, 1990].

Several flights occurred at night to investingate NO_3/N_2O_5 chemistry [*Brown et al.*, 2006] providing the opportunity to examine nocturnal oxidation using sulfuric acid

as a photochemical tracer. Flights paths were focused on the greater New York City area and the Ohio valley as shown in Figure 4.5. The mean observed [H_2SO_4] was 1.5 $\times 10^6$ molecules cm^{-3}. In comparison, nighttime sulfuric acid measured during PEM-TROPICS A at high altitude in a dry air mass (RH < 20%) had an average concentration of 10-11$\times 10^6$ molecules cm^{-3}; in wetter air masses the average concentration was ~1 $\times 10^6$ molecules cm^{-3} [*Mauldin et al.*, 1999b]. In general, observed nighttime sulfuric acid is quite low. Sulfuric acid observed could be due to a combination of two sources: OH oxidation of SO_2 or the evaporation from aerosols. The latter possibility could represent the vapor pressure over aerosols, although since there is not a correlation between relative humidity or temperature and sulfuric acid, this has been discounted. However, the derived OH levels from observations of sulfuric acid must be considered an upper limit at night.

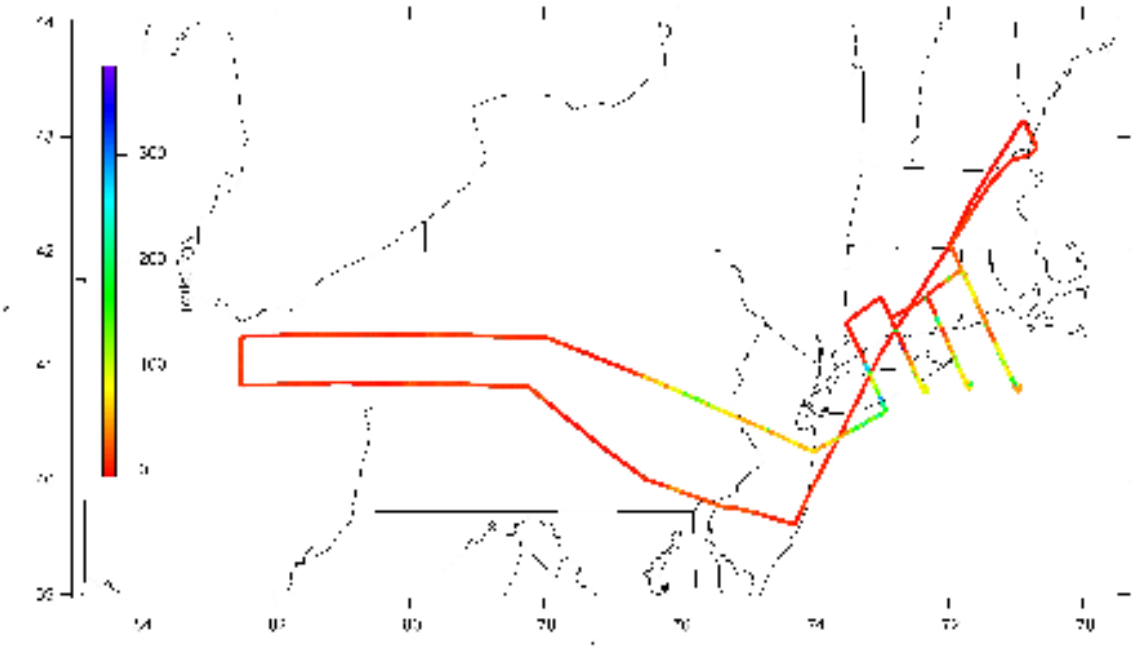

Figure 4.5: Flight track for night flight beginning on 9 August into 10 August 2004. Color code corresponds to observed nitrate concentration (pptv).

The maximum nighttime concentration of sulfuric acid, 2×10^6 molecules cm^{-3}, was measured around NYC on 09 August 2004. This corresponds to a maximum calculated OH level of 3.9×10^5 molecules cm^{-3}. Although many power plants are located within the Ohio Valley, enhanced nocturnal sulfuric acid concentrations were not observed in this region. Average sulfur dioxide encountered was 3.5 ppbv with several plumes reaching in excess of 150 ppbv downwind of the power plants. Large mixing ratios of NO_3 were also encountered but not within the power plant plumes. In fact, enhanced sulfuric acid ($> 5\times10^6$ molecules cm^{-3}) was only observed when SO_2 was at least 30 ppbv and NO_3 concentrations were greater than 100 pptv. Figure 4.6 illustrates the time series of measured SO_2, NO_3, and H_2SO_4 for the flight – enhanced sulfuric acid is seen toward the end over New Jersey and eastern Pennsylvania where there was both high levels of SO_2 and NO_3.

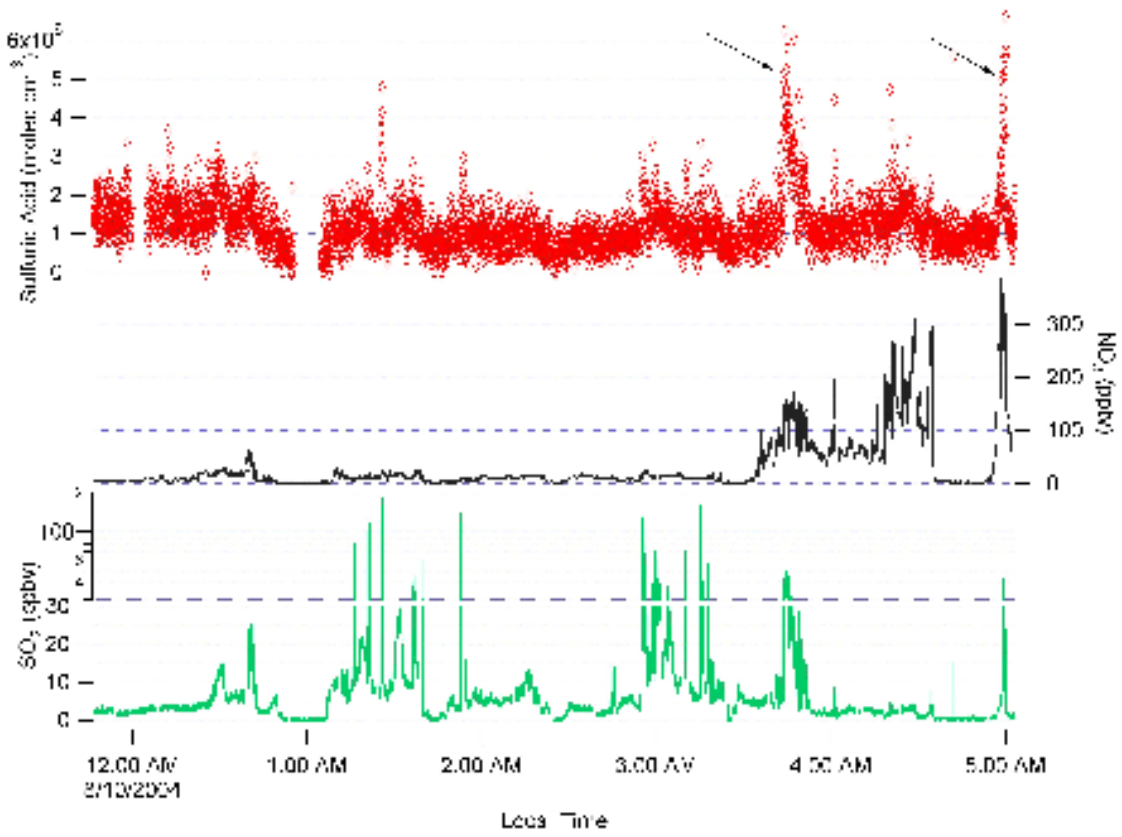

Figure 4.6: Sulfuric acid, nitrate radical, and sulfur dioxide for flight occurring on 10 August 2004. Plumes of enhanced NO_3 and SO_2 are correlated to the production of enhanced sulfuric acid (>5×10^6 molecules/cm^3) as indicated by arrows. Enhanced sulfuric acid seen in urban plumes in the New York City area.

To better understand the enhanced sulfuric acid levels, steady-state OH was calculated for the flight. The median steady-state OH concentration for the greater New York City area was 3.3×10^5 molecules cm^{-3}. Comparing to other night measurements, this OH concentration is considerably less than what has been reported in U.S. urban areas. In Nashville, typical nighttime OH levels measured by laser-induced fluorescence (LIF) was 1×10^6 molecules cm^{-3} [*Martinez et al.*, 2003] and in New York City, OH concentration during the early night was ~1.3×10^6 molecules cm^{-3} [*Ren et al.*, 2003b].

Consequently, the sulfuric acid observed on the nocturnal flights is not compatible with the relatively high levels of OH observed by LIF.

As mentioned above, relatively high levels of sulfuric acid were observed at night but only when high SO_2 and NO_3 levels were encountered. In fact at H_2SO_4 levels above 2×10^6 molecules cm^{-3}, the product of $[SO_2][NO_3]$ has a reasonably strong correlation to the observed sulfuric acid ($R^2 = 0.50$). This indicates that the nitrate radical is responsible for increased sulfuric acid production as the aerosol surface area was not highly variable on these flights. However, the reaction of NO_3 with SO_2 is inefficient and can't account for the observed sulfuric acid [*IUPAC*, 2003]. One possibility is the oxidation of SO_2 via OH produced from the reaction of HO_2 radicals with NO_3, reaction (R4.8):

$$NO_3 + HO_2 \rightarrow OH + NO_2 + O_2 \qquad \text{R4.8}$$

The OH production rate calculated with measured nitrate and peroxy radical was found to be roughly 10^6 molecules/cm^3 sec, assuming a lifetime of 0.05 sec [*Ren et al.*, 2006a] the possible OH concentration is 50000 molecules/cm^3. This is an upper limit to the sulfuric acid production rate as much as the OH would react with NO_x and other species. However, less than three percent of the radical production via this mechanism is required to account for the observed sulfuric acid. For this reason, we believe that the enhanced nocturnal sulfuric acid is likely due to interaction of NO_3 radicals with HO_2.

4.3.4 Sulfuric Acid and Nucleation

The nucleation parameter, *L*, was calculated using equation (5) for a total of 8 daylight flights and was found below 1, indicating that nucleation is probable, 10% of the time. There was no indication that nucleation occurred when $L>1$ (*e.g.* significant number

densities of the smallest particle sizes were not observed). Nucleation was observed when L was less than 1 but not all the time. This is likely due to the rapid traverse of the different air masses by the aircraft and the finite amount of time needed for particles to grow to a detectable size 4 nm. Consequently, our observations are consistent with the conclusion of *McMurry et al*. [2005] that the simple parameter L can be used to predict when nucleation is likely. For this campaign, L was observed to be less than 1 at a median sulfuric acid concentration is 4×10^7 molecules cm^{-3} with a minimum value of 2.2×10^6 molecules cm^{-3}. Nucleation, as defined by *L*, was found to be most probable in urban plumes and was driven by sulfuric acid levels since the surface area density of aerosols remained relatively constant throughout the study region as shown in Figure 4.7.

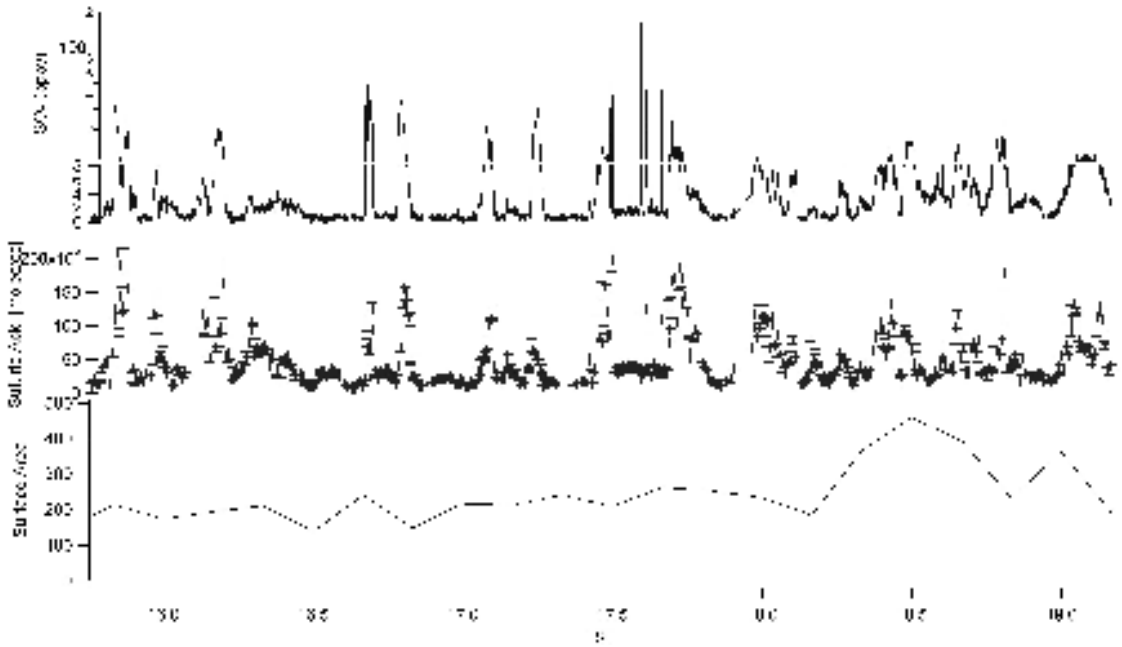

Figure 4.7: Highlight of 06 August 2004 flight in which power plant plumes were encountered. Portion of flight shown is concentrated on Ohio Valley. Fine aerosol surface area (averaged for 10 minutes) is shown on bottom panel; it remains relatively constant. On the middle panel observed sulfuric acid is shown. The upper panel is the observed sulfur dioxide. It can be concluded the OH variance is needed in addition to sulfur dioxide to explain values of H_2SO_4.

Interestingly, in the 1990s, governmental action enacted reductions in NO_x emissions from power plants [*EPA*, 2004]. [*Frost et al.*, 2006] found that summertime NO_x emissions rates from the eastern U.S. power plants dropped ~50% between 1999 and 2003 while SO_2 emission rates did not significantly decrease for the same period. This reduction in NO_x emissions can suppress the oxidative capacity of the power plant plumes, thus resulting in lower sulfuric acid and in turn, impacting nucleation within the plumes. In order to test the reduction of NO_x levels on photochemistry and its importance to sulfuric acid and nucleation, the NO concentration was increased by 50% in power plant plumes and sulfuric acid levels were predicted using the NASA box model. The resulting sulfuric acid increased up to 40% in some of the power plant plumes, on average there was an increase in the concentration of sulfuric acid by 20% in power plant plumes. The increased NO_x within the power plant plumes also increased the probability of nucleation since the occurrence of $L < 1$ increased by 60%. This indicated that the NO_x reductions may have also les to a significant decrease in nucleation in power plant plume emissions.

4.4 Conclusion

Airborne measurements of sulfuric acid were made in July and August of 2004 over the northeastern portion of United States. The sulfuric acid concentration in the boundary layer for the field campaign varies between 1.6×10^5 molecules cm^{-3} and 5.4×10^8 molecules cm^{-3} and was found to be highly variable, *i.e.* concentration would change by an order of magnitude or more in less than 1 kilometer. The one second observations of sulfuric acid, sulfur dioxide, and aerosol surface area were used to calculate OH levels

assuming steady state. These results compared well with predicted OH levels from the NASA photochemical box model. However, correlation between model and steady state calculation was often poor. This is attributed to the variability of VOCs that could not be captured with observations of high time resolution. It is shown that when VOCs were found to correlate with the observed CO levels that excellent agreement could be found from the model predictions and steady state calculations based on H_2SO_4 observations. These results demonstrate the difficulty of predicting OH and sulfuric acid levels in a highly inhomogeneous environment (e.g. highly variable VOC) such as the northeast U.S. Finally, the results also indicate that in areas with high sulfur loadings that sulfuric acid is an excellent photochemical tracer that can be used at integration times as short as one second.

Nocturnal observations of sulfuric acid were used to calculate OH levels. Within the greater New York City area, low nighttime sulfuric acid was observed, 1.5×10^6 molecules cm^{-3} and thus low OH mixing ratios were calculated, median value of 3.3×10^5 molecules cm^{-3}. This finding is in strong contrast to the high levels of nighttime OH reported by [*Ren et al.*, 2003b]. High levels of sulfuric acid were observed. However, these levels corresponded to OH levels less than 3.9×10^5 molecules cm^{-3}. Instead, the high nocturnal sulfuric acid mixing ratios were found to correspond to enhanced levels of NO_3.

The nucleation parameter, L, was found to be consistent with observations from this field experiment. Nucleation events were observed when L was less than one but not when L was greater than one. During daylight flights nucleation was found to be probable 10% of the time with most of these occurrences in urban plumes at sulfuric acid

levels of greater than 4 x 10^7 molecules cm^{-3}. There was little evidence for nucleation in power plant plumes. However, calculations suggest that this may in part be suppressed by NO_x reductions leading to decreased levels of OH and sulfuric acid.

4.5 References

Arnold, F., J. Schneider, K. Gollinger, H. Schlager, P. Schulte, D. E. Hagen, P. D. Whitefield, and P. vanVelthoven (1997), Observation of upper tropospheric sulfur dioxide- and acetone-pollution: Potential implications for hydroxyl radical and aerosol formation, *Geophysical Research Letters*, *24*(1), 57-60.

Berndt, T., O. Boge, F. Stratmann, J. Heintzenberg, and M. Kulmala (2005), Rapid formation of sulfuric acid particles at near-atmospheric conditions, *Science*, *307*(5710), 698-700.

Berresheim, H., T. Elste, H. G. Tremmel, A. G. Allen, H. C. Hansson, K. Rosman, M. Dal Maso, J. M. Makela, M. Kulmala, and C. D. O'Dowd (2002), Gas-aerosol relationships of H2SO4, MSA, and OH: Observations in the coastal marine boundary layer at Mace Head, Ireland, *Journal of Geophysical Research-Atmospheres*, *107*(D19), 12.

Boy, M., M. Kulmala, T. M. Ruuskanen, M. Pihlatie, A. Reissell, P. P. Aalto, P. Keronen, M. Dal Maso, H. Hellen, H. Hakola, R. Jansson, M. Hanke, and F. Arnold (2005), Sulphuric acid closure and contribution to nucleation mode particle growth, *Atmospheric Chemistry and Physics*, *5*, 863-878.

Brock, C. A., F. Schroder, B. Karcher, A. Petzold, R. Busen, and M. Fiebig (2000), Ultrafine particle size distributions measured in aircraft exhaust plumes, *Journal of Geophysical Research-Atmospheres*, *105*(D21), 26555-26567

Brock, C. A., M. Trainer, T. B. Ryerson, J. A. Neuman, D. D. Parrish, J. S. Holloway, D. K. Nicks, G. J. Frost, G. Hubler, F. C. Fehsenfeld, J. C. Wilson, J. M. Reeves, B. G. Lafleur, H. Hilbert, E. L. Atlas, S. G. Donnelly, S. M. Schauffler, V. R. Stroud, and C. Wiedinmyer (2003), Particle growth in urban and industrial plumes in Texas, *Journal of Geophysical Research-Atmospheres*, *108*(D3).

Brown, S. S., T. B. Ryerson, A. G. Wollny, C. A. Brock, R. Peltier, A. P. Sullivan, R. J. Weber, W. P. Dube, M. Trainer, J. F. Meagher, F. C. Fehsenfeld, and A. R. Ravishankara (2006), Variability in nocturnal nitrogen oxide processing and its role in regional air quality, *Science*, *311*(5757), 67-70.

Chen, G., L. G. Huey, M. Trainer, D. Nicks, J. Corbett, T. Ryerson, D. Parrish, J. A. Neuman, J. Nowak, D. Tanner, J. Holloway, C. Brock, J. Crawford, J. R. Olson, A. Sullivan, R. Weber, S. Schauffler, S. Donnelly, E. Atlas, J. Roberts, F. Flocke, G. Hubler, and F. Fehsenfeld (2005), An investigation of the chemistry of ship emission plumes during ITCT 2002, *Journal of Geophysical Research-Atmospheres*, *110*(D10), 15.

Crawford, J., D. Davis, J. Olson, G. Chen, S. Liu, G. Gregory, J. Barrick, G. Sachse, S. Sandholm, B. Heikes, H. Singh, and D. Blake (1999), Assessment of upper

tropospheric HOx sources over the tropical Pacific based on NASA GTE/PEM data: Net effect on HOx and other photochemical parameters, *Journal of Geophysical Research-Atmospheres*, *104*(D13), 16255-16273.

Dube, W. P., S. S. Brown, H. D. Osthoff, M. R. Nunley, S. J. Ciciora, M. W. Paris, R. J. McLaughlin, and A. R. Ravishankara (2006), Aircraft instrument for simultaneous, in situ measurement of NO3 and N2O5 via pulsed cavity ring-down spectroscopy, *Review of Scientific Instruments*, *77*(3), 11

Edwards, G. D., C. A. Cantrell, S. Stephens, B. Hill, O. Goyea, R. E. Shetter, R. L. Mauldin, E. Kosciuch, D. J. Tanner, and F. L. Eisele (2003), Chemical ionization mass spectrometer instrument for the measurement of tropospheric HO2 and RO2, *Analytical Chemistry*, *75*(20), 5317-5327.

Eisele, F. L. (1989), Natural and Anthropogenic Negative-Ions in the Troposphere, *Journal of Geophysical Research-Atmospheres*, *94*(D2), 2183-2196

Eisele, F. L., and D. J. Tanner (1993), MEASUREMENT OF THE GAS-PHASE CONCENTRATION OF H2SO4 AND METHANE SULFONIC-ACID AND ESTIMATES OF H2SO4 PRODUCTION AND LOSS IN THE ATMOSPHERE, *Journal of Geophysical Research-Atmospheres*, *98*(D5), 9001-9010

Eisele, F. L., R. L. Mauldin, D. J. Tanner, J. R. Fox, T. Mouch, and T. Scully (1997), An inlet/sampling duct for airborne OR and sulfuric acid measurements, *Journal of Geophysical Research-Atmospheres*, *102*(D23), 27993-28001.

Eisele, F. L., and P. H. McMurry (1997), Recent progress in understanding particle nucleation and growth, *Philosophical Transactions of the Royal Society of London Series B-Biological Sciences*, *352*(1350), 191-200.

EPA (2004), NOx Budget Trading Program 2003 progress and compliance reprot.

Faloona, I., D. Tan, W. Brune, J. Hurst, D. Barket, T. L. Couch, P. Shepson, E. Apel, D. Riemer, T. Thornberry, M. A. Carroll, S. Sillman, G. J. Keeler, J. Sagady, D. Hooper, and K. Paterson (2001), Nighttime observations of anomalously high levels of hydroxyl radicals above a deciduous forest canopy, *Journal of Geophysical Research-Atmospheres*, *106*(D20), 24315-24333.

Fehsenfeld, F. C., C. J. Howard, and A. L. Schmeltekopf (1975), GAS-PHASE ION CHEMISTRY OF HNO3, *Journal of Chemical Physics*, *63*(7), 2835-2842.

Fehsenfeld, F. C., G. Ancellet, T. S. Bates, A. H. Goldstein, R. M. Hardesty, R. Honrath, K. S. Law, A. C. Lewis, R. Leaitch, S. McKeen, J. Meagher, D. D. Parrish, A. A. P. Pszenny, P. B. Russell, H. Schlager, J. Seinfeld, R. Talbot, and R. Zbinden (2006), International Consortium for Atmospheric Research on Transport and Transformation (ICARTT): North America to Europe - Overview of the 2004

summer field study, *Journal of Geophysical Research-Atmospheres*, *111*(D23), 36.

Fiedler, V., M. Dal Maso, M. Boy, H. Aufmhoff, J. Hoffmann, T. Schuck, W. Birmili, M. Hanke, J. Uecker, F. Arnold, and M. Kulmala (2005), The contribution of sulphuric acid to atmospheric particle formation and growth: a comparison between boundary layers in Northern and Central Europe, *Atmospheric Chemistry and Physics*, *5*, 1773-1785.

Frost, G. J., S. A. McKeen, M. Trainer, T. B. Ryerson, J. A. Neuman, J. M. Roberts, A. Swanson, J. S. Holloway, D. T. Sueper, T. Fortin, D. D. Parrish, F. C. Fehsenfeld, F. Flocke, S. E. Peckham, G. A. Grell, D. Kowal, J. Cartwright, N. Auerbach, and T. Habermann (2006), Effects of changing power plant NOx emissions on ozone in the eastern United States: Proof of concept, *Journal of Geophysical Research-Atmospheres*, *111*(D12), 19.

Geyer, A., K. Bachmann, A. Hofzumahaus, F. Holland, S. Konrad, T. Klupfel, H. W. Patz, D. Perner, D. Mihelcic, H. J. Schafer, A. Volz-Thomas, and U. Platt (2003), Nighttime formation of peroxy and hydroxyl radicals during the BERLIOZ campaign: Observations and modeling studies, *Journal of Geophysical Research-Atmospheres*, *108*(D4), 16.

Holloway, J. S., R. O. Jakoubek, D. D. Parrish, C. Gerbig, A. Volz-Thomas, S. Schmitgen, A. Fried, B. Wert, B. Henry, and J. R. Drummond (2000), Airborne intercomparison of vacuum ultraviolet fluorescence and tunable diode laser absorption measurements of tropospheric carbon monoxide, *Journal of Geophysical Research-Atmospheres*, *105*(D19), 24251-24261

Jacob, D. J. (2000), Heterogeneous chemistry and tropospheric ozone, *Atmospheric Environment*, *34*(12-14), 2131-2159

Kulmala, M., V. M. Kerminen, T. Anttila, A. Laaksonen, and C. D. O'Dowd (2004a), Organic aerosol formation via sulphate cluster activation, *Journal of Geophysical Research-Atmospheres*, *109*(D4), 7.

Kulmala, M., H. Vehkamaki, T. Petajda, M. Dal Maso, A. Lauri, V. M. Kerminen, W. Birmili, and P. H. McMurry (2004b), Formation and growth rates of ultrafine atmospheric particles: a review of observations, *Journal of Aerosol Science*, *35*(2), 143-176.

Lovejoy, E. R., D. R. Hanson, and L. G. Huey (1996), Kinetics and products of the gas-phase reaction of SO3 with water, *Journal of Physical Chemistry*, *100*(51), 19911-19916.

Martinez, M., H. Harder, T. A. Kovacs, J. B. Simpas, J. Bassis, R. Lesher, W. H. Brune, G. J. Frost, E. J. Williams, C. A. Stroud, B. T. Jobson, J. M. Roberts, S. R. Hall,

R. E. Shetter, B. Wert, A. Fried, B. Alicke, J. Stutz, V. L. Young, A. B. White, and R. J. Zamora (2003), OH and HO2 concentrations, sources, and loss rates during the Southern Oxidants Study in Nashville, Tennessee, summer 1999, *Journal of Geophysical Research-Atmospheres*, *108*(D19), 17

Mauldin, R. L., D. J. Tanner, J. A. Heath, B. J. Huebert, and F. L. Eisele (1999), Observations of H2SO4 and MSA during PEM-Tropics-A, *Journal of Geophysical Research-Atmospheres*, *104*(D5), 5801-5816 Observations of H2SO4 and MSA during PEM-Tropics-A *J. Geophys. Res.-Atmos*.

McMurry, P. H., M. Fink, H. Sakurai, M. R. Stolzenburg, R. L. Mauldin, J. Smith, F. Eisele, K. Moore, S. Sjostedt, D. Tanner, L. G. Huey, J. B. Nowak, E. Edgerton, and D. Voisin (2005), A criterion for new particle formation in the sulfur-rich Atlanta atmosphere, *Journal of Geophysical Research-Atmospheres*, *110*(D22), 10.

Neuman, J. A., L. G. Huey, R. W. Dissly, F. C. Fehsenfeld, F. Flocke, J. C. Holecek, J. S. Holloway, G. Hubler, R. Jakoubek, D. K. Nicks, D. D. Parrish, T. B. Ryerson, D. T. Sueper, and A. J. Weinheimer (2002), Fast-response airborne in situ measurements of HNO3 during the Texas 2000 Air Quality Study, *Journal of Geophysical Research-Atmospheres*, *107*(D20), 16

Olson, J. R., J. H. Crawford, G. Chen, W. H. Brune, I. C. Faloona, D. Tan, H. Harder, and M. Martinez (2006), A reevaluation of airborne HOx observations from NASA field campaigns, *Journal of Geophysical Research-Atmospheres*, *111*(D10), 12.

Peltier, R. E., A. P. Sullivan, R. J. Weber, C. A. Brock, A. G. Wollny, J. S. Holloway, J. A. de Gouw, and C. Warneke (2007), Fine aerosol bulk composition measured on WP-3D research aircraft in vicinity of the Northeastern United States - results from NEAQS, *Atmospheric Chemistry and Physics*, *7*(12), 3231-3247.

Platt, U., G. Lebras, G. Poulet, J. P. Burrows, and G. Moortgat (1990), PEROXY-RADICALS FROM NIGHTTIME REACTION OF NO3 WITH ORGANIC-COMPOUNDS, *Nature*, *348*(6297), 147-149

Ren, X. R., H. Harder, M. Martinez, R. L. Lesher, A. Oliger, T. Shirley, J. Adams, J. B. Simpas, and W. H. Brune (2003a), HOx concentrations and OH reactivity observations in New York City during PMTACS-NY2001, *Atmospheric Environment*, *37*(26), 3627-3637

Ren, X. R., H. Harder, M. Martinez, R. L. Lesher, A. Oliger, J. B. Simpas, W. H. Brune, J. J. Schwab, K. L. Demerjian, Y. He, X. L. Zhou, and H. G. Gao (2003b), OH and HO2 chemistry in the urban atmosphere of New York City, *Atmospheric Environment*, *37*(26), 3639-3651.

Ryerson, T. B., M. P. Buhr, G. J. Frost, P. D. Goldan, J. S. Holloway, G. Hubler, B. T. Jobson, W. C. Kuster, S. A. McKeen, D. D. Parrish, J. M. Roberts, D. T. Sueper, M. Trainer, J. Williams, and F. C. Fehsenfeld (1998), Emissions lifetimes and ozone formation in power plant plumes, *Journal of Geophysical Research-Atmospheres*, *103*(D17), 22569-22583

Ryerson, T. B., L. G. Huey, K. Knapp, J. A. Neuman, D. D. Parrish, D. T. Sueper, and F. C. Fehsenfeld (1999), Design and initial characterization of an inlet for gas-phase NOy measurements from aircraft, *Journal of Geophysical Research-Atmospheres*, *104*(D5), 5483-5492

Sander, S. P. e. a. (2003), Chemical kinetics and photochemical data for use in stratospheric modeling: Evaluation 14, *JPL Publ.*, *02-25*.

Schauffler, S. M., E. L. Atlas, D. R. Blake, F. Flocke, R. A. Lueb, J. M. Lee-Taylor, V. Stroud, and W. Travnicek (1999), Distributions of brominated organic compounds in the troposphere and lower stratosphere, *Journal of Geophysical Research-Atmospheres*, *104*(D17), 21513-21535

Schauffler, S. M., E. L. Atlas, S. G. Donnelly, A. Andrews, S. A. Montzka, J. W. Elkins, D. F. Hurst, P. A. Romashkin, G. S. Dutton, and V. Stroud (2003), Chlorine budget and partitioning during the Stratospheric Aerosol and Gas Experiment (SAGE) III Ozone Loss and Validation Experiment (SOLVE), *Journal of Geophysical Research-Atmospheres*, *108*(D5), 18

Sjostedt, S., L. G. Huey, D. J. Tanner, J. Peischl, G. Chen, J. E. Dibb, B. Lefer, M. A. Hutterli, A. J. Beyersdorf, N. J. Blake, D. R. Blake, D. Sueper, T. Ryerson, J. Burkhart, and A. Stohl (2007), Observations of hydroxyl and the sum of peroxy radical at Summit, Greenland during summer 2003, *Atmospheric Environment*, *41*, 5122-5137.

Stolzenburg, M. R., P. H. McMurry, H. Sakurai, J. N. Smith, R. L. Mauldin, F. L. Eisele, and C. F. Clement (2005), Growth rates of freshly nucleated atmospheric particles in Atlanta, *Journal of Geophysical Research-Atmospheres*, *110*(D22), 10.

Weber, R. J., J. J. Marti, P. H. McMurry, F. L. Eisele, D. J. Tanner, and A. Jefferson (1997), Measurements of new particle formation and ultrafine particle growth rates at a clean continental site, *Journal of Geophysical Research-Atmospheres*, *102*(D4), 4375-4385.

Weber, R. J., P. H. McMurry, R. L. Mauldin, D. J. Tanner, F. L. Eisele, A. D. Clarke, and V. N. Kapustin (1999), New particle formation in the remote troposphere: A comparison of observations at various sites, *Geophysical Research Letters*, *26*(3), 307-310.

Weber, R. J., K. Moore, V. Kapustin, A. Clarke, R. L. Mauldin, E. Kosciuch, C. Cantrell, F. Eisele, B. Anderson, and L. Thornhill (2001), Nucleation in the equatorial

Pacific during PEM-Tropics B: Enhanced boundary layer H2SO4 with no particle production, *Journal of Geophysical Research-Atmospheres*, *106*(D23), 32767-32776.

CHAPTER 5

PHOTOCHEMICAL ACTIVITY IN MEXICO CITY DURING MILAGRO 2006: RESULTS FROM THE T1 SITE

5.1 Summary

A large suite of instruments were deployed at a ground based site in Tecámac, México (near the northern boundary of Mexico City) to measure SO_2, NO, CO, O_3, H_2SO_4, OH and HO_2 +RO_2 during MIRAGE-Mex field campaign (March 2006). These and other measurements are used to characterize atmospheric oxidation and predict sulfuric acid and OH concentrations at the site. The observations in conjunction with the NASA LARc Photochemical box model are used to explore ozone production, nitrate and sulfate formation, and radical levels and radical production rates during the day. The one minute observations of sulfuric acid, sulfur dioxide, and aerosol surface area were used to calculate OH levels assuming steady state. The sulfuric acid derived OH values agreed well with observation of OH (R^2 = 0.7). Maximum ozone production was calculated from the observations and found to be 25 ppb/hr, peaking at 10 am LST. The NASA photostationary state model predicts considerably less ozone production with a solar noon peak. Photochemical activity is found to be maximum during the morning hours, as seen in ozone and nitrate formation. Although the model predictions capture the observed diurnal profile, the model underpredicts RO_2 concentrations in the morning hours and overpredicts in the afternoon (HO_2 + RO_2 radical Model/observed (M/O) ~1.15 and OH M/O ~ 1.2). There is significant disagreement between the model and

observations in the early morning that is attributed to non-standard radical sources not defined in the model.

5.2 Experimental Methods

5.2.1 Field Campaign and site description

The MIRAGE 2006 field campaign took place in Mexico during the spring of 2006. MIRAGE combined several aircraft platforms and surface sites in order to understand the chemistry, transport, and dispersion of pollutants in the greater region. The T1 surface site was the base for the Georgia Tech trailer which included trace gas instrumentation to measure NO, SO_2, O_3, CO, H_2SO_4, OH, and $HO_2 + RO_2$. The site is situated 35 km northwest of the center of Mexico City at the Universidad Tecnológica de Tecámac as shown in Figure 5.1. It was an arid climate with sparse vegetation. Other trailers at the site housed a suite of other aerosol and gas phase measurements. The site was situated next to a major road. As a result, if the wind blew from the east local pollution from vehicles was captured. For more information on the campaign and a complete description of the surface sites and aircraft payload, see *http://www.eol.ucar.edu/projects/milagro/*. Description of specific trace gas instrumentation and methods at the T1 site follows.

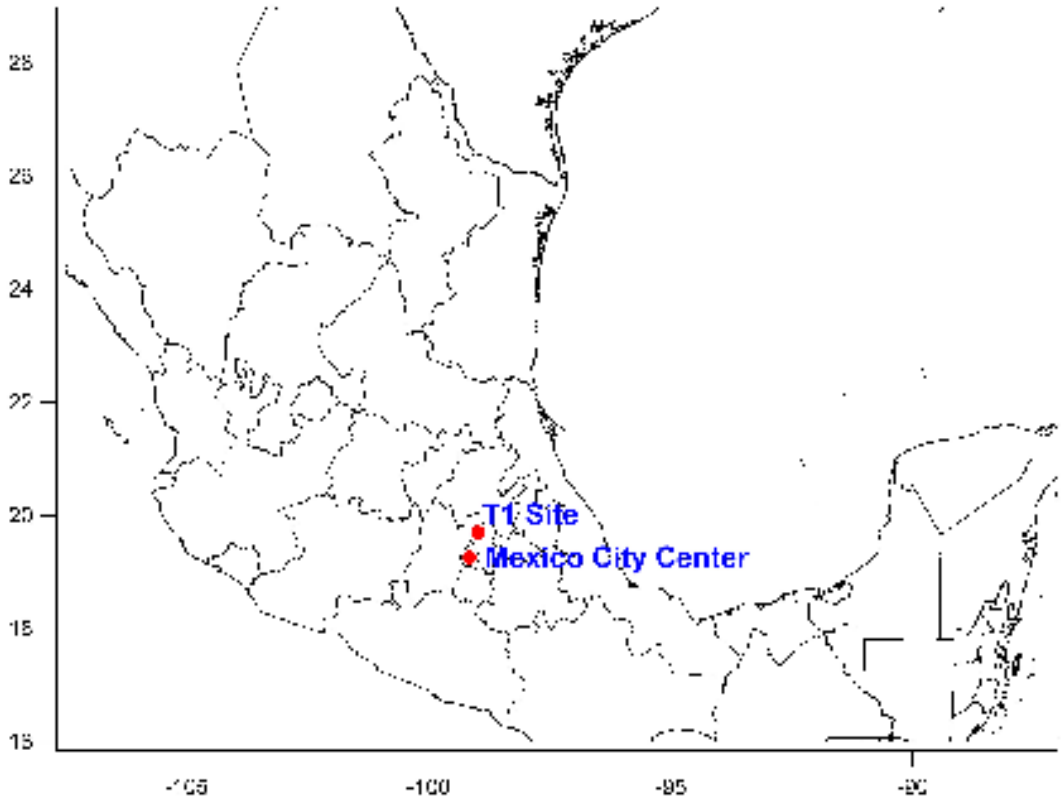

Figure 5.1: The T1 surface site was located at the Universidad Tecnológica de Tecámac; it is a suburban location located 35 km northwest of Mexico City Center.

5.2.2 CIMS Instrument

Gas-phase H_2SO_4, OH and $HO_2 + RO_2$ were measured by chemical ionization mass spectrometry (CIMs) as described in detail in [*Sjostedt et al.*, 2007]. The CIMs instrument was mounted in an enclosure on the roof of the trailer (approximately 4 meters above ground). A brief description of the relevant measurement features are given here. OH radicals are measured by conversion to $H_2{}^{34}SO_4$ via titration with $^{34}SO_2$ [*Eisele*, 1989]. RO_2 and HO_2 radicals are also converted to $H_2{}^{34}SO_4$ via reaction with NO and $^{34}SO_2$ [*Edwards et al.*, 2003]. Both labeled and naturally occurring sulfuric acid are detected as HSO_4^- (97 amu) by reaction (R5.1)

$$H_2SO_4 + NO_3^- \cdot (HNO_3) \rightarrow HSO_4^- \cdot (HNO_3) + HNO_3 \qquad \text{R5.1}$$

The photolysis of water provides the calibration of OH and peroxy radicals [*Sjostedt et al.*, 2007]. The sulfuric acid calibration is inferred from the OH titration. It should be noted that the calibration of the CIMS instrument was carried out in zero air due to the high VOC loading in Mexico City. This increases the uncertainty of both measurements (OH and RO_2) relative to previous campaigns in remote environments [*Sjostedt et al.*, 2007]. However, it should be noted that the sulfuric acid measurement is independent of conversion chemistry and therefore provides another assessment of OH concentrations measured in Mexico City [*Case Hanks et al.*, in prep]. This is especially important as high NO levels were often present at T1. These high levels have the potential to influence both the OH and RO_2 measurements via both HONO formation and enhanced OH production from HO_2 in the CIMS. We estimate measurement uncertainty as 50% for all three measurements. This is larger than in remote regions due to the presence of the high levels of VOC and NO. The 3σ limit of detection for H_2SO_4 is 6 $\times 10^5$ molecules cm^{-3} in 1 second while OH and peroxy radical limit of detections are 6 $\times 10^5$ molecules cm^{-3} and 1 $\times 10^7$ molecules cm^{-3} respectively in 1 second.

5.2.3 Other measurements

The instruments were located within the trailer with their sampling inlet, 3/8 inch OD Teflon tube, located 5 m above the ground affixed to a tower. Measurements ran continuously from 9 March -1 April 2006. Nitric oxide was measured with a custom chemiluminescence instrument [*Sjostedt et al.*, 2007]. NO was averaged for 5 seconds and had a 3σ detection limit of 25 pptv. Carbon monoxide was detected via a CO

analyzer from Thermo Electron Corporation (model 48C). It was modified to control temperature around the optics bench and a Palladium scrubber was added in order to verify background signal [*Holloway et al.*, 2000]. The 3σ limit of detection for carbon monoxide was 32 ppbv for a 1 minute average. The SO_2 detector (ThermoElectron Corporation, model 42C) was also modified to verify background signal by adding an activated charcoal scrubber. Finally, the ozone analyzer was a commercial instrument from Thermo Electron Corporation, model 49C. Calibrations were performed for each species besides ozone at least every other day during the campaign. Ancillary measurements at the site include temperature, pressure, relative humidity, wind speed, wind direction, and photolysis frequencies. Volatile organic compounds, VOCs, were measured via whole air sampling. A total of 200 whole air samples were collected for the duration of the campaign. The canisters were filled over a mean period of ~1.5 hours. A description of the analysis techniques can be found in [*Barletta et al.*, 2006]. As a comparison, VOCs were also measured using gas chromatography/flame ionization detection and proton transfer reaction mass spectrometer [*de Gouw et al.*, 2006]. Lastly, photolysis frequencies were acquired via a scanning spectral radiometer [*Lefer et al.*, 2003].

5.2.4 NASA LARc Photochemical Box Model

The NASA photochemical model [*Crawford et al.*, 1999; *Olson et al.*, 2006] was used to evaluate oxidative capacity and photochemistry at the T1 site. Details of the model and a chemical reaction scheme can be found elsewhere [*Crawford et al.*, 1999] although it is important to note that updates to the model have occurred, reflecting the most current reaction rate coefficients [*Sander*, 2003]. The model calculations were constrained to

measured parameters such as temperature, pressure, dew point, photolytic fluxes, and chemical species including O_3, CO, NO, VOCs, HCHO and H_2O. The VOCs included as constraints were alkanes, alkenes, aromatics, benzene, and isoprene; no oxygenated VOCs were used to constrain except for HCHO due to lack of observations of higher order species. Standard model runs were also not constrained to HONO levels due to lack of *in situ* measurements. Consequently, the model calculations should be considered base case runs with standard chemistry.

A 10 minute time resolution was used for all measured parameters including volatile organic compounds. Recall, VOC concentrations used within model simulations were measured by means of a whole air sampling technique followed by gas chromatography [*Barletta et al.*, 2006]. The VOC data was for this reason interpolated to the 10 minute timescale through a 1^{st} order polynomial correlation to measured CO concentrations. This correlation was only used when the VOC was well correlated to CO concentration ($R^2 > 0.50$). When the VOC did not correlate well ($R^2 < 0.49$), a time interpolation was used. This allowed for a comprehensive 10 minute data set for daytime coverage from 9 March to 31 March 2006. The model constraints provided 1368 data points which fulfilled the above requirements. The output chemical species were calculated using photostationary steady state portion of the model and are considered to be in steady state as their concentrations were integrated in time until no variations occurred.

5.3 Observations

The weather during March of 2006 for the T1 site was typically sunny with few clouds. Average daytime (time of sunrise to sunset which is roughly 6:50 am to 7:10 pm LST) temperature was 18.7°C with a maximum temperature of 30°C occurring on 13 March 2006. The T1 site encountered light breezes with an average wind speed of 1.6 m/sec and the prevailing winds coming from the southeast. The sunset around 7:10 LST and average nighttime temperature was 13.2°C. Rain occurred sporadically towards the end of the campaign. The average relative humidity was 47 % for the campaign. Trace gases, NO, SO_2, O_3, CO were measured continuously from 9 March to 1 April 2006. RO_x ($OH + HO_2 + RO_2$) and H_2SO_4 were also measured continuously from 7 March to 1 April 2006. The CIMS instrument was down from early 17 to late 19 of March due to a power surge from thunder storms. Ambient concentrations of measured species are shown as a time series for the campaign in Figures 5.2 and 5.3. *Table 5.1* summarizes the data statistics for the trace gas species at the T1 site in Mexico City for the duration of the campaign.

Briefly, nitric oxide and carbon dioxide showed similar daily profiles where concentrations peaked just before 6 am LST. This sharp increase in their concentrations can be attributed to the early morning commute beginning along with heating and cooking activities. Nitric oxide had a median value of 1524 pptv during the day. It peaked sometime after 6 am LST with lowest concentrations around noon. In contrast, during the night median NO concentration was 1171 pptv. Sulfur dioxide had no discernable diurnal profile at the T1 site. On 18 March 2006, a localized burst around 9 am (maximum value of 300 ppbv, highest of the measurement period) of SO_2 was

captured. An analysis of wind direction for this morning indicated that the prevailing wind was coming from the south east and the FLEXPART back trajectory (available at http://catalog.eol.ucar.edu/milagro/index.html) confirms the wind was indeed coming from southeast of the T1 site. This surge could be due to sulfur rich air from the Popcatepetl volcano south east of greater Mexico City. Major refineries around the T1 site include PEMEX and Tula in which both are northwest of the site.

Table 5.1: Measured Data Statistics for T1 site during March 2006

Species[a]	Median	Mean	Noontime Average[b]
NO	1.4	13.3	1.2
CO	380	515	295
SO_2	1.2	5.2	5.2
O_3	35	39	77
OH	1×10^6	2×10^6	5×10^6
$HO_2 + RO_2$	6.4×10^7	1.1×10^8	2.6×10^8
H_2SO_4	2.1×10^6	7×10^6	1.6×10^7

[a]NO, CO, SO_2, and O_3 are reported in ppbv; OH, $HO_2 + RO_2$, and H_2SO_4 are reported in molecules cm^{-3}.
[b]Noontime average is defined as 10 am-2 pm local standard time.

During the measurement period, ozone's median concentration was 35.1 ppbv. Daytime ozone concentration had a mean value of 55 ppbv and began increasing immediately with the sunrise. The highest concentration of ozone during the day was 168 ppbv on 09 March 2006. During the evening hours, ozone ranged from below the detection limit to72 ppbv. Previous measurements around downtown Mexico City revealed that ozone exceeded 100 ppbv everyday [*Dunlea et al.*, 2007]. On the contrary,

concentrations of ozone at T1 only exceeded 100 ppbv during the day 52% of the campaign, reflecting its suburban locale.

Sulfuric acid and HO_x mixing ratios are highest during the day while at night there is little of these species. Sulfuric acid had a median value of 1.1×10^7 (1.1×10^6) molecules cm^{-3} and had a maximum value of 1.1×10^8 (6.2×10^6) molecules cm^{-3} at the T1 site during the day (night). The median value of OH observed during the day was 2.8×10^6 molecules cm^{-3}. During MCMA-2003, OH and HO_2 radical concentrations were measured by laser induced fluorescence. *Shirley et al*., [2006] observed a mean mixing ratio of OH to be 2.6×10^6 molecules cm^{-3} at midday. This is comparable to the values observed at the T1 site. Local noon values for OH also are similar to *Shirley et al*., who measured ~ 7×10^6 molecules cm^{-3} and our observed OH mixing ratio was 5×10^6 molecules cm^{-3}. The median nighttime mixing ratio observed for OH was 2.2×10^5 molecules cm^{-3} which is the limit of detection of the LIF instrument used during MCMA 2003. Peroxy radicals measured by the CIMS instrument are a sum of $HO_2 + RO_2$. At the T1 site, median daytime value was 1.6×10^8 molecules cm^{-3} with variations similar to MCMA-2003 (5.5×10^6 to 12×10^8 molecules cm^{-3}). The diurnal profile of the measured peroxy radicals reveals that it peaks around 1300 LST.

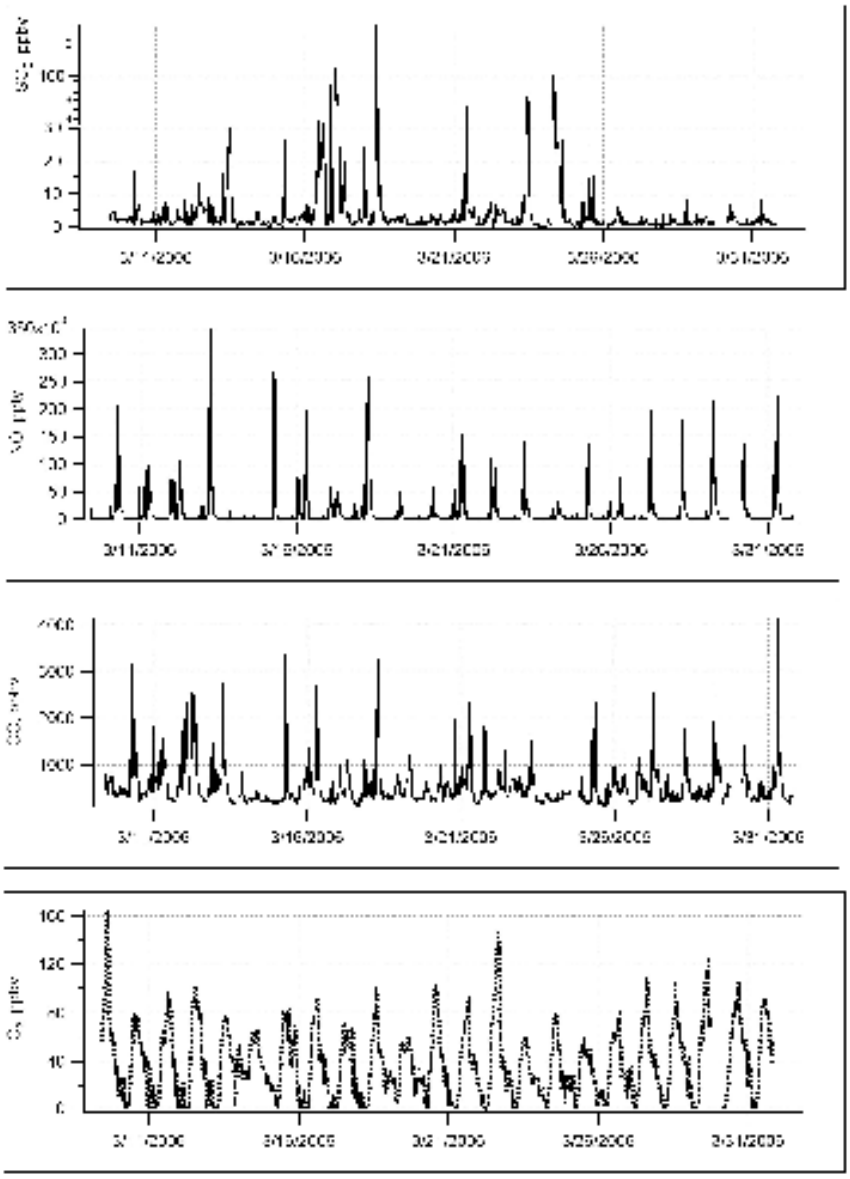

Figure 5.2. Time series of concentrations of O_3, CO, NO, and SO_2 from 9 March to 31 March 2006.

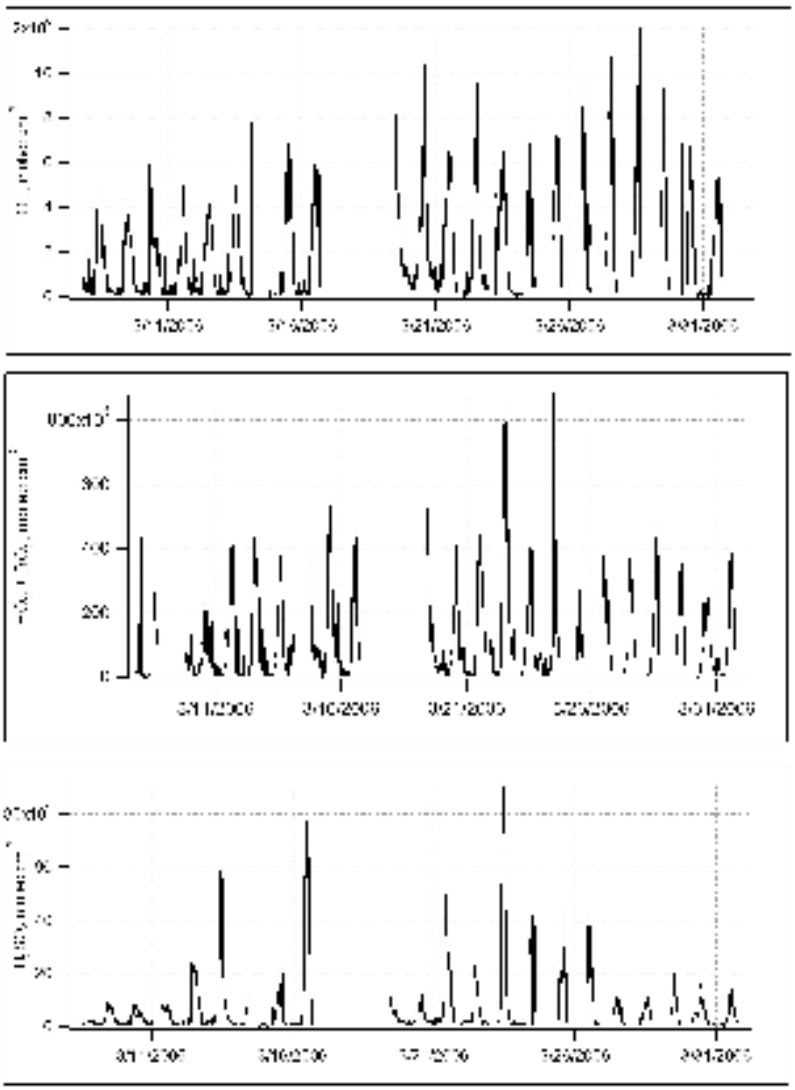

Figure 5.3. Time series of concentrations of H_2SO_4, $HO_2 + RO_2$, and OH as measured by CIMS from 9 March to 31 March 2006.

The total OH reactivity was examined for the T1 site. The total OH reactivity ($R_{OH,total}$, s^{-1}) is defined as the OH loss at the T1 site with the following species CO, CH_4, NO_2, and VOCs:

$$R_{OH,total} = k_{CO+OH}[CO] + k_{CH_4+OH}[CH_4] + k_{NO_2+OH}[NO_2] + \sum k_{n+OH}[nVOC] \qquad \text{E5.1}$$

where *nVOC* is the anthropogenic VOC species, k_{n+OH} is the rate coefficient in cm^3 $molecules^{-1}$ sec^{-1} calculated from measured temperature and pressure, and *[nVOC]* is the measured number density of the species. As stated earlier, three techniques, whole air sampling, gas chromatography/flame ionization detection, and proton transfer reaction mass spectrometer, were used to measure VOCs. When the techniques measured the same species, the VOC reactivity was calculated for the different technique and reported as an average of the techniques. Average concentrations are also reported where appropriate. *Table 5.2* is a summation of these parameters and indicates the individual contribution of the VOC to the total OH reactivity for the morning rush hours of 6-10 am LST.

Table 2: VOC reactivity and their average ambient concentrations at the T1 site for the morning rush hour from 6-10 am LST.

Species	OH reactivity (s^{-1})	Concentration (ppbv)	$k_{OH} \times 10^{-12}$ (cm^3 $molec^{-1}$ s^{-1})#	Classification
Acetaldehyde	1.46	3.74	15.8	Oxygentated
Acetylene	0.15	6.55	0.78	Alkyne
Benzene	0.04	1.2	1.2	Aromatic
cis-2-butene	0.12	0.14	56.4	Olefin
cis-2-pentene	0.12	0.08	65	Olefin
C_8 Benzenes	1.9	2.63	30.2+	Aromatic
C_9 Benzenes	0.78	1.53	20.8+	Aromatic
C_{10} Benzenes	0.13	0.45	11.2+	Aromatic
C_{11} Benzenes	0.06	0.12	20.7+	Aromatic
Ethane	0.03	5.6	0.24	Alkane
Ethene	1.38	7.35	7.9	Olefin
Ethylbenzene	0.07	0.42	7.1	Aromatic
i-butane	0.24	4.41	2.2	Alkane
i-pentane	0.26	2.66	3.94	Alkane
n-butane	0.68	12.8	2.34	Alkane
n-heptane	0.05	0.29	7.0	Alkane
n-hexane	0.14	1.09	6.76	Alkane
n-pentane	0.16	1.89	8.69	Alkane
o-xylene	0.17	0.52	13.7	Olefin
Propane	0.94	34.66	1.1	Alkane
Propene	1.87	2.49	29	Olefin
Toluene	0.41	2.94	6.18	Aromatic
trans-2-butene	0.01	0.15	1.5	Olefin
trans-2-pentene	0.23	0.14	67.0	Olefin
1-butene	0.25	0.29	31.3	Olefin
1-pentene	0.10	0.13	31.4	Olefin
3-methyl-1-butene	0.04	0.04	31.8	Olefin

#Rate constants are from IUPAC (http://www.iupac-kinetic.ch.cam.ac.uk/) or Atkinson et al., 1999 unless otherwise noted and stated for the conditions of 298 K and 1 atm.

+ Rate constant is an estimate based on average of known C_n Benzene rate constants.

Total OH reactivity was calculated to be 27.1 s^{-1}. The contribution from anthropogenic non-oxygenated VOCs is 10.3 s^{-1}. The importance of oxygenated VOCs, aldehydes, and biogenic VOCs to the total OH reactivity cannot be explored due to the lack of measurements. Although it is expected that if oxygenated VOCs and aldehydes were included, the total OH reactivity would increase. The suburban location of the T1 site and its arid climate do not indicate that biogenic VOCs would greatly impact the total OH reactivity. Within the suburban atmosphere, the significant VOCs which contribute to OH reactivity included the C_8-benzenes, propene, ethene, and propane. Only one oxygenated VOC, acetaldehyde, was consider in this analysis and it contributes significantly to OH reactivity. Shirley et al., [2006] used the Total OH Loss Measurement instrument at an urban site to measure a $R_{OH,\ total}$ value of 120 s^{-1} during the morning rush hours. It was estimated that VOCs contributed to about 72% of that reactivity. The lower $R_{OH,total}$ at the T1 site can be attributed to the limited VOC measurements particularly the lack of oxygenated VOCs and a different locale.

During MCMA 2002 and 2003, [*Velasco et al.*, 2007] analyzed VOC concentrations from 4 urban monitoring sites and found that the most abundant VOCs included propane (127±63 ppbv), n-butane (50±25 ppbv), ethylene (20±11 ppbv), i-butane (18±9 ppbv), and ethane (17±11 ppbv). These species are the most abundant at the T1 site as well although slightly lower in concentration. It is noted that *Velasco et al.,* [2007] observed at urban sites during the MCMA 2002 and 2003 studies that concentrations of VOCs depended strongly on meteorological processes and vehicular activity. Therefore, a meticulous comparison is not possible but overall trends indicate similar behavior of VOC reactivity and ambient concentration from the MCMA 2002 &

2003 with those at the T1 site. Measured $R_{OH,\ total}$ in North American cities include Nashville with a median value of 11 s^{-1} [*Martinez et al.*, 2003] and New York City with a median value of 19 s^{-1} [*Ren et al.*, 2003d]. Comparison of these urban values to the suburban T1 site in Mexico indicates that the suburban T1 atmosphere has much significantly higher loadings of VOCs.

5.4 Analysis and Discussion

To understand the photochemical activity at the T1 site, RO_2 data measured by the CIMS instrument has been compared to model output from the NASA photochemical model as presented in the following section. Henceforth, morning time is defined as 6-10 AM LST and noontime is defined as 10-2 pm LST. Figure 5.4 shows the mean diurnal profile of the model predictions versus the observed at the T1 site which indicate similar diurnal variations. In general, the model does a reasonable job of capturing the diurnal profile and the shape and magnitude of the concentration over time as illustrated in Figure 5.5. The overall model-to-observed ratio (M/O) had a median (mean) value of 0.95(1.2) for OH and 0.6(1.06) for $HO_2 + RO_2$ and correlation coefficients, R^2, of 0.5 and 0.6, respectively. On average the model predictions are within the error of the CIMS measurement for both OH and RO_2. However, the radical behavior in the morning (6-10 am LST) decreases the correlation between model and observations and drives the difference between the median and mean values especially for the $HO_2 + RO_2$ data.

In both observations and model predictions the OH shows a peak around solar noon and the peak for $HO_2 + RO_2$ follows as hour later (1 pm LST). However, both

measured species have higher concentrations than model predictions in the early morning hours. Morning radical activity can be seen during the rush hour time period of 6-10 LST where the median M/O, 0.63 for OH and 0.45 for $HO_2 + RO_2$. This is consistent with predictions that other radical sources such as HONO may be important relative to standard sources such as ozone photolysis [*Shirley et al.*, 2006; *Volkamer et al.*, 2007]. However, this time period is also when NO concentrations are at the highest and are more likely to interfere with the CIMS measurement of OH and RO_2.

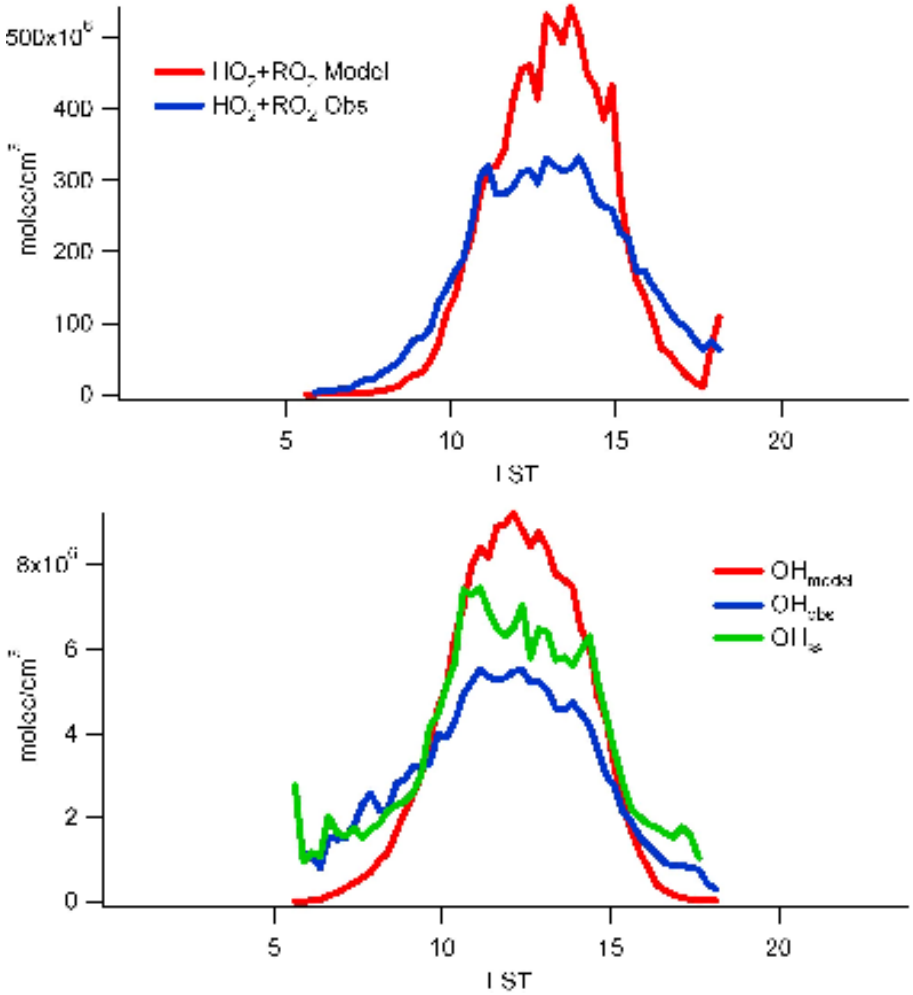

Figure 5.4: Diurnal profile of (top panel) $HO_2 + RO_2$ and (bottom panel) OH.

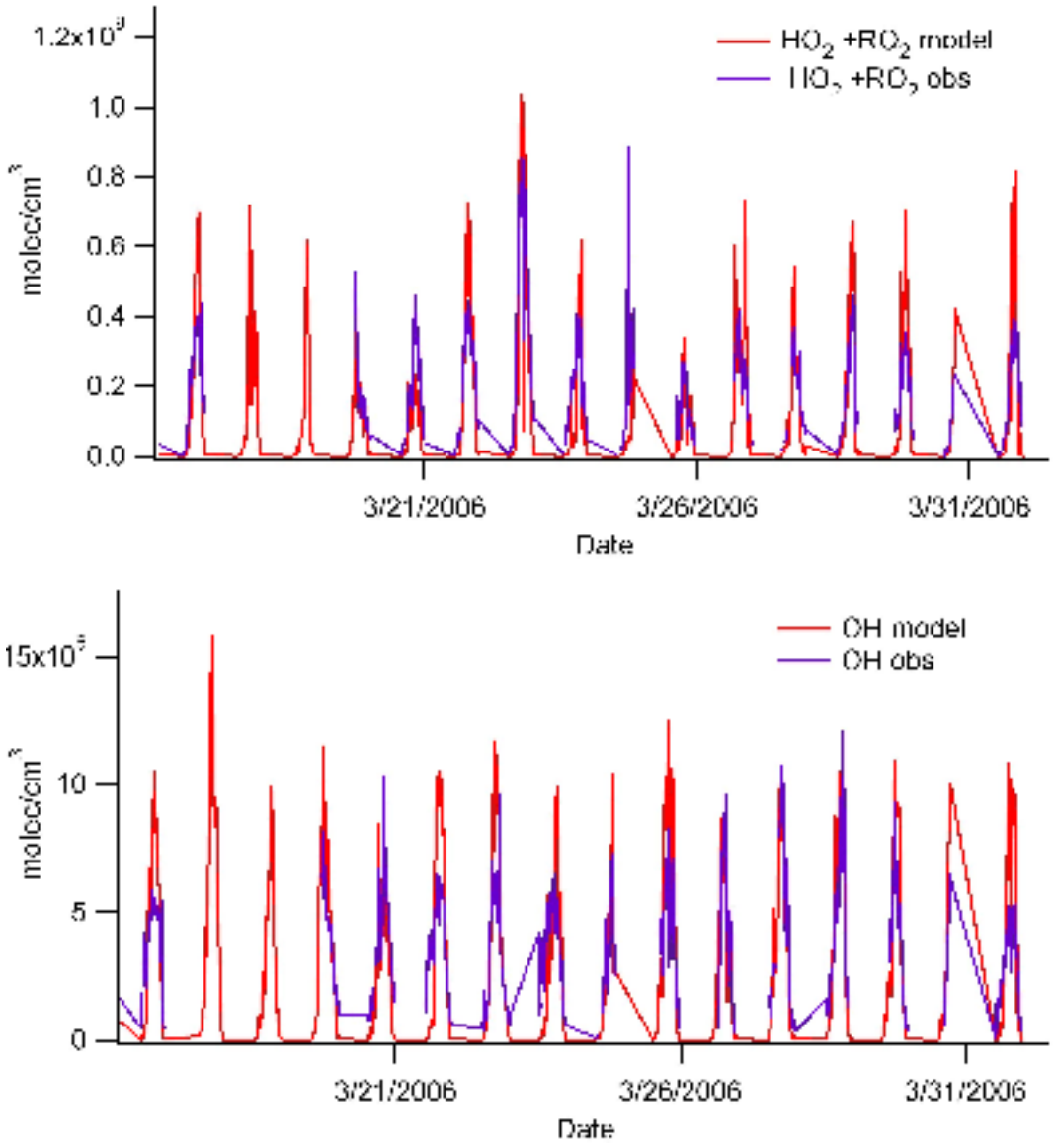

Figure 5.5: Time series of model predicted and observed HO_2 + RO_2 (top panel);time series model and observed OH (bottom panel).

In order to address the potential impact of high NO levels on the CIMS radical measurements sulfuric acid levels were used to calculate steady state OH levels. Note that the sulfuric acid measurement is immune to interference from high NO levels. As a result, the OH concentration can be calculated through a steady state approximation assuming diffusion limited uptake of H_2SO_4 by the aerosol, $R_{AerosolUptake}$,

$$[OH]_{ss} = \frac{R_{AerosolUptake}}{k[SO_2]} \quad \text{E5.2}$$

$$R_{AerosolUptake} = \left(\frac{4}{v\alpha}\right)^{-1} An_x \quad \text{E5.3}$$

where v is the molecular speed, α is the mass accommodation coefficient, A is the Fuchs surface area, and n_x is $[H_2SO_4]_{(g)}$ [*Jacob*, 2000]. The average lifetime of sulfuric acid at the T1 site is 100 seconds. The steady-state OH calculation has been used in a highly variable environment to estimate the OH concentration and proved a valuable tool [*Case Hanks et al.*, in prep]. At the T1 site, the steady-state calculations of OH levels are in excellent agreement with observations. The correlation coefficient is 0.7 with a median (mean) SS/O (steady-state-to-observed) ratio of 1.10(1.23). In addition, the steady-state calculation supports the high morning radical levels as shown in the mean diurnal profile in Figure 5.4. Effectively, there is no difference between the median morning and noon SS/O ratios as there are roughly the same 1.2. Consequently, the observed sulfuric acid levels are consistent with enhanced OH levels in the morning. These data indicate that NO is not interfering with the OH measurements at this time and further implies that the observed RO_2 levels are probably not impacted by high NO_x.

One potential important morning radical source is HONO. There were no *in situ* measurements of HONO at the T1 site which is why it is not included in standard model

runs. However, on several days the HONO vertical column was obtained by Max-DOAS [*Sinreich et al.*, 2007]. For days in which HONO was measured at the site (14 total), the average boundary layer height was 325 m for the morning hours. Assuming uniform distribution in the boundary layer, median (mean) measured HONO values were 279 pptv (389 pptv) in the morning. As a primary RO_2 source and an upper limit for the possible impact of HONO as a source, the observed HONO provided an average of 526 pptv hr^{-1} around between 7 and 8 am LST. This makes HONO a significant morning source when compared to other RO_2 sources at the T1 site including photolysis of ozone and HCHO. During the same time interval, each provided an average value of production for RO_2 of 300 pptv hr^{-1}. This upper limit of HONO production can account for up to 30% of the OH observed during that time interval, signifying that other sources in the morning are needed. Recent literature has also suggested the photolysis of nitrous acid is a significant source of OH in urban areas [*Aumont et al.*, 2003; *Platt et al.*, 2002; *Ren et al.*, 2003c]. In fact, *Volkamer et al.* [2007] concluded that early morning production of OH radicals during MCMA 2003 was dominated by photolysis of HONO, followed by photolysis of O_3 and O_3/alkene reactions. As HONO concentration decreases and photochemical O_3 is produced, photolysis of O_3 became the major source of primary OH radicals.

The high levels of observed RO_2 indicate that ozone production is at a maximum in the morning. This is a contrast to the model results which show ozone production maximum at noon as illustrated in Figure 5.6. Photochemical ozone production rates were estimated from observations using equation 5.4. The loss terms include photolysis and water vapor reaction, nitric acid formation, estimate of organic nitrate formation, and ozone reaction with alkenes and HO_x.

$$P(O_3)_{net} = k_{RO_2+NO}[RO_2][NO] - J(O^1D)[H_2O] - k_{OH+O_3}[OH][O_3]$$
$$- k_{RO_2+O_3}[RO_2][O_3] - k_{alkene+O_3}[alkene][O_3] \qquad \text{E5.4}$$
$$- k_{OH+NO_2}[M][OH[NO_2] - P(Nitrate)_{organic}$$

Nitrogen dioxide was measured at the site from 17 March to 30 March 2006 [*Thornton et al.*, 2000]; in order to get a more complete NO_2 profile, it was calculated based on measured photochemical parameters. When compared to the NO_2 measured, the calculated was within 25% and was typically higher. The calculated NO_2 was used to determine the calculated ozone production rate at the T1 site. All kinetic rate constants were calculated based on recommended equation from IUPAC [*Atkinson et al.*, 2006]. The resulting production rates were compared to the calculated ozone production ($P(O_3)_{pss}$) from the NASA photochemical model. Figure 5.6 shows the diurnal profile of the rates along with the observed O_3 and NO.

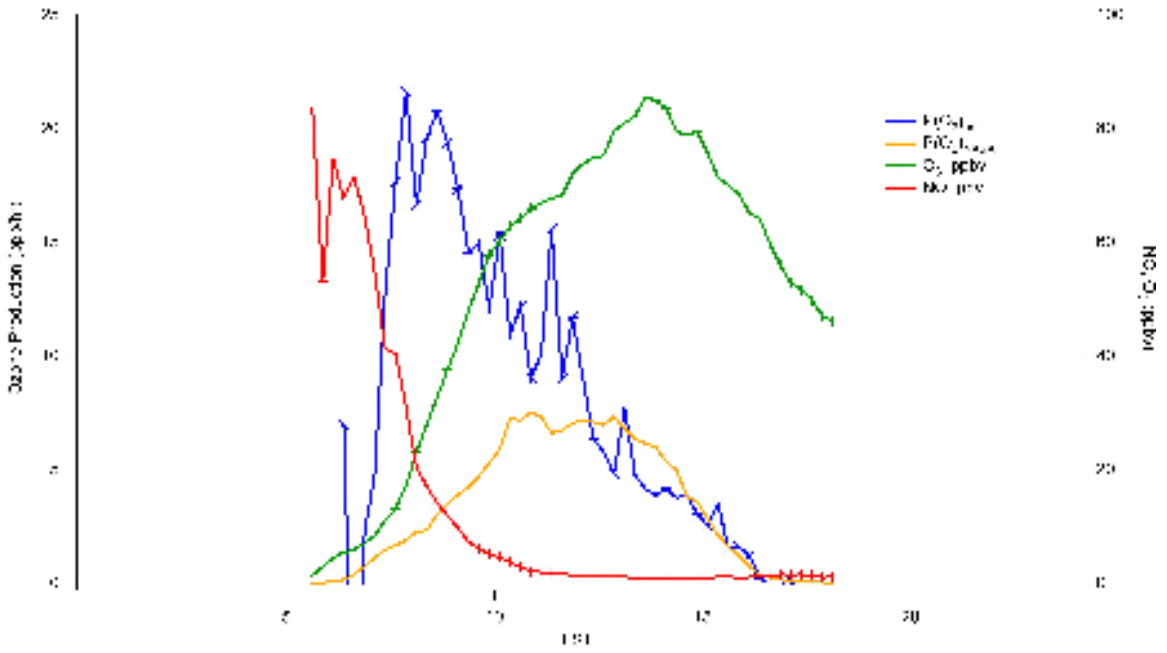

Figure 5.6 : Profile of ozone production calculated and modeled; also shown is measured ozone and nitric ozone. The calculated ozone production peaks early in the morning and observed NO rapidly decreases. Modeled ozone production peaks at noontime and observed ozone peaks around 3 pm LST.

The NASA model predicts that ozone production is maximum (~ 9 ppb/hr) around solar noon. However, the NO profile and the $P(O_3)_{net}$ have a similar shape with maximum production occurring around 9 am LST. By noon, ozone production has fallen to about 10 ppb/hr. An estimate of which ozone production rate is more realistic can be found by integrating the observed ozone production from 7 am – 12 pm LST. This yields an average calculated noontime value around 75 ppb which compares well to the observed noontime ozone of 77 ppb. In comparison, the same method can be employed with the modeled ozone production. Modeled ozone production does not include increased morning production of ozone and that is reflected in the average predicted noontime ozone value of 19 ppb. Ozone production can be compared to other megacities. It was calculated during MCMA 2003 in downtown Mexico City and was 48 ppb/hr with

maximum production occurring at 10 am LST [*Ren et al.*, 2006b]. In New York City, instantaneous ozone production peaked at 11 am LST and had a median value of 12 ppb/hr [*Ren et al.*, 2003c], similar to that at the suburban T1 site.

Ozone production in the morning can be impacted by the nighttime reservoir of NO_2. For that reason, nighttime NO_2 was examined to determine if conversion into O_3 as the sun rises was an important production term for morning ozone. The average NO_2 concentration at night was about 15 ppbv. Steady state ozone concentration is proportional to the $[NO_2]/[NO]$ ratio. At 7 am, the ratio is on average ≥ 2. Assuming that for each NO_2 molecule there is complete conversion into an O_3 molecule, it can be discounted as a possible source for the high morning ozone production.

The above ozone production calculations do not account for physical processes. Another possible source is the entrainment of free-tropospheric ozone. This can cause concentration changes within the boundary layer. For that reason, entrainment of free tropospheric air enriched with ozone was examined to see if the discrepancy in $P(O_3)$ could be explained. Morning time boundary layer height was determined from radiosonde data [*Shaw et al.*, 2007], ozone data was used from ozonesondes [*Thompson et al.*, 2007], and the entrainment velocity was defined as 1.5 cm s^{-1} [*Baumann et al.*, 2000]. Average ozone concentration at a height of 1 km above the boundary layer was 30 ppbv. The contribution of entrainment of air aloft to the morning ozone concentration when ozone concentration was sufficiently high aloft was estimated to be no more than 10% of observations for a boundary layer of 325 meters indicating that photochemical production was far more important.

The enhanced morning radical activity can impact other important processes. Gas-phase nitrate and sulfate production rates were also calculated for the T1 from observed species. Interestingly, these production rates along with ozone production (see above) were not centered around solar noon. Production rates peaked in the mid-morning, around 9-10 am local time. It can be seen that morning activity begins with the sunrise and rapidly increases with solar radiation. This phenomenon has also been reported by *Volkamer et al.,* [*2007*] during the MCMA-2003 and it was concluded that the processing of morning pollutants gets amplified by radical production from secondary pollutants that are trapped within Mexico City's natural basin and once pollution is exported, radical production dramatically decreases.

Analysis of aerosol measurements revealed that nitrate was a substantial portion of the inorganic aerosol fraction and had high morning production rates which were highly correlated to water-soluble organic carbon [*Hennigan et al.*, in submission]. At the T1 site, calculated photochemical production of nitrate from observed OH as described in equation 5.5 for the morning had a median value of 7.4 μg m^{-3} hr^{-1}.

$$P(nitrate)_{gas-phase} = k_{OH+NO_2}[OH][NO_2] \qquad \text{E5.5}$$

Hennigen et al., [in submission] suggest that aerosol nitrate at the T1 site is photochemical in nature due to the rapid increase in concentration with solar radiation and the correspondence to the observed HNO_3 production rate. A similar photochemical driven increase of gas-phase nitrate within the morning hours was also observed during MCMA [*Salcedo et al.*, 2006]. Figure 5.7 illustrates the early morning rise of gas-phase nitrate production from the observed values and the modeled. The measured aerosol nitrate fraction revealed a strong diurnal profile. In regards to photochemical sulfate

production, its median value in the morning is 0.35 μg m^{-3} hr^{-1}. It does not demonstrate a strong diurnal profile because measured SO_2 at the T1 site does not present a distinct diurnal pattern. Maximum gas-phase sulfate production occurs around 10 am LST and there is still a significant production rate for the morning that decreases sharply shortly after solar noon.

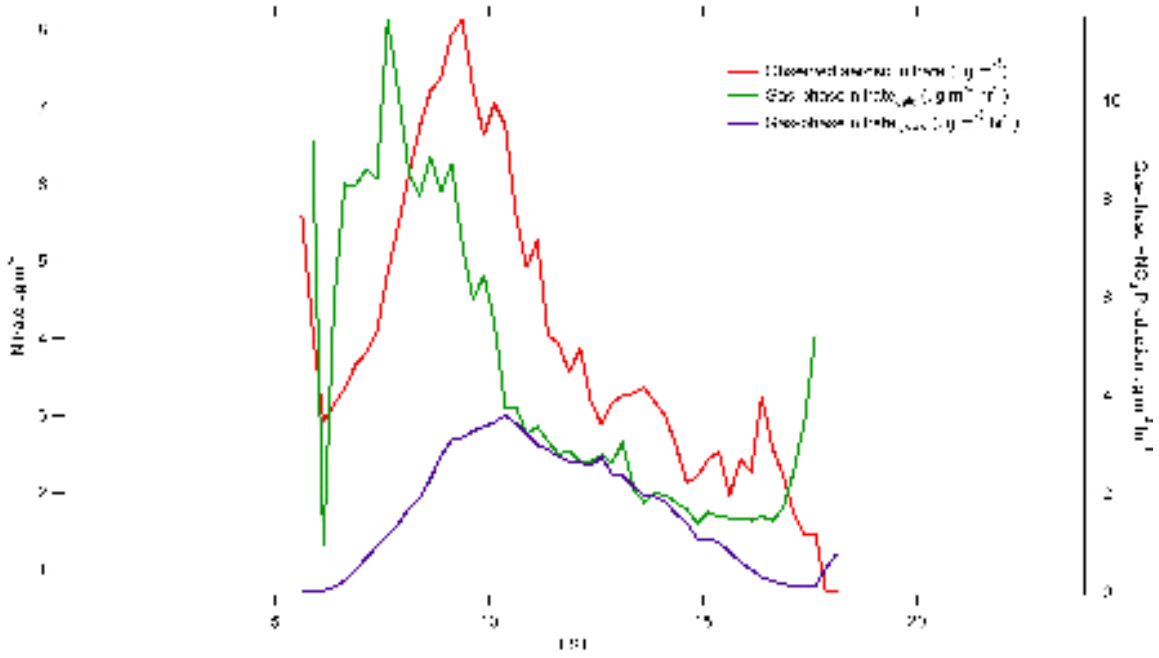

Figure 5.7: The diurnal profile of aerosol nitrate and the calculated and modeled gas-phase production rate of HNO_3. The observed production rate peaks in the morning hours around 7 am LST and falls sharply, indicating the importance of radical activity in the morning. The modeled nitrate production rate peaks after 10 am LST.

5.5 Summary and Conclusions

In this paper we have analyzed measurements of OH, $HO_2 + RO_2$, and H_2SO_4 obtained at the T1 site in suburban Mexico City in the spring of 2006. Median daytime observations for the species are as follows, sulfuric acid: 1.1×10^7 molecules cm^{-3}, OH: 2.8×10^6 molecules cm^{-3} and peroxy radicals: 1.6×10^8 molecules cm^{-3}. The suite of observations obtained has allowed for a detailed examination of photochemical activity at the suburban T1 site. Observations have shown that there is an enhancement of morning concentrations for OH and RO_2 species.

By using the observations to constrain to the NASA photochemical box model we were able to further understand the morning activity. In general, the NASA photochemical model captured the basic diurnal profile, including the shape and magnitude of the concentration of the species over time. The overall model-to-observed ratio (M/O) had a median (mean) value of 0.95(1.2) for OH and 0.6(1.06) for $HO_2 + RO_2$. There was a large disagreement between model and observed values in the morning. This could be due to other radical sources such as HONO or oxygenated VOCs which were not considered in this analysis.

The impact of the morning radical activity can also be seen in the rapid rise of ozone and aerosol nitrate production. This rise is compatible with our OH and HO_2+RO_2 observations but not the model predictions which include only conventional radical sources. In conclusion, a suite of observations including OH, nitrate and ozone production, indicate that oxidation processes are dominant within the morning. Further studies to characterize the source for this high morning time activity need to be carried out.

5.6 References:

Aumont, B., F. Chervier, S. Laval, and El (2003), Contribution of HONO sources to the NOx/HOx/O-3 chemistry in the polluted boundary layer, *Atmospheric Environment*, *37*(4), 487-498.

Barletta, B., S. Meinardi, I. J. Simpson, F. S. Rowland, C.-Y. Chan, X. Want, S. Zou, L. Y. Chan, and D. R. Blake (2006), Ambient Halocarbon Mixing Ratios in 45 Chinese Cities *Atmospheric Environment*, *40*, 7706-7719.

Baumann, K., E. J. Williams, W. Angevine, J. Roberts, R. Norton, G. Frost, F. Fehsenfeld, S. Springston, S. Bertman, and B. Hartsell (2000), Ozone production and transport near Nashville, Tennessee: results from the 1994 study at New Hendersonville, *Journal of Geophysical Research*, *105*(D7), 9137-9153.

Brock, C. A., M. Trainer, T. B. Ryerson, J. A. Neuman, D. D. Parrish, J. S. Holloway, D. K. Nicks, G. J. Frost, G. Hubler, F. C. Fehsenfeld, J. C. Wilson, J. M. Reeves, B. G. Lafleur, H. Hilbert, E. L. Atlas, S. G. Donnelly, S. M. Schauffler, V. R. Stroud, and C. Wiedinmyer (2003), Particle growth in urban and industrial plumes in Texas, *Journal of Geophysical Research-Atmospheres*, *108*(D3).

Case Hanks, A. T., L. G. Huey, D. Tanner, and C. Brock (in prep), Boundary Layer Sulfuric Acid Measurements during NEAQS-ITCT 2k4: Implications for Photochemistry and Aerosols.

Crawford, J., D. Davis, J. Olson, G. Chen, S. Liu, G. Gregory, J. Barrick, G. Sachse, S. Sandholm, B. Heikes, H. Singh, and D. Blake (1999), Assessment of upper tropospheric HOx sources over the tropical Pacific based on NASA GTE/PEM data: Net effect on HOx and other photochemical parameters, *Journal of Geophysical Research-Atmospheres*, *104*(D13), 16255-16273.

de Gouw, J. A., C. Warneke, A. Stohl, A. G. Wollny, C. A. Brock, O. R. Cooper, J. S. Holloway, M. Trainer, F. C. Fehsenfeld, E. L. Atlas, S. G. Donnelly, V. Stroud, and A. Lueb (2006), Volatile organic compounds composition of merged and aged forest fire plumes from Alaska and western Canada, *Journal of Geophysical Research-Atmospheres*, *111*(D10), 20.

Dunlea, E. J., S. C. Herndon, D. D. Nelson, R. M. Volkamer, F. San Martini, P. M. Sheehy, M. S. Zahniser, J. H. Shorter, J. C. Wormhoudt, B. K. Lamb, E. J. Allwine, J. S. Gaffney, N. A. Marley, M. Grutter, C. Marquez, S. Blanco, B. Cardenas, A. Retama, C. R. R. Villegas, C. E. Kolb, L. T. Molina, M. J. Molina (2007), Evaluation of nitrogen dioxide chemiluminescence monitors in a polluted urban environment, *Atmospheric Chemistry and Physics*, *7*(10), 2691-2704.

Edwards, G. D., C. A. Cantrell, S. Stephens, B. Hill, O. Goyea, R. E. Shetter, R. L. Mauldin, E. Kosciuch, D. J. Tanner, and F. L. Eisele (2003), Chemical ionization

mass spectrometer instrument for the measurement of tropospheric HO2 and RO2, *Analytical Chemistry*, *75*(20), 5317-5327.

Eisele, F. L. (1989), Natural and Anthropogenic Negative-Ions in the Troposphere, *Journal of Geophysical Research-Atmospheres*, *94*(D2), 2183-2196

Fast, J. D., and S. Y. Zhong (1998), Meteorological factors associated with inhomogeneous ozone concentrations within the Mexico City basin, *Journal of Geophysical Research-Atmospheres*, *103*(D15), 18927-18946.

Guttikunda, S. K., Y. H. Tang, G. R. Carmichael, G. Kurata, L. Pan, D. G. Streets, J. H. Woo, N. Thongboonchoo, and A. Fried (2005), Impacts of Asian megacity emissions on regional air quality during spring 2001, *Journal of Geophysical Research-Atmospheres*, *110*(D20), 27.

Hennigan, C. J., A. P. Sullivan, C. I. Fountoukis, A. Nenes, A. Hecobian, O. Vargas, A. T. Case Hanks, L. G. Huey, B. L. Lefer, A. G. Russell, and R. J. Weber (in submission), On the Volatility and Production Mechanisms of Newly Formed Nitrate and Water Soluble Organic Aerosol in Mexico City, *Atmospheric Chemistry and Physics*.

Holloway, J. S., R. O. Jakoubek, D. D. Parrish, C. Gerbig, A. Volz-Thomas, S. Schmitgen, A. Fried, B. Wert, B. Henry, and J. R. Drummond (2000), Airborne intercomparison of vacuum ultraviolet fluorescence and tunable diode laser absorption measurements of tropospheric carbon monoxide, *Journal of Geophysical Research-Atmospheres*, *105*(D19), 24251-24261

Jacob, D. J. (2000), Heterogeneous chemistry and tropospheric ozone, *Atmospheric Environment*, *34*(12-14), 2131-2159

Kanaya, Y., and H. Akimoto (2002), Direct measurements of HOx radicals in the marine boundary layer: Testing the current tropospheric chemistry mechanism, *Chemical Record*, *2*(3), 199-211.

Kanaya, Y. G., R. Q. Cao, S. G. Kato, Y. K. Miyakawa, Y. Kajii, H. Tanimoto, Y. Yokouchi, M. Mochida, K. Kawamura, and H. Akimoto (2007), Chemistry of OH and HO2 radicals observed at Rishiri Island, Japan, in September 2003: Missing daytime sink of HO2 and positive nighttime correlations with monoterpenes, *Journal of Geophysical Research-Atmospheres*, *112*(D11), 17.

Kleinman, L. I., P. H. Daum, Y. N. Lee, L. J. Nunnermacker, S. R. Springston, J. Weinstein-Lloyd, and J. Rudolph (2002), Ozone production efficiency in an urban area, *Journal of Geophysical Research-Atmospheres*, *107*(D23), 12.

Lefer, B. L., R. E. Shetter, S. R. Hall, J. H. Crawford, and J. R. Olson (2003), Impact of clouds and aerosols on photolysis frequencies and photochemistry during TRACE-P: 1. Analysis using radiative transfer and photochemical box models, *Journal of Geophysical Research*, *108*(D21).

Martinez, M., H. Harder, T. A. Kovacs, J. B. Simpas, J. Bassis, R. Lesher, W. H. Brune, G. J. Frost, E. J. Williams, C. A. Stroud, B. T. Jobson, J. M. Roberts, S. R. Hall, R. E. Shetter, B. Wert, A. Fried, B. Alicke, J. Stutz, V. L. Young, A. B. White, and R. J. Zamora (2003a), OH and HO2 concentrations, sources, and loss rates during the Southern Oxidants Study in Nashville, Tennessee, summer 1999, *Journal of Geophysical Research-Atmospheres*, *108*(D19), 17.

Martinez, M., H. Harder, T. A. Kovacs, J. B. Simpas, J. Bassis, R. Lesher, W. H. Brune, G. J. Frost, E. J. Williams, C. A. Stroud, B. T. Jobson, J. M. Roberts, S. R. Hall, R. E. Shetter, B. Wert, A. Fried, B. Alicke, J. Stutz, V. L. Young, A. B. White, and R. J. Zamora (2003b), OH and HO2 concentrations, sources, and loss rates during the Southern Oxidants Study in Nashville, Tennessee, summer 1999, *Journal of Geophysical Research-Atmospheres*, *108*(D19), 17

Olson, J. R., J. H. Crawford, G. Chen, W. H. Brune, I. C. Faloona, D. Tan, H. Harder, and M. Martinez (2006), A reevaluation of airborne HOx observations from NASA field campaigns, *Journal of Geophysical Research-Atmospheres*, *111*(D10), 12.

Platt, U., B. Alicke, R. Dubois, A. Geyer, A. Hofzumahaus, F. Holland, M. Martinez, D. Mihelcic, T. Klupfel, B. Lohrmann, W. Patz, D. Perner, F. Rohrer, J. Schafer, J. Stutz, and Cj (2002), Free radicals and fast photochemistry during BERLIOZ, *Journal of Atmospheric Chemistry*, *42*(1), 359-394.

Ren, X. R., H. Harder, M. Martinez, R. L. Lesher, A. Oliger, T. Shirley, J. Adams, J. B. Simpas, and W. H. Brune (2003a), HOx concentrations and OH reactivity observations in New York City during PMTACS-NY2001, *Atmospheric Environment*, *37*(26), 3627-3637.

Ren, X. R., H. Harder, M. Martinez, R. L. Lesher, A. Oliger, J. B. Simpas, W. H. Brune, J. J. Schwab, K. L. Demerjian, Y. He, X. L. Zhou, and H. G. Gao (2003b), OH and HO2 chemistry in the urban atmosphere of New York City, *Atmospheric Environment*, *37*(26), 3639-3651.

Ren, X. R., W. H. Brune, J. Q. Mao, M. J. Mitchell, R. L. Lesher, J. B. Simpas, A. R. Metcalf, J. J. Schwab, C. X. Cai, Y. Q. Li, K. L. Demerjian, H. D. Felton, G. Boynton, A. Adams, J. Perry, Y. He, X. L. Zhou, and J. Hou (2006a), Behavior of OH and HO2 in the winter atmosphere in New York city, *Atmospheric Environment*, *40*, S252-S263.

Ren, X. R., W. H. Brune, A. Oliger, A. R. Metcalf, J. B. Simpas, T. Shirley, J. J. Schwab, C. H. Bai, U. Roychowdhury, Y. Q. Li, C. X. Cai, K. L. Demerjian, Y. He, X. L. Zhou, H. L. Gao, and J. Hou (2006b), OH, HO2, and OH reactivity during the PMTACS-NY Whiteface Mountain 2002 campaign: Observations and model comparison, *Journal of Geophysical Research-Atmospheres*, *111*(D10), 12.

Salcedo, D., T. B. Onasch, K. Dzepina, M. R. Canagaratna, Q. Zhang, J. A. Huffman, P. F. DeCarlo, J. T. Jayne, P. Mortimer, D. R. Worsnop, C. E. Kolb, K. S. Johnson,

B. Zuberi, L. C. Marr, R. Volkamer, L. T. Molina, M. J. Molina, B. Cardenas, R. M. Bernabe, C. Marquez, J. S. Gaffney, N. A. Marley, A. Laskin, V. Shutthanandan, Y. Xie, W. Brune, R. Lesher, T. Shirley, and J. L. Jimenez (2006), Characterization of ambient aerosols in Mexico City during the MCMA-2003 campaign with Aerosol Mass Spectrometry: results from the CENICA Supersite, *Atmospheric Chemistry and Physics*, *6*(4), 925-946.

Sander, S. P. e. a. (2003), Chemical kinetics and photochemical data for ise in stratospheric modeling: Evaluation 14, *JPL Publ.*, *02-25*.

Shaw, W. J., M. S. Pekour, R. L. Coulter, T. J. Martin, and J. T. Walters (2007), The daytime mixing layer observed by radiosonde, profiler, and lidar during MILAGRO, *Atmospheric Chemistry and Physics Discussion*, *7*, 15025-15065.

Shirley, T. R., W. H. Brune, X. Ren, J. Mao, R. Lesher, B. Cardenas, R. Volkamer, L. T. Molina, M. J. Molina, B. Lamb, E. Velasco, T. Jobson, and M. Alexander (2006), Atmopsheric oxidation in the Mexico City Metropolitan Area (MCMA) during April 2003, *Atmospheric Chemistry and Physics*, *6*, 2753-2765.

Sinreich, R., R. Volkamer, F. Filsinger, C. Kern, U. Platt, O. Sebastian, and T. Wagner (2007), MAX-DOAS measurement of Glyoxal during ICARTT-2004, *Atmospheric Chemistry and Physics*, *7*, 1293-1303.

Sjostedt, S., L. G. Huey, D. J. Tanner, J. Peischl, G. Chen, J. E. Dibb, B. Lefer, M. A. Hutterli, A. J. Beyersdorf, N. J. Blake, D. R. Blake, D. Sueper, T. Ryerson, J. Burkhart, and A. Stohl (2007), Observations of hydroxyl and the sum of peroxy radical at Summit, Greenland during summer 2003, *Atmospheric Environment*, *41*, 5122-5137.

Thompson, A. M., J. E. Yorks, S. K. Miller, J. C. Witte, K. M. Dougherty, G. A. Morris, D. Baumgardner, L. Ladino, and B. Rappenglueck (2007), Free tropospheric ozone sources and wave activity over Mexico City and Houston during Milagro/Intercontinental Transport Experiment (INTEX-B) Ozonesonde Network Study, 2006 (IONS-06), *Atmospheric Chemistry and Physics Discussion*.

Thornton, J. A., P. J. Wooldridge, and R. C. Cohen (2000), Atmospheric NO2: In Situ Laser-Induced Fluorescence Detection at Parts per Trillion Mixing Ratios, *Analytical Chemistry*, *72*.

Velasco, E., B. Lamb, H. Westberg, E. Allwine, G. Sosa, J. L. Arriaga-Colina, B. T. Jobson, M. L. Alexander, P. Prazeller, W. B. Knighton, T. M. Rogers, M. Grutter, S. C. Herndon, C. E. Kolb, M. Zavala, B. de Foy, R. Volkamer, L. T. Molina, and M. J. Molina (2007), Distribution, magnitudes, reactivities, ratios and diurnal patterns of volatile organic compounds in the Valley of Mexico during the MCMA 2002 & 2003 field campaigns, *Atmospheric Chemistry and Physics*, *7*, 329-353.

Volkamer, R., P. M. Sheehy, L. T. Molina, and M. J. Molina (2007), Oxidative capacity of the Mexico city atmosphere --Part 1: A radical source perspective, A*tmospheric Chemistry and Physics Discussion*, *7*, 5365-5412.